Transition to turbulence in particle laden pipe flows

Vasudevan Krishnan

Technische Universiteit Delft

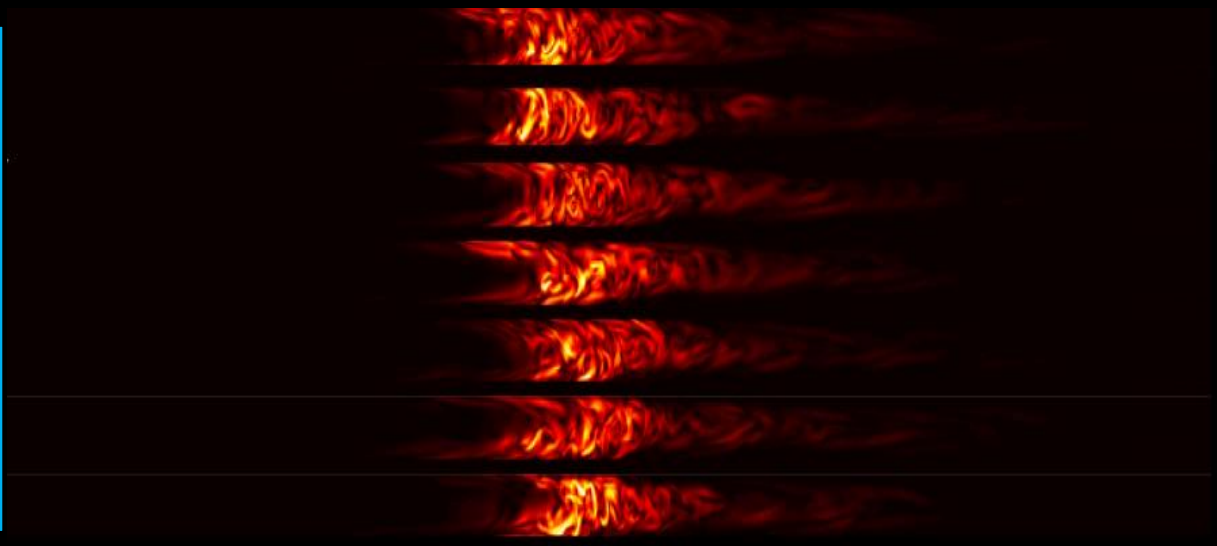

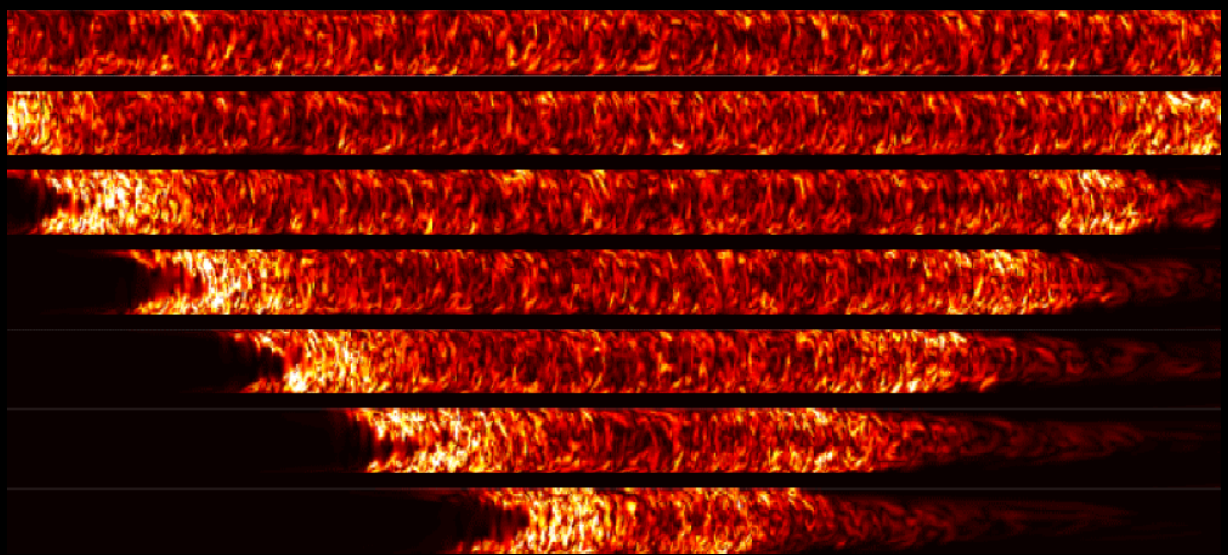

Transition to turbulence in particle-laden pipe flows

by

Vasudevan Krishnan

to obtain the degree of Master of Science
at the Delft University of Technology,
to be defended publicly on 23 November 2020.

Student number:	4796632	
P & E report number:	3037	
Project duration:	October 21, 2019 – November 23, 2020	
Thesis committee:	Dr. ir. C. Poelma,	TU Delft, supervisor
	Dr. Ir. J. Westerweel,	TU Delft
	Ir. W. Hogendoorn,	TU Delft, Daily supervisor

An electronic version of this thesis is available at `http://repository.tudelft.nl/`.

TU Delft

Preface

The thesis marks the completion of required credits to obtain for the Masters in Mechanical Engineering under the track '*Energy and Process technology*'. The research was carried out at the Laboratory of Aero Hydrodynamics in the department of Process and Energy under the supervision of Dr.ir. Christian Poelma. The report explains the work done to the study the effect of neutrally buoyant particles on transition of pipe flows.

The report aims to provide documentation of the experimental campaign, literature reviewed to understand the problem and the results obtained from the experiments. The readers interested in the theory of transition and the effect of particles are advised to go to Chapter 1 and directly to Chapter 4 and 5. The readers who would like to repeat or build similar experiments are directed to Chapter 3 and further refer Appendix A, Appendix B and Appendix C. The aforementioned sections explains the construction of the setup and the calibration procedure of the apparatus used.

I take full responsibilities for the contents detailed in this report and therefore I will be accountable for any anomaly or lack clarity in the report. constructive criticism on the experimental procedure or logical flaws found in the document are welcome. I strive to learn from any mistakes that may have been committed. The data used in the document will be available upon request for any validation or experiments conducted in the future. Experiments to study transition behavior using different particle and tube diameters are currently in progress.

The cover page shows the visualization of puffs and slugs along the length of pipe. The image is taken from the experiments conducted to study the speed and structure of turbulent fronts by Song et al. [1]

Vasudevan Krishnan
Delft, November 6, 2020

Acknowledgements

The current work was started on October, 2019 as part of my Master thesis worth 45 credits. It would not have been possible to complete the work without the help of many people. I would like to take this moment to thank them for their time and involvement to help me set up and perform experiments. I would like to thank **Jasper** for fabricating all the parts I needed to perform the experiments. Since, this was my first attempt at building an experimental setup from scratch, I designed parts that were eventually rendered redundant and Jasper fabricated all my designs and provided me promptly. The perturbation mechanism used in the current setup had not been used in any recent experiments and therefore **Jan** helped me acquiring the parts to make it functional. The system needed to be tuned for the specific needs of the experiments eg. creating a new velocity profile for the motor, setting up the data acquisition system for the mechanism and troubleshooting the mechanism in event of malfunctioning.

The work would not have been possible without the help offered by the PhD students in the lab. I would like to thank **Sudarshan** for taking time out of his schedule to discuss any problem that I faced during the experimental campaign. I would also like to thank him for lending his camera to perform the particle size distribution explained in Appendix B. I would like to thank **Udhav** for helping me with his insights when I encountered problems with the perturbation mechanism. I also wanted to thank him for his help in processes like draining the setup etc. I would like to thank **Dr. Bidhan** for helping me with building the setup and sharing components from his setup for my experiments. I would like to thank him for assisting me in the calibration process and his insights on various areas throughout my thesis. I would like to thank **Dr. Delfos** for taking his time from his busy schedule and helping me with the calibration process and in particularly helping me troubleshooting it. I will be grateful for his voluntary involvement in the calibration process as he provided me some key insights to understand it better.

The thesis would have not been completed successfully without the able guidance from my supervisors. I will be grateful to **Dr. Christian Poelma** for giving me the opportunity to perform this research and guiding me through it. I would like to thank him for the freedom provided to perform the research in my own direction and providing me invaluable advice and feedback regularly. I would like to thank him for motivating me through difficult times during my thesis. I would like to thank **Willian** who was my daily supervisor during my thesis. It is impossible to overstate his help and guidance in this work. I would like to thank him for sharing his code for particle size characterization an helping me with calibrating the pressure sensors when I started to perform the experiments. I would like to thank him for helping me with understanding the physical phenomena and important insights for performing experiments in a pragmatic way. I learned a lot about planning experimensts and the relevnat procedures in advance and accounting for all factors and uncertainties while performing experiments.

This work would not have been possible without the motivation and support shown by my **friends** in a particularly difficult and stressful year. The discussions over coffee table or during dinner relieved lot of stress and enabled me to be focused while performing the experiments. I would also like to thank my **family** for financing my study and thereby supporting my dreams and aspirations.

Abstract

Multiphase flows are found in abundant natural phenomena and industrial processes. In particular, pipe flows are widely popular in industries involving chemical processing, dredging and oil transport to name a few. Particle laden flows are often observed in applications like dredging, sediment and slurry transport through pipes etc. Therefore, it is imperative to understand the flow phenomenon in detail. The most important parameter in pipe flow is the pressure drop across a given length. This relates directly to the pumping power which is a significant parameter for industries when viewed from an economic standpoint. This lays emphasis on understanding the different regimes for particle laden flows and impact of particles on transition in particular. Research on transition behavior for particle laden pipe flows is scarce and the behavior is far from being completely understood.

The literature is replete with study of transition for single phase pipe flows. Different perturbation mechanisms were analyzed and the lifetime studies indicated that the puffs are memoryless in nature. The literature provided different formulations to accommodate for the presence of particles with regards to modify viscosity of the suspension. The research in multiphase flows have provided inconclusive results in determining the critical Reynolds number for transition as different criteria were provided in different works.

The goal of the current thesis is to perform experiments to understand the transition behavior of particle laden pipe flows for different particle concentrations. The novelty of this work is the use of active perturbation mechanism that enabled the study of transition in perturbed and unperturbed flows. The experiments involves varying the particle concentration and keeping the ratio of pipe to particle diameter constant. The study concentrates on understanding the transition behavior using Moody diagrams. The experiments rely on pressure drop measurements to record the average pressure drop across the pipe and study the intermittent structures that drive the transition behavior. The study uses glycerol to make the solution neutrally buoyant when using particles. Single phase measurements are performed to validate the setup including the pressure sensors and the perturbation mechanism. The Moody chart indicates that the transition is sub-critical with spatio-temporal intermittency for particle concentrations less than 1.5%. Interestingly, the particle induced disturbances are significant and the transition behavior is identical for perturbed and unperturbed flow. This suggests that the disturbance created by the particles are qualitatively similar to that of the perturbation mechanism. However, the transition becomes super-critical for higher particle concentrations as the transition is driven by the fluctuations generated by the particles and the additional friction created by them. The friction factor decreases monotonically for very high particle concentrations ($\geq 15\%$). The transition behavior is investigated further by analyzing the time series data of pressure drop for different particle concentrations at an intermittency of $10-20\%$. The transition criteria is analyzed based on deviation from Poiseuille line in the Moody chart and spike in pressure fluctuations in the flow. The latter provides inconclusive evidence for higher particle concentrations. The former holds good for the current study, however, it needs to be revisited for other particle sizes.

Nomenclature

Re - Reynolds number (-)

f - Friction factor (-)

D_h - Hydraulic diameter of the flow geometry (m)

ϵ - Wall roughness (-)

D - Pipe diameter (m)

t - Time (s)

ρ - Density (kg/m^3)

u - Bulk velocity of fluid (m/s)

μ - Viscosity of fluid (kg/ms)

Δp - Pressure drop in flow (Pa)

L - Length of pipe (m)

h^* - Non dimensional height of obstacle (-)

h - Height of obstacle (m)

A - Amplitude of perturbation (-)

μ_{adj} - Viscosity of suspension after accounting for particle concentration ($kg/m\ s$)

ϕ - Particle concentration expressed as wt/wt % of suspension (-)

ϕ_m - Maximum particle concentration in suspension (-)

γ - Intermittency in flow (-)

f_{puffs} - Friction factor corresponding to puffs (-)

f_{lam} - Friction factor corresponding to laminar regime (-)

Δp_{mean} - mean pressure drop in flow (Pa)

Φ_{inj} - Mass flux of fluid injected (kg/min)

Φ_{inj} - Mass flux of fluid flow in pipe (kg/min)

v - Instantaneous velocity of piston (m/s)

v_{max} - Maximum velocity of piston (m/s)

T - Time period of perturbation (s)

L_{entry} - Entrance length of pipe (m)

D/d - Ratio of diameter of pipe to diameter of particle (-)

f_{add} - Additional friction (-)

f_{actual} - Measured value of friction factor (-)

$f_{blasius}$ - Friction factor calculated using Blasius correlation (-)

$\Delta p'$ - Pressure fluctuations obtained after subtracting mean value of pressure drop (Pa)

$\bar{t}$ - Non dimensional time (-)

L_{puff} - Length of turbulent puff normalized by pipe diameter (-)

Re_c - Critical Reynolds number for transition in flow regime (-)

Contents

List of Figures

List of Tables

1

Introduction

In fluid mechanics, multi-phase flow is the simultaneous flow of materials with two or more thermodynamic phases. They can consist only a single chemical component (eg. water vapour in water) or multiple components (eg. dust suspended in air). The flow generally has two distinct phases: continous phase and dispersed phase. Multi-phase flows have numerous applications from atmospheric phenomena, oil and gas, dredging industry, pollution dispersion to process industries. During the mid 20th century, advances in nucleate boiling fueled the research in mutiphase flows to develop models for predicting friction factor and heat transfer. Later, it was extensively researched by the oil and gas industry to improve productivity and efficiency of oil extraction. Multi-phase flow metering technology is the result of prolonged research by companies like BP, Texaco that has become industry standard. Other applications include fluidized bed reactors used in process industries. Applications in nature include sediment transport in rivers where the suspended particles are treated as dispersed particles interacting with continuous fluid phase. Blood flow and flow in the intestinal tract are some common examples of multi-phase flow. In some cases, the dispersed phase can affect the physical properties of the suspension like viscosity, density etc. Therefore, it is important to understand the impact of the dispersed phase on the flow regime itself. Therefore, understanding the flow phenomena is crucial towards development of new technologies.

Some of the important parameters in pipe flows are pressure drop, friction factor and volume flow rate etc. The pressure drop is a direct indicator of pumping power required to keep the fluid flowing and also directly corresponds to the running cost when viewed from an industrial standpoint. Also, identifying the flow regime plays a crucial role in calculating the aforementioned parameters. The presence of the second phase is also significant as it alters the flow behaviour and the parameters discussed here. For instance, friction factor is inversely proportional to the Reynolds number ($\propto Re^{-1}$) in the laminar regime. In turbulent regime this proportionality changes to $Re^{-0.25}$. This has a direct impact on the pressure drop across the pipe. Also addition of dispersed phase alters the viscosity and thus the Reynolds number itself, which will be explained in detail in section 2.1.2. The impact of size of the dispersed phase on the transition and flow phenomena in general will also be discussed. Since the particles have a big influence on some important parameters like friction factor, viscosity and density, it is important to understand the impact of their presence on the transition behavior. This understanding of the transition behavior is crucial to model or predict behavior of important parameters for different flow regimes for multi-phase flows.

The study of transition to turbulent regime in a pipe is an age-old problem. Numerous attempts have been made to analyse the nature of transition and the point of transition in a Hagen - Poiseuille flow. The research towards the understanding of laminar and turbulent regimes for single phase flows are well documented using theoretical and empirical relations. But transition, specially in multiphase systems, need deeper inspection. Therefore, transition to turbulence in particle laden flows has caught attention recently and have been researched extensively since then. However, prior to diving into multi-phase systems, it is important to understand pertinent theory on transition in single phase flow in pipes. The chapter details on some important theoretical concepts that are relevant to understand the physical processes in turbulence and parameters relevant to it.

1.1. Theory

The current work involves the study of transition in pipe flows for multi-phase systems. Therefore it is important to understand the different flow regimes and important terminologies in Hagen-Poiseuille flow. Some of the important terminologies related to transition in pipe flow and impact of addition of particles are discussed in the section.

1.1.1. Laminar flow regime

The laminar flow regime is characterized by smooth orderly motion of fluid where it moves in layers and the individual layers do not mix with the each other. This indicates that the layers move in direction parallel to the wall in the case of pipe flow. Therefore, the flow regime does not involve presence of swirls or eddies. The laminar flow is typically observed at lower Reynolds numbers (Re < 1000) where flow regime typically involves low velocities, smaller length-scales or high viscosity. Furthermore, the flow regime is characterized by high momentum diffusion and low momentum convection. The diffusion of momentum is possible due to the influence of viscous forces over the inertial forces in the flow. This property will later be exploited in the design of entrance chamber in the experimental setup to facilitate break down of eddies. The friction factor scales inversely the Reynolds number with and agrees with the Poiseuille line ($f = 64/Re$) [17] and often this will be used a quick method for validating the experimental setup.

1.1.2. Turbulent flow regime

The turbulent flow regime is the widely observed regime in everyday phenomena and is often characterized by chaotic fluctuations in pressure and flow velocity. The fluid layers constantly mix with each other and thus constantly exchanging energy. Different empirical correlations were formulated to characterize the friction factor in the flow. The turbulent regime has some important characteristic phenomena like high diffusivity, irregularity, rotationality and dissipation [18]. Unlike the laminar regime, the correlations were developed based on experimental evidence and solving the logarithmic law for the fluid velocity analytically [19] [20]. The friction factor of the flow is heavily influenced by the wall roughness in the pipe. Colebrook and White combined experimental results for smooth and rough pipes to formulate a correlation for friction factor [21] as given in equation 1.1.

$$\frac{1}{\sqrt{f}} = -2\ log\left(\frac{\epsilon}{3.7D_h} + \frac{2.51}{Re\sqrt{f}}\right) \tag{1.1}$$

The correlation uses surface roughness ϵ and hydraulic diameter D_h to calculate friction factor for a given Reynolds number. The formulation has wide range of applicability, however, it is implicit in nature and therefore difficult to obtain a value for friction factor directly. It is for this reason, a more explicit relation formulated by Blasius is used in the thesis to calculate the friction factor of the flow. The correlation is valid for Re < 10^5 and is given in equation 1.2.

$$f = \frac{0.316}{Re^{1/4}} \tag{1.2}$$

1.1.3. Stability of flow and Intermittent structures

Pipe flow is theoretically stable for all volume flow rates and consequently all Reynolds numbers. It is considered that, for a given set of mathematically ideal initial and boundary conditions, it should be possible to find a solution of the Navier-Stokes equation. When the problem is considered well posed, it indicates that any small perturbations in the initial or the boundary conditions will remain small. This particular criterion is satisfied only in the laminar flow regime. However, it was clear from the literature and daily experience that pipe flows are stable only up to a certain Reynolds number after which non-linear effects play a dominant role in the growth of small disturbances into finite perturbations. Under these circumstances, small disturbances will grow into finite amplitude perturbations in a finite amount of time. Such solutions to the Navier-Stokes problem is not physically feasible and the problem becomes ill-posed [22]. This behavior, referred to as deterministic chaos, is often associated with turbulent flow.

As discussed above, the flow becomes unstable after a certain Reynolds number where non-linear growth of perturbations take prominence. These finite amplitude perturbations grow into chaotic turbulent struc-

tures like eddies which are the fundamental blocks in the intermittent structures observed in the flow regime. These intermittent structures are referred to as '*puffs*' and '*slugs*' depending on the Reynolds number. The turbulent puffs are often observed at Re < 2700 while slugs are observed for Re > 3000. The typical velocity profiles of these turbulent structures are shown in figure 1.1. The turbulent structures are spatially localized in the pipe in the transition regime. Arguments were made that the relaminarization of flow behind the chaotic turbulent region is due to the sudden drop in Reynolds number to a value where turbulence cannot be maintained [23].

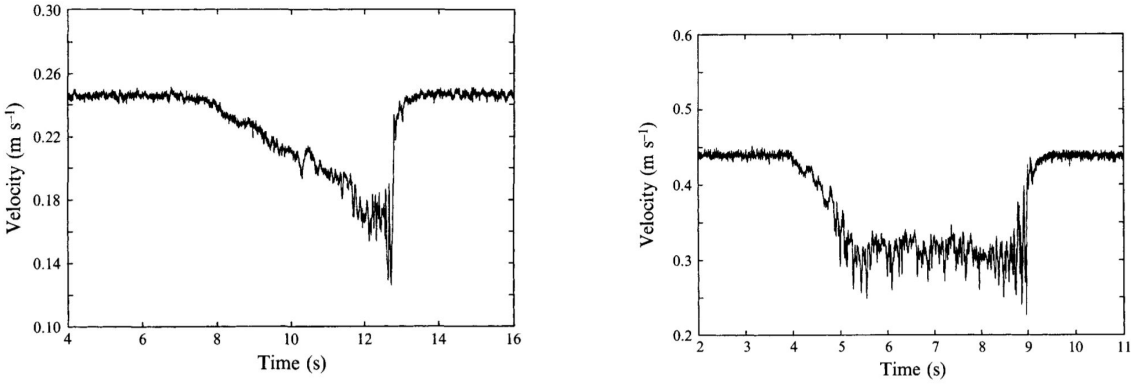

(a) Velocity profile of turbulent puff

(b) Velocity profile of turbulent slug

Figure 1.1: (a) Centerline velocity profile of a turbulent puff at Re = 2300 recorded at 140 D from the inlet using Laser doppler anemometry. (b) Centerline velocity profile of a turbulent puff at Re = 4260 recorded at 140 D from the inlet using Laser doppler anemometry. Figure reproduced from Darbyshire et al. [2]

The turbulent puffs represent the incomplete relaminarization process in the flow. The velocity of the puffs reduce gradually in the leading edge. The velocity reduces to a minimum after which it sharply jumps back to the value observed for the laminar region. This reduction in centerline velocity can be explained by a flatter velocity profile observed in the turbulent regime compared to the parabolic velocity profile in the laminar regime. Helical wave-like structures were observed in the central region of the flow. Furthermore, the turbulent region of the fluid covers the entire cross-section of the pipe. The relative size and scales of the eddies within the puffs are not the same for different puffs. This holds true even when the puffs are triggered without changing the Reynolds number and the perturbation parameters. However, the overall length of the puff and the intensity are similar for any two puffs. The puffs were reported to be the result of gradual increase in turbulence intensity from the inlet due to incomplete relaminarization. Therefore, the turbulent intensity and length-scales of these structures vary in the upstream region where the puffs are developing. However, there is no observable difference in the overall length-scale of puffs when they are fully developed making them independent of their source. As the leading edge travels at higher velocity, the puffs split into smaller structures and if the Reynolds number is high enough the individual structures grow into separate puffs. However, there are instances where the turbulence cannot be sustained and puff decays after being split. The figure 1.2 shows the puff splitting at two different Reynolds numbers [3].

The intermittent structures, referred to as slugs, have sharp interfaces in the leading and trailing edge and a sharp decrease in the velocity is observed. Unlike puffs, slug do not originate from the entrance as the turbulence measured at entrance was low. The slugs are reportedly the result of transition in the developing boundary layer downstream of the entrance. Slugs originate from a single spot of disturbance in the boundary layer on one side of the tube wall and grows until its dimensions become comparable to the diameter of the pipe. Studies performed by Wygnanaski et. al. [23] reported slugs were observed to envelope the entire cross-section of the pipe by 40 D. While turbulent spots were observed at smaller axial distances, the slugs represented the occurence of turbulence at larger axial distances.

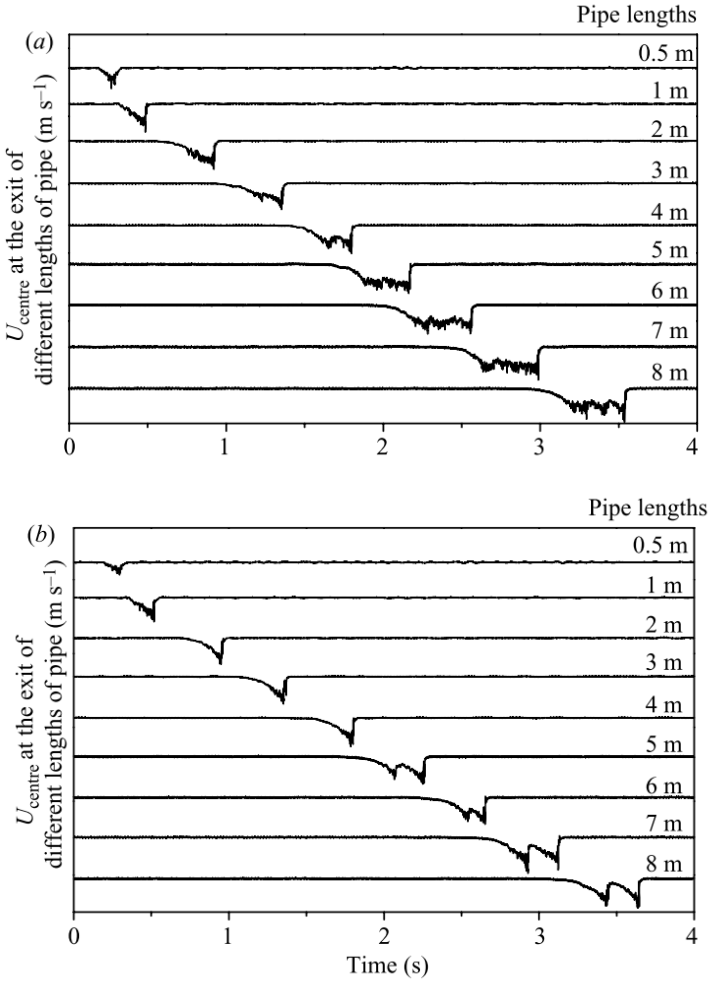

Figure 1.2: Development of turbulent puffs at (a) Re = 2680 (b) Re = 2495 for different pipe lengths [3]

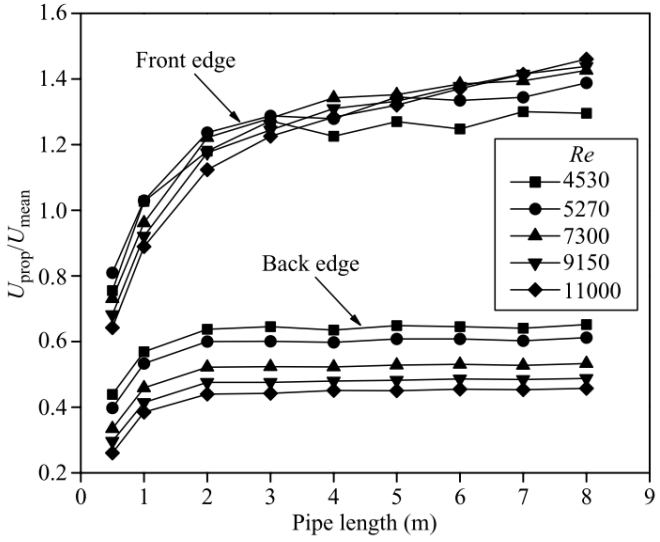

Figure 1.3: Propagation velocities of typical slugs along the length of the pipe. The propagation velocity of the slugs was normalized with the mean velocity of the bulk flow. The higher velocity of the front edge indicates the expanding nature of slugs [3]

The propagation velocity of the front and back of slugs are shown in figure 1.3. The propagation velocities of the slugs are normalized with the mean velocities of the bulk flow. It can be seen that the leading part of the slugs advect at velocities greater than the trailing edge and therefore, the slugs merge with others in the upstream direction and fill the pipe with turbulence completely. The figure 1.4 shows the development of slugs triggered at different time intervals at Re = 4200.

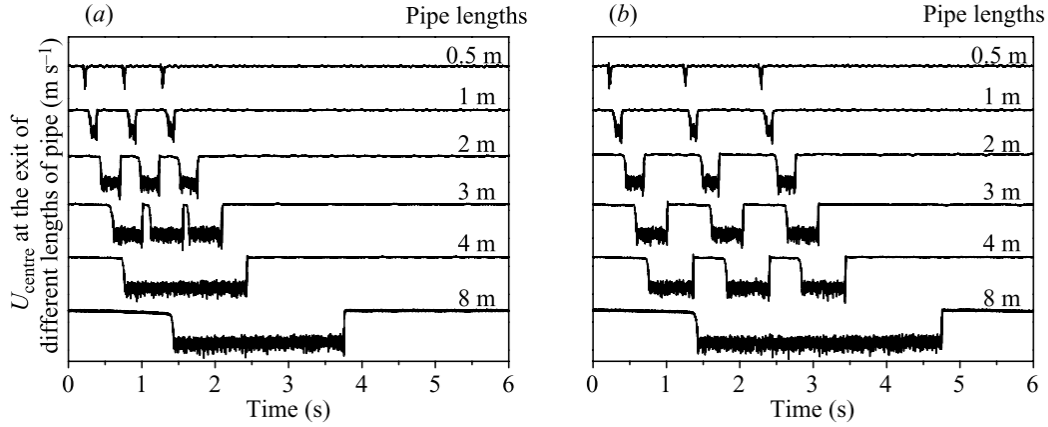

Figure 1.4: Development of slugs along the pipe length showing the merging phenomena at Re = 4200 when the flow was perturbed at an interval of (a) t = 1s (b) t = 1.5s [3]

1.1.4. Relevant dimensionless numbers

The current section describes the relevant dimensionless numbers used for the experimental campaign. These dimensionless numbers make it possible to compare the findings from this work with the literature and draw meaningful inferences. The first dimensionless number to be visited is the Reynolds number as formulated in equation 1.3. The Reynolds number is significant because of it can be used to compare flow in different length-scales and fluids with different physical properties.

$$Re = \frac{\rho u D}{\mu} \tag{1.3}$$

The current work uses the Moody diagram extensively for studying transition phenomena. The diagram plots the variation of friction factor with Reynolds number. The friction factor, as given in equation is a non dimensional form of pressure drop for a given flow condition. The Δp measures the pressure drop across a given length of tube which is then normalized by the dynamic pressure in the denominator.

$$f = \frac{\Delta p}{\frac{1}{2}\rho u^2 \frac{L}{D}} \tag{1.4}$$

The study involves the impact of particles in transition behavior in flow. The particle size is normalized with the diameter of the pipe in order to compare with other studies from the literature.

1.2. Structure of report

The report proceeds with a review of research performed towards transition behavior in single phase and multi-phase systems in chapter 2. It also encompasses the work done to analyse different perturbation systems. Chapter 3 continues by explaining the experimental setup used for performing the experiments and the methodology used by the measurement systems used in the setup. The results are discussed in chapter 4 and inferences are drawn based on them. Finally, chapter 5 summarizes the results and conclusions are drawn as well as recommending some possible research areas for the future. The appendices contain some important information like calibration of pressure sensor, estimation of particle size and density along with Moody chart for multi-phase flows. The procedure followed during the experimental campaign is also provided in the Appendix before mentioning the list of references.

2

Overview of previous research: A Literature review

The current chapter provides information about previously conducted numerical and experimental studies that are relevant to transition in multi-phase pipe flows. The section 2.1 explains the results of relevant research and its impact on current study. The section 2.2 points out the gaps in available research literature and list out the goals of this current thesis.

2.1. Literature review

Reynolds [24] performed his landmark experiment and found that the flow became unstable after certain flow rates and also the fact that the transition flow rate varied if the inlet disturbances were varied. The research on transition to turbulence then focused on stability of flows at relatively lower Reynolds number. The study performed by Wygnanski et al [23] analyzed different experimental settings to study the fluctuations in the transition regime. Different types of perturbation devices triggered transition at different Reynolds numbers. The article suggested that the transition between the laminar and turbulent flows at the beginning and end of a turbulent patch was abrupt relative to its duration. The fluctuations were indeed confirmed to be pockets of turbulence by comparing the velocity data at two different Reynolds numbers, namely, 4200 and 50000. It was also observed that the turbulent puffs do not grow with distance of the pipe while slugs grow in the order of the bulk velocity of the pipe. Furthermore, the article suggested that, puffs are the result of growing disturbance propagating from the inlet section, the slugs seem to be the product of transition in the developing boundary layer downstream of entrance.

The packets of turbulence (*puffs* and *slugs*), as mentioned earlier, have slightly different characteristics. The turbulent signatures called *puffs* exist when the Reynolds number was below 2600 while *slugs* are found after that Reynolds number [25]. The study used injection mechanism to perturb the flow and explained the development of the disturbances using travelling wave solutions. The advection velocities of slugs and puffs were recorded in the study. Similar study was performed where puffs were reported to be observed for $Re < 2300$ while slug formation occurred for $Re > 3000$ [3]. The puffs have a slow trailing edge and sharp interface while slugs have sharp interfaces at both edges and travel at a speed slightly higher than the bulk flow. The puffs split as they advect with the flow as shown by Mukund et al [4]. The interactions between the puffs maintains balance between decay and splitting and thus maintaining the intermittency in the flow. Although the interaction has an effect on the nature of the transition, it has little bearing on the critical point of transition.

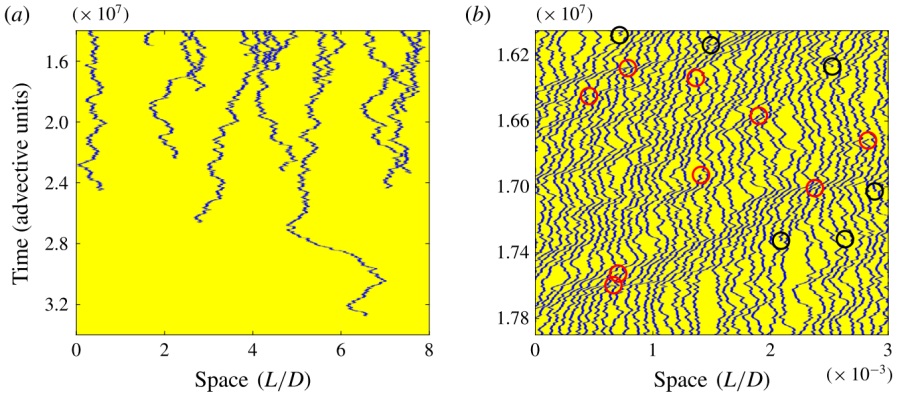

Figure 2.1: Splitting and decay of puffs observed by Hof et al [4]. Space–time plots with the puffs shown in blue on a yellow laminar background. (a) Portion of a space–time plot for Re = 2020, where all of the puffs eventually decay. (b) Portion of a space–time plot under a statistical steady-state condition for Re=2060. Splitting and decay events are marked with red and black circles respectively

Quantitative measurements of lifetime of turbulent puffs were conducted based on accurate pressure drop measurements combined with laser doppler anemometry [5].The characteristic lifetime is calculated based on the lifetime probability of puffs. The pressure drop was measured between 125 D and 250 D from pipe inlet. The figure 2.2 shows the pressure signal of a stable and decaying puffs. The black and grey threshold lines are used to determine the point of decay and disintegration of the puff respectively. The rise in the pressure drop in the surviving puff (illustrated by black line) is due to the local deceleration of bulk velocity of the turbulent puff near the first sensor. This signaled the entry of the puff. The pressure drop reduces sharply as the puff passes through the second sensor due to increase in the flow velocity resulting in a sub-laminar pressure drop.

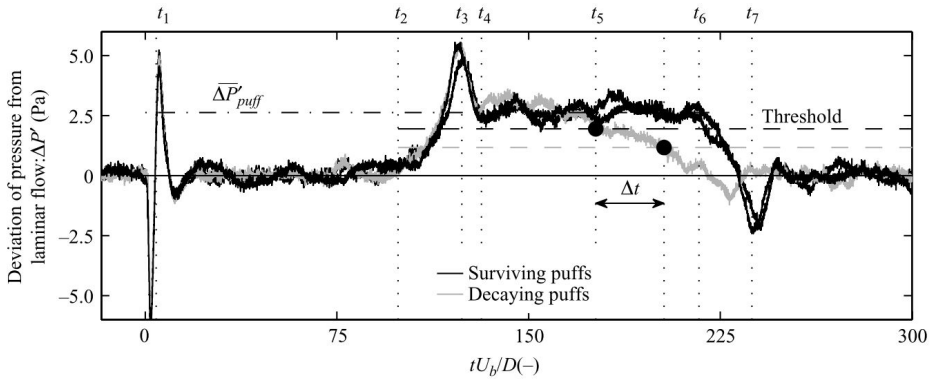

Figure 2.2: Instantaneous time series of pressure drop recorded across 125 D. The black line shows a stable puff while the grey line shows a decaying puff at Re = 1822. Figure is reproduced from Kuik et al. [5]

The experiment conducted by Cerbus et al [6] concurred with the range of Reynolds number for the occurrence of puffs and slugs. They characterized the puffs by measuring the radial velocity at the centreline and observe fluctuations of an identifier function based on this parameter. The friction factor of the turbulent patches are indeed equal to the friction factor corresponding to turbulent flow regime. It is evident that the puffs are patches of turbulence and intermittent in nature, yet, there is no method to calculate intermittency for a given Re. Therefore, intermittency remains a parameter that could be calculated from the results but not estimated for a given Re before the experiment was performed. Their plot of friction factor is shown in the figure 2.3.

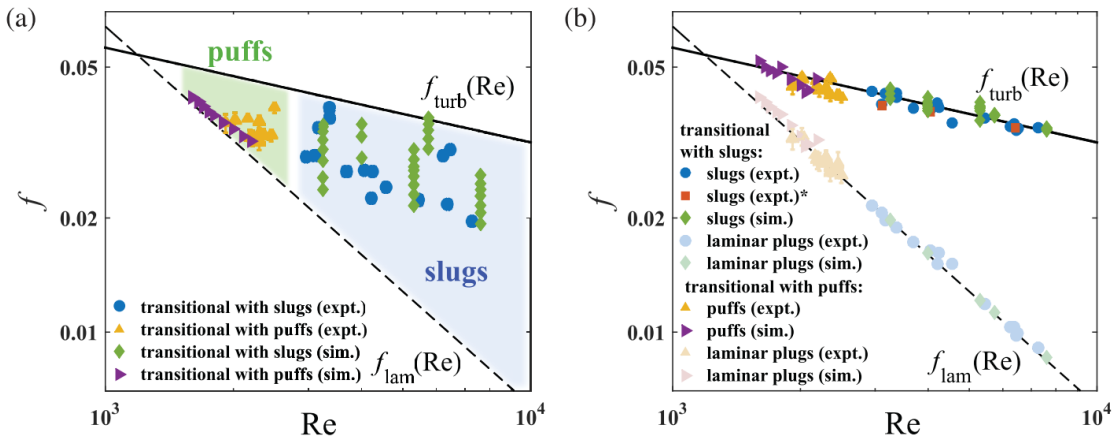

Figure 2.3: Experimental and numerical estimation of friction factor for transitional regime of the flow (a) shows the friction factor having contributions from laminar and turbulent patches (b) shows the values of friction factor after disentangling them. Figure reproduced from Cerbus et al. [6]

Avila at al [7] studied the onset of turbulence using experimental and computational techniques. In their previous research, they identified that a sustained disturbance of large amplitude could not induce turbulence for lower Reynolds number (Re ≈ 2000). Therefore, they injected water jets to induce single turbulent puffs for each Re. They understood that the puffs, beyond their initial formation time, are memoryless and the probability of splitting does not depend on the age of the puff. They confirmed that the probability of splitting downstream increases with Re as shown in figure 2.4.

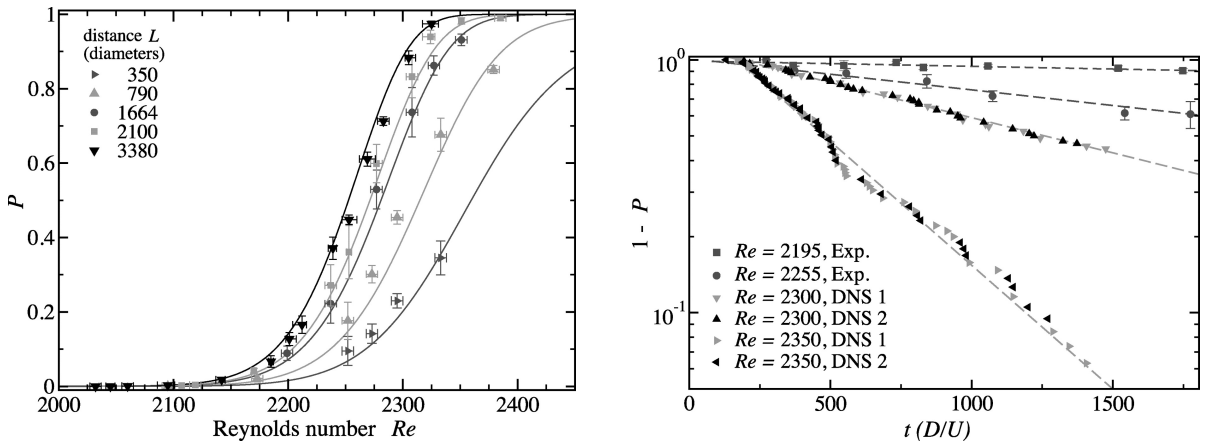

(a) Probability of puff splitting

(b) Probability of puff survival

Figure 2.4: (a) Probability of the puff to split after travelling a distance L with the error bars indicating 95% confidence level. (b) Probability for the puff to survive after some non-dimensional time which are collected at fixed locations and converted to time units with propagation speed of the puffs. Figure reproduced from Avila et al. [7]

2.1.1. Perturbation mechanism

There are many methods through which finite amplitude disturbances can be induced in the flow to trigger turbulence. The detailed study conducted by Durst et al [26] studied the effect of obstacles like perturbation ring and electronically controlled iris diaphragm (shown in figure 2.5) and compared the results to transition without any external disturbances. The transition occurred at $Re = 13000$ without using any flow perturbation mechanisms. The transition involved slug like disturbances interspersed between laminar plugs. They also observed that the transition started from the inlet which required further investigation. The transition to turbulence occurred over a finite range of Reynolds number when an obstacle was used. The critical Reynolds number decreased with increasing obstacle height and they were able to identify a non-dimensional height based on wall friction velocity and viscosity of the fluid using dimensional analysis. The non-dimensional height used in the article is given in equation 2.1.

$$h^* = \frac{hU_\tau}{\nu} \tag{2.1}$$

where h is the height of the obstacle, U_τ is the wall friction velocity and ν is the kinematic viscosity. Also, the laminar - turbulent transition occurs over a small range of Re. While the current setup was reliable in creating transition at a specified Re, it was unable to control the occurrence of puffs or slugs. It was for this reason they used an electronically controlled diaphragm. A solenoid valve was used to actuate the diaphragm at the required frequency. The height of the iris diaphragm was adjusted using calculations performed for static ring obstacles. It was also observed that the turbulent slugs were identical to the ones that were generated with the ring type obstacle.

The research conducted by Hof et. al. [27] formulated a scaling law between the amplitude of perturbation and Reynolds number. The flow was perturbed by a single box car pulse of fluid through a ring of six equally spaced 0.5 mm holes. The injection was controlled by high speed solenoid valves and the quantities of water injected were in the range of 0.01 % to 0.1 % of the total volume flux. The scaling law formulated from the experiments is given in equation 2.2.

$$A = O(Re^{-1}) \tag{2.2}$$

The experiments carried out by Mullin et. al. [28] compared the single jet injection with injection/extraction mechanism as shown in figure 2.6. Flow visualization was performed to understand the growth and decay of disturbances at different perturbation amplitudes. The study also compared the visualization of perturbations at two different amplitudes to study the decay and growth of puffs by injection and suction mechanism. It was found that the amplitude required for suction type perturbation was two orders larger than that of injection perturbation system.

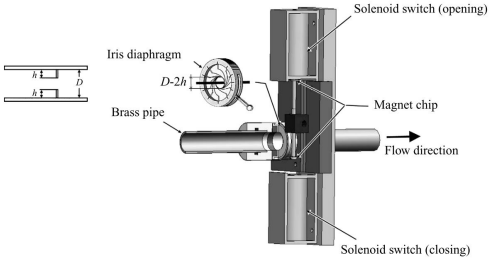

Figure 2.5: Three dimensional representation of electronic diaphragm used to trigger transition. Figure reproduced from Nishi et al. [3]

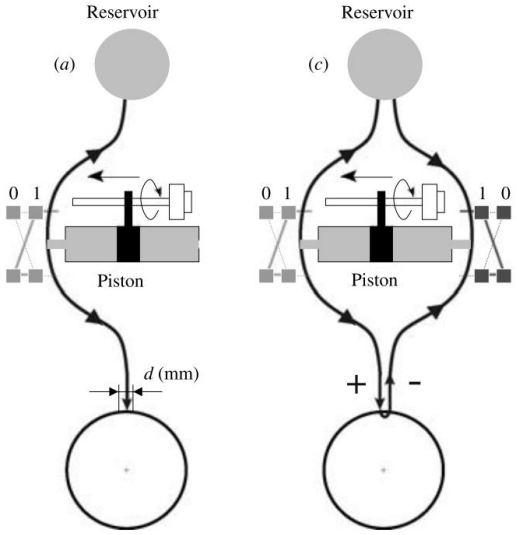

Figure 2.6: (a) Injection perturbation mechanism along with (b)zero net mass system where fluid is injected and extracted simultaneously. Figure reproduced from Mullin et al. [8]

The research performed by Willis et. al. [29] reproduced the scaling relationship between the amplitude of perturbation and Reynolds number mentioned earlier [28]. The experiment also conducted a lifetime study of puffs before they relaminarized. It was concluded that a turbulent puff can be sustained for Reynolds numbers greater than 1750.

Laminar flow could be observed upto a Reynolds number of 23000 in the research conducted by Peixinho and Mullin [8]. They compared two types of disturbances, namely, single jet disturbance and push-pull disturbance. The single jet disturbance, as the name suggests, injects water through a hole with predetermined constant mass flux for a specific amount of time. The push-pull disturbance injects and removes equal quantity of water for specific amount of time through holes in different locations. The volume flux of water was

around 0.0001 % - 0.1 % depending on the Reynolds number. The effect of the hole diameters were also studied. It was found that using multiple jets (six in azimuthal direction) required lower amplitude of perturbation (a factor of two) when compared to perturbing with a single jet. Also, the push-pull configuration reduced the amplitude of perturbation by an order of magnitude when compared to single jet perturbation. Figure 2.7 shows the relation between the perturbation required corresponding to each Re and compares the amplitude of the single jet data to push-pull disturbance.

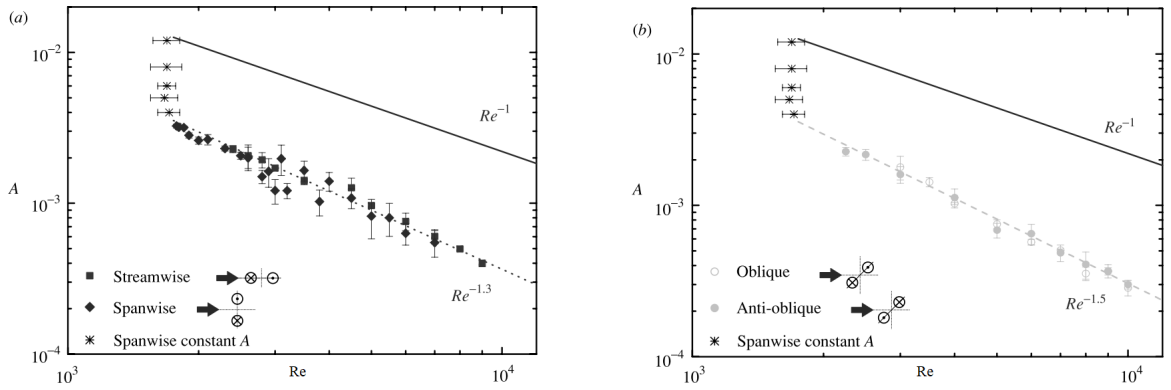

Figure 2.7: (a) shows the scaling law for push-pull disturbance aligned in stream wise and span wise directions (b) shows the scaling law for push-pull disturbance, aligned in oblique and non-oblique directions, compared with single jet disturbance. Figure reproduced from Mullin et al. [8]

As it has been made clear that there are different methods to trigger turbulent puffs, it is important to understand the impact of these mechanisms on the puffs themselves. The research conducted by De Lozar et al [9] compared the effects of different types of perturbation on parameters like survival probability of puffs, advection velocity of puffs etc. Four different types of perturbation were compared and the survival or decay of the puffs after a time t was studied based on the angle of outflow at the pipe exit. The perturbation systems used were single jet injection, injection and extraction of fluid, reduction of Re and static obstacle. The method of Reynolds number reduction is one where a puff was created at higher Re and after the puff has propagated a certain distance, the Reynolds number was reduced by 150 (ΔRe = 150). This was made possible by using pipes of two different diameters in parallel connection and blocking flow through the larger pipe so that the pressure drop increases for the segment with smaller diameter resulting in reduction of Re. The figures 2.8 and 2.9 show the statistics recorded for the puffs generated by single jet perturbation method.

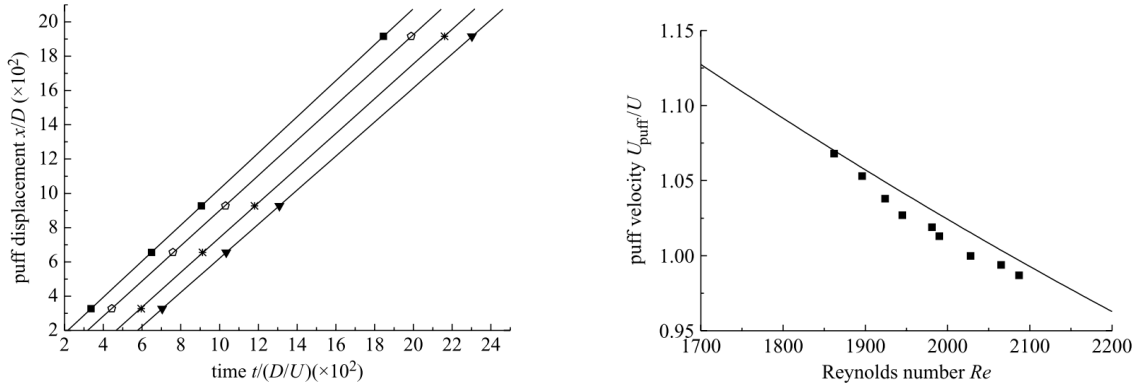

Figure 2.8: (a) Space travelled by puffs after a time t. The data for Re=1896 is unaltered while the others are shifted by 100D/U on the time axis. Square, Re=1896, U_{puff}=1.053; pentagon, Re=1945, U_{puff} = 1.027; asterisk, Re=1990, U_{puff} = 1.013; down triangle, Re=2065, U_{puff} = 0.994. (b) Non dimensional propagation velocities of turbulent puffs. Figure reproduced from De Lozar et al. [9]

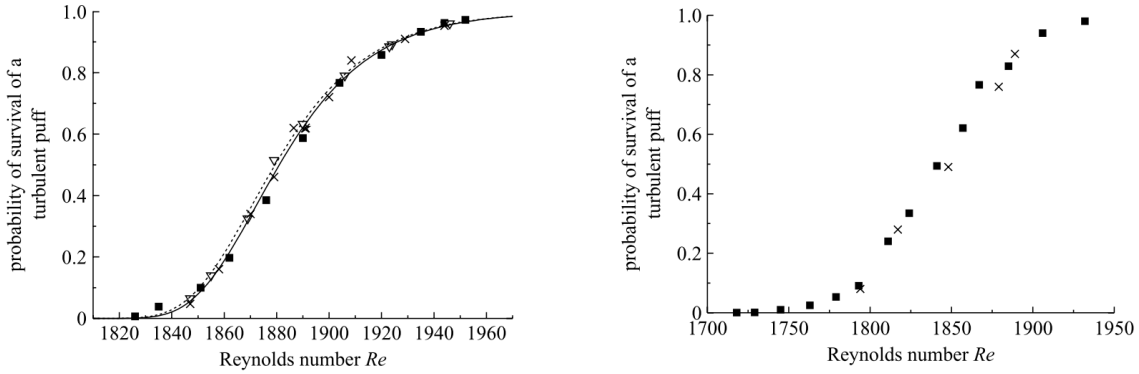

Figure 2.9: (a) Survival rate of puffs for an observation time/distance of 933D. Square, injection; cross, injection/extraction; down triangle, decreasing Re; star, obstacle. (b) Survival rate of puffs at 269D from the perturbation point. Square, injection; cross, injection/extraction. Figure reproduced from De Lozar et al. [9]

Over 7500 experiments were were carried out for plotting figure 2.9. Their research concluded that the decay statistics of the puffs are identical for all disturbance mechanisms. The collapse of all data sets to the single curve suggests that the method of perturbation has an insignificant effect on the behaviour of the puffs generated.

2.1.2. Multi-phase flows

One of the seminal studies made in this field was by Matas et al [10]. The objective of the study was to study transition of neutrally buoyant particle laden pipe flow and relate it to the particle size and concentration. A ring type perturbation was used to create transition at Re $\approx$ 2100, while a pressure transducer was used to obtain pressure drop spectrum for characterizing transition. The point of transition was identified based on frequencies observed in the pressure drop spectrum. The gravity driven flow does not have any peak frequency, unlike pump driven flow where a peak at pump frequency and its associated harmonics can be observed. The Reynolds number was calculated once the intermittency threshold was reached. The figure 2.10 shows the pressure spectrum and the critical Reynolds number with corrected viscosity. The viscosity was corrected for presence of particles using Krieger's viscosity correction as shown in equation 2.3. The equation is obtained based on rheological experiments performed with mono-disperse polystyrene lattices. The relation between viscosity and concentration is formulated by fitting data of viscosity with volume fraction between 0.01 and 0.5. $\phi_m = 0.68$, is the random close packing concentration for spherical particles when the relative viscosity approaches infinity. However, it should be noted that the value of random close packing efficiency is reported to be 0.64 in other literature [30].

$$\frac{\mu_{adj}}{\mu_0} = (1 - \phi/\phi_m)^{-1.82} \tag{2.3}$$

In case of smaller particles, (D/d $\geq$ 65), the critical Reynolds number remains largely unchanged for different concentration when compared to pure fluid. The study suggested that there is an additional mechanism for dissipation. For larger particles, (D/d $\leq$ 65), the critical Reynolds number decreases till a certain volume concentration was reached after which the transition was delayed. Also the minima of the critical Reynolds number were lesser for larger particles. One more interesting observation from their experiments was that the sub-critical transition is triggered by the particles as they can replicate the curve without the use of perturbation devices.

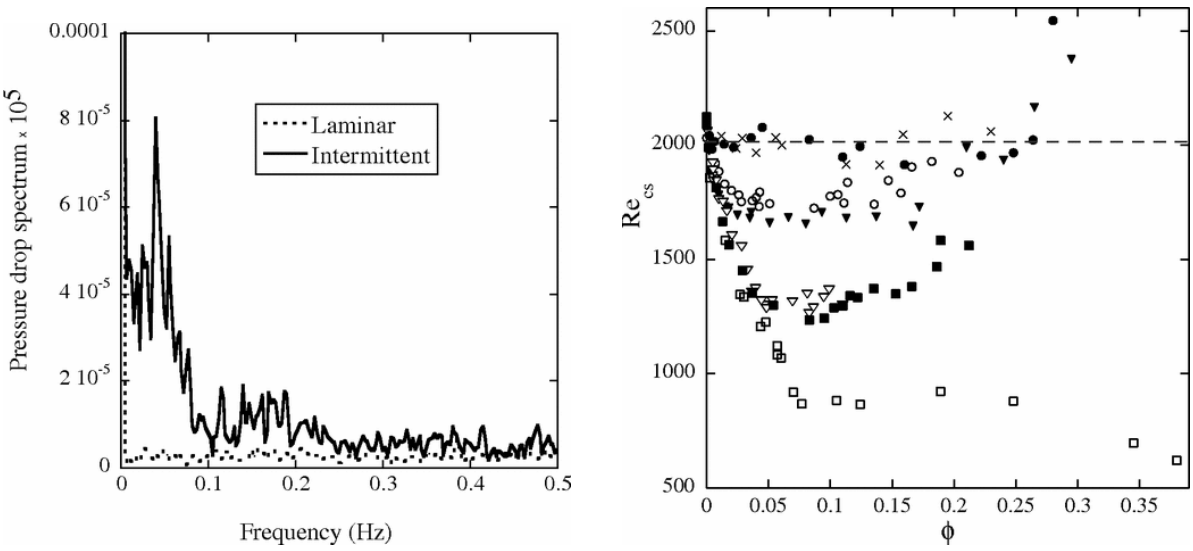

Figure 2.10: (a) Pressure drop spectrum for laminar intermittent flow regime for volume fraction of ϕ = 0.1. The zero frequency value of the spectrum relates to the mean pressure drop is much larger ans not represented in the graph. (b) Critical Reynolds number after correcting for viscosity. Tube $D_1(8mm)$ with d = 215 μm (◯), 510 μm (▽), 780 μm (□). Tube $D_2(14mm)$ with d = 40 μm (×), 215 μm (•), 510 μm (▼), 780 μm (■) Figure reproduced from Matas et al. [10]

.

Since the addition of particles changes the viscosity of the suspension and thereby the parameters reliant on it, it is prudent to understand the rheology of suspensions. One such research was performed by Boyer et al [11]. The objective of this particular study was to understand rheology of dense suspensions from the hydrodynamic viewpoint and contact interactions in suspensions. The rheology of suspensions is governed by a single control parameter called the *non-dimensional viscous number*. It is given by equation 2.4.

$$I_v = \frac{\eta_f \dot{\gamma}}{P^P} \tag{2.4}$$

where $\dot{\gamma}$ is the strain rate, η_f is the fluid viscosity and P^P is the particle pressure. When a suspension is sheared at a constant volume fraction, shear and normal stresses scale viscously i.e. $\propto \eta_f \dot{\gamma}$ and can be expressed with $\eta_s(\phi)$ and $\eta_n(\phi)$ which are dimensionless effective shear and normal viscosity.

$$\tau = \eta_s(\phi)\eta_f \dot{\gamma} \tag{2.5}$$

$$P^P = \eta_n(\phi)\eta_f \dot{\gamma} \tag{2.6}$$

The experimental setup of Boyer et al consisted of an annular shear cell with the suspension confined between a truncated cone and a rotating annulus. The particles were large and neutrally buoyant, thereby eliminating Brownian motion and colloidal effects from gaining importance. The value of friction coefficient tend to a constant value at vanishing viscous number and increased for increasing I_v. In contrast to dry granular rheology, the value of μ does not saturate at large I_v. The maximum value of volume concentration is obtained when ϕ is plotted against I_v which closely matches with the values reported in studies that used dry granular media. The figure 2.12 shows the relationship between effective shear and normal viscosity with volume fraction. Scaling laws for friction factor, viscosity and volume fraction were proposed as result of this study. It should also be noted that the scaling law for viscosity agrees with the Krieger formulation mentioned previously. This can be seen from figure 2.12 along with the experimental setup in figure 2.11.

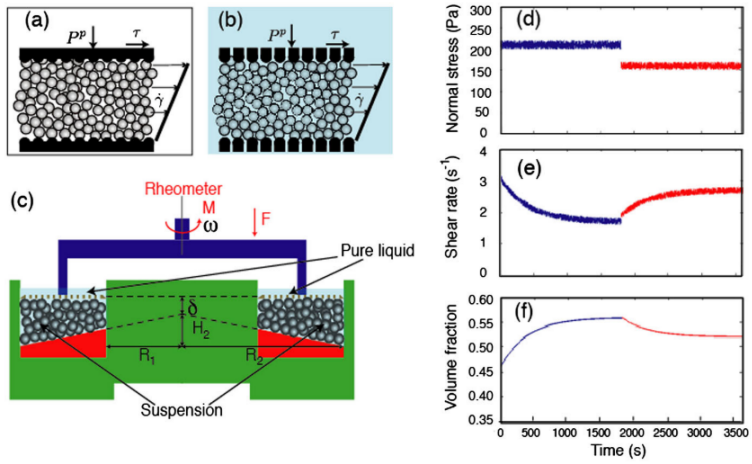

Figure 2.11: Paradigmatic configuration of (a) dry and (b) immersed granular media. (c) shows the experiment setup used by Boyer [11]. (d) and (e) show the variation of shear rate and volume fraction respectively in response to change in (d) applied normal stress. The shear stress τ is constant and is set to 150 Pa.

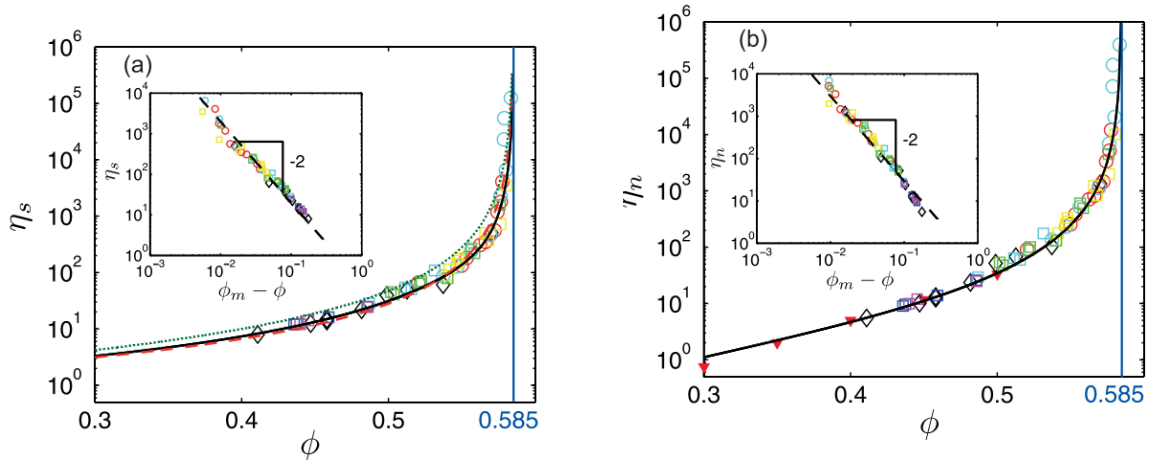

Figure 2.12: Effective (a) shear and (b) normal viscosities versus ϕ. (a) Empirical correlations of Eilers (red dashed line) and Krieger-Dougherty (green dashed line). (b) particle-pressure measurements (red down-triangles). Insets: logarithmic plots of η_s and η_n versus ϕ_m - ϕ. Figure reproduced from Boyer et al. [11]

.

Another important study on rheology was performed by Lashgari et al [12]. The analysis was based on data from numerical simulations of channel laden with rigid neutrally buoyant particles. The numerical code coupled an uniform Eulerian mesh for fluid phase with a Lagrangian mesh for solid phase along with use of periodic boundary conditions in streamwise and spanwise directions. The flow was perturbed by streamwise vortices. Root mean square values of streamwise velocity fluctuations were used to characterize transition of flow to turbulent regime. While a threshold was identified for transition when the volume fraction is negligible (ϕ = 0.001 %), it was very difficult to do so for high volume fraction (ϕ = 30 %). This was attributed to the continuous background disturbance due to presence of particles.

The figure 2.13a shows the plot of RMS value of streamwise velocity fluctuations over time for two different particle concentrations. The presence of particles creates continuous background disturbances such that the threshold of sustaining turbulence decreases to 1750 < Re < 2000. But, the velocity fluctuations rise gradually in case of ϕ = 0.3, thereby making the point of transition very sensitive to the threshold value. Also the peak value of the fluctuations seems to be lesser when the volume fraction was higher. Figure 2.13b shows map of velocity fluctuations of flow and particles obtained by ensemble averaging. The threshold 0.07 suggests a non-monotonic behaviour of transition Reynold number. The regions marked with letters a, b and c are

labelled as laminar-like, inertial shear thickening and turbulent-like regimes.

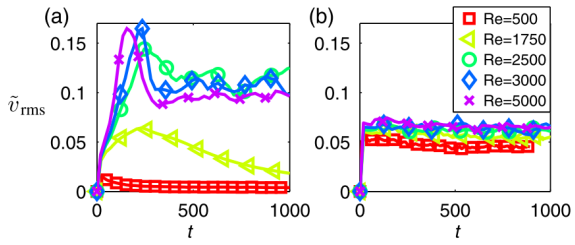

(a) RMS value of streamwise velocity fluctuations for different particle concentrations

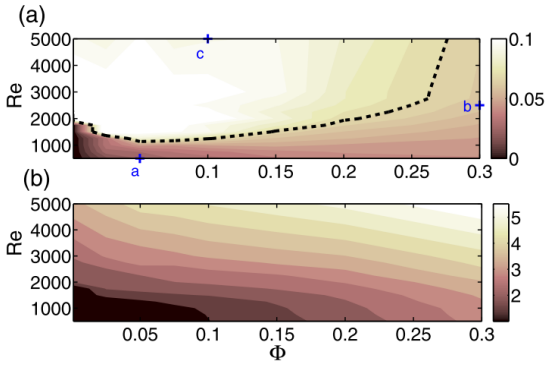

(b) (a) Map of velocity fluctuations for different Reynolds number and particle concentrations (b) Relative viscosity (ν_r) in (Re, ϕ) plane using 96 data points from simulations

Figure 2.13: Velocity fluctuations and flow regime map showing the influence of addition of particles on transition behaviour and difficulty in identifying threshold for transition. Figure reproduced from Lashgari et al.[12]

Upon investigating this further using the momentum budget to understand contribution from different stresses, as shown in figure 2.14a, it is evident that the viscous stress dominates the laminar-like regime when compared to Reynolds shear stress and particle stress. Also Reynolds shear stress dominates both viscous stress and particle stress which was typical of turbulent regime. The particle stresses dominates in the inertial shear thickening regime and contributed to over 78% of the momentum transport. This stress is particularly higher near the wall due to particle migration and rise in mean local concentration. The turbulent stress dominates near the centre suggesting that the momentum transport is done by the fluid. Figure 2.14b shows the region of existence of the three regimes described above. The black lines in the contour map indicate when the term is over 50% in the stress budget. The transition between laminar and turbulent regime is straightforward when $\phi \longrightarrow 0$ and it is dependant on the threshold value set for the velocity fluctuations for finite values of ϕ. At $\phi = 0.3$, the relative viscosity increases smoothly which can be attributed to the increase in particle-induced stress. The behaviour suggests that in dense cases the inertial shear thickening may prevent the transition to a fully turbulent regime at arbitrary high speed of the flow.

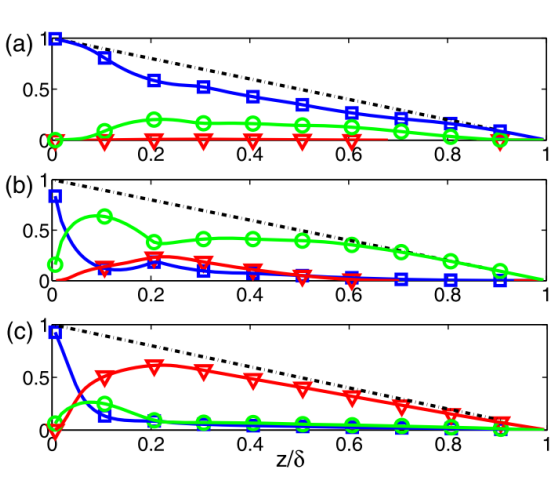

(a) Momentum budget showing the contributions of different stresses based on particle concentration. Red triangle represents Reynolds stress; blue square, viscous stress; and green circle, particle stress

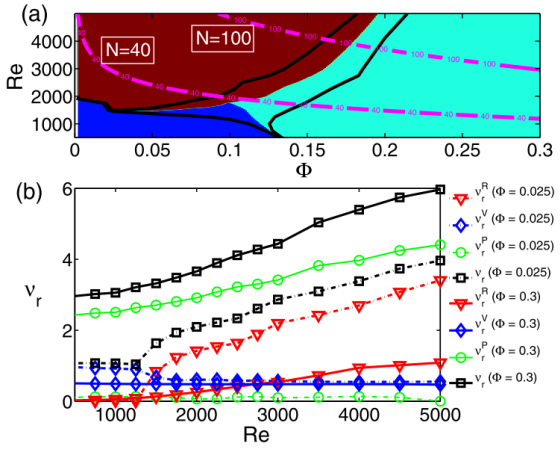

(b) (a) Flow regime map based on particle concentration in Re - ϕ plane (blue, red, and green colors indicate laminar-like, turbulent-like, and inertial shear-thickening regime). (b) Contribution to total wall friction (no superscript) from viscous stress (superscript ν), particle stress (superscript P) and Reynold stress (superscript R)

Figure 2.14: Momentum budget and contribution of different types of stresses are used to construct the flow regime map. Figure reproduced from Lashgari et al. [12]

A numerical study was performed by Yu et al [13] to understand the effect of large neutrally buoyant particles on transition. Their study was divided into two parts where the first section concerned study of particle induced flow instability while keeping the pressure gradient constant. The second part involved examining the effect of particles on the critical Reynolds number based on mean velocity when the mass flux is maintained constant. The presence of particles disturbs the smoothness of the flow even at low Reynolds number and thus makes it difficult to predict the flow regime. They used the energy of streamswise velocity fluctuations as indicator of transition in flow. This parameter is set based on size of streamwise vortices generated. The decision on the threshold is made by monitoring the values of fluctuation energies. The formulation of E is given in equation 2.7,

$$E(t) = \int\int\int [u_z'(x,y,z;t)]^2 dxdydz, \tag{2.7}$$

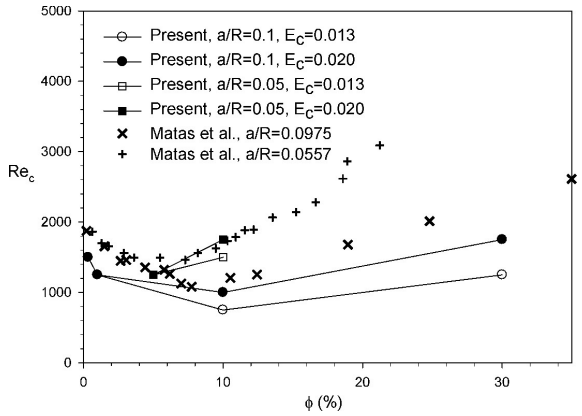

Figure 2.15: Critical Reynolds number plotted as a function of particle concentration for a/R = 0.1 and 0.05, where *a* indicates the particle size which is normalized by the pipe radius. The results obtained by characterizing transition using streamwise energy fluctuations agreed with the results produced by Matas et al. [10]. Figure reproduced from Yu et al. [13]

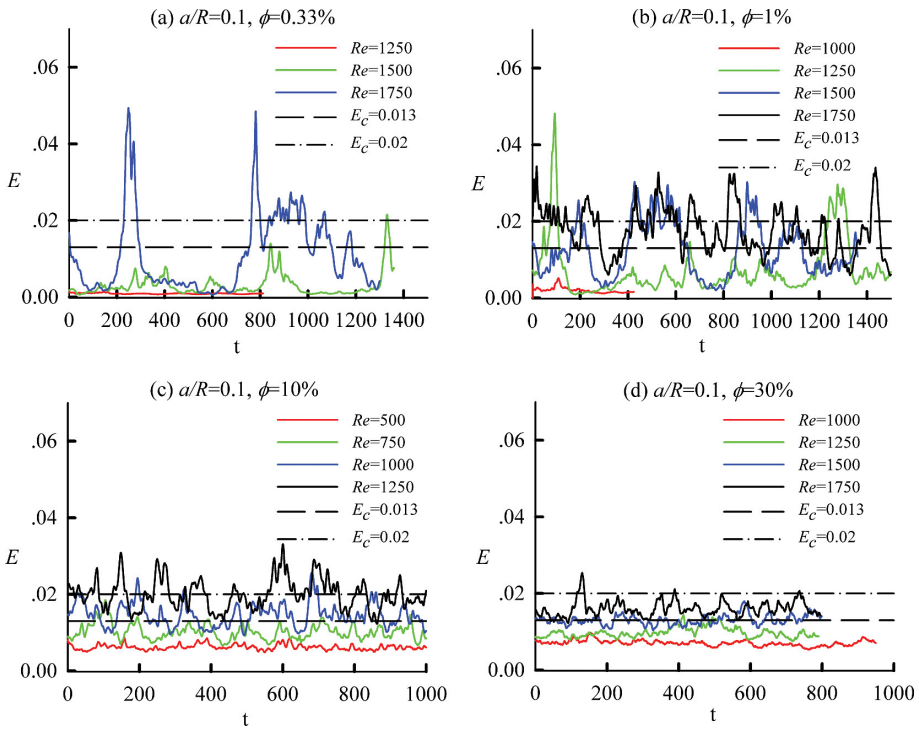

Figure 2.16: Fluctuation parameter for different volume fraction and Reynolds number for a/r = 0.1 where a is the radius of particle and R being the radius of the tube. Figure reproduced from Yu et al. [13]

It can be observed from the figure that the length-scale of the largest streamwise vortices are smaller than the particle size for E < 0.013. Thus E = 0.02 was chosen as the upper critical value as there was strong spatial intermittency. The findings agrees with the experimental results from Matas et al [10]. However the article does not offer an explanation for the reduction in critical Reynolds number for increase in particle concentration. One possibility suggested by the paper was that the drag and pressure drop increase for higher particle concentration, and consequently more energy was injected into the system. The fluctuation parameter for different Reynolds number and particle volume concentration is shown in figure 2.16. The variation of critical Reynolds number for particle concentration are shown in 2.15 which agree well with Matas et al [10].

One of the more recent experimental research was performed by Agarwal et al [14] where impact of particles on transition was studied in pipe flows. Particles used were $1/20^{th}$ of the pipe diameter and the flow was driven by piston to ensure constant mass flux. Figure 2.17 shows the pressure fluctuations for different volume fractions. There is a sharp peak in the pressure fluctuations for case with $\phi = 0$ while the peak reduces and the curve becomes smoother as the particle concentration increases.

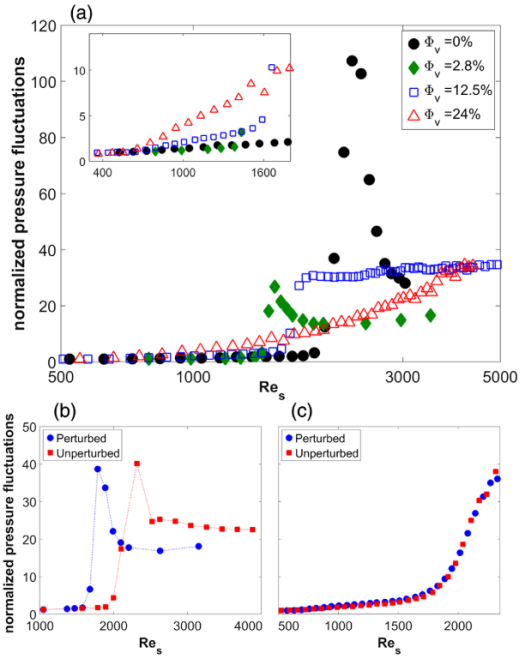

Figure 2.17: Pressure fluctuations for different volume concentrations and comparison for hysteresis in perturbed and unperturbed flow. Figure reproduced from Agarwal et al. [14]

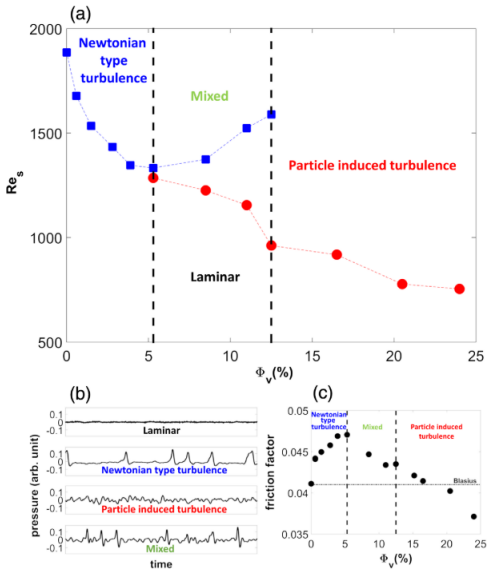

Figure 2.18: Critical Reynolds number and pressure signal for different flow regime over time. Figure reproduced from Agarwal et al. [14]

The report agreed with the results from Matas et al [10] and observed no spatio-temporal intermittency at any Reynolds number for ϕ = 12.5 %. Also the article reported that the transition showed hysteresis at lower particle concentration while the same was non-existent at higher concentrations (ϕ = 16 %). It shows that turbulence is triggered with or without continuous perturbation pointing towards the particle induced turbulence. This has been reaffirmed by figure 2.18 where a plot of suspension Reynolds number is plotted against particle concentration. The 'Newtonian-like' regime has abrupt transition where the initial perturbation was critical to transition and the volume fraction (ϕ) is less than 5%. For 5 < ϕ < 12.5 %, the fluctuations increases globally and there is a secondary transition beyond a certain Re_s where spatially intermittent puffs appear on top of fluctuating background flow. For ϕ > 12.5 %, the flow becomes turbulent gradually without intermittency or hysteresis. It is also observed that the friction factor is a non-monotonic function of Reynolds number.

Lastly, the current work is related to the experiments performed by Hogendoorn and Poelma [15], where a similar study effect of neutrally buoyant particle on transition in pipe flow was investigated. The particle diameter was 1/19 of the pipe diameter and the flow was gravity driven. The experiment used Ultrasound

Image Velocimetry (UIV) to examine the velocity field. It was calculated by cross-correlation of location of tracer particles obtained through echography. The spatial resolution was found to be adequately small compared to the length scale of typical turbulent puff.

The paper characterized transition based on the friction factor of the flow regime. The flow was considered to be in transition when the friction factor deviated from the Poisuelle law by 10%. Figure 2.19a shows the Moody diagram and it can be seen that the transition behaviour changes for increasing volume fraction. The sharp jump in friction factor observed for volume fractions below 14% is absent for the case of ϕ = 17.5% where a smooth change in f is observed for increasing Reynolds number. The minimum of transition Reynolds number is reported as 1350 at ϕ = 8% which agreed with the results from Matas et al [10] and Yu et al [13]. To further understand the transition behaviour, UIV was used to observe the intermittency as shown in figures 2.20 and 2.21. The results are semi-qualitative in nature as the eddies below the size of particles are lost and only the location of the particles can be tracked with UIV. The intermittency is obtained from equation 2.8 which is formulated in the article from Cerbus et al [6].

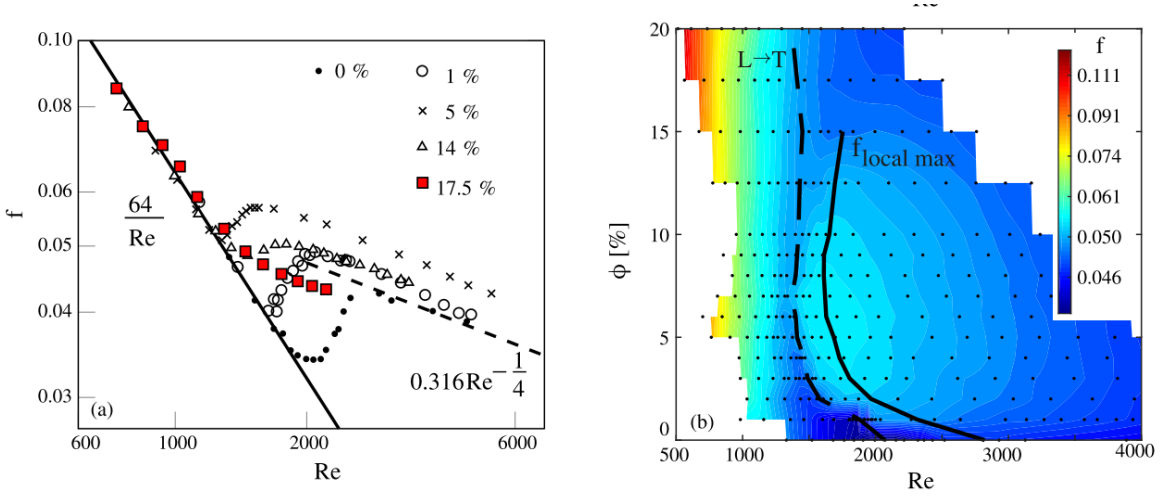

(a) Moody chart for particle concentrations. Sub-critical transition was observed for particle concentrations less than 14 % while super-critical transition was observed for higher concentrations

(b) Point of transition for different volume fractions. The points are individual measurements. The transition Reynolds number decreases for lower concentrations suggesting earlier onset of transition

Figure 2.19: Moody chart and transition behaviour for different particle concentrations. Figure reproduced from Hogendorrn et al. [15]

$$f = \gamma f_{puffs} + (1-\gamma) f_{lam}, \tag{2.8}$$

The figure 2.20 shows origin of puffs by superimposition of the centerline velocity to form a saw tooth shape which are typical puff signatures. The puffs start to appear at more locations and then the flow becomes fully turbulent when γ = 1. From these observations, the effect of the particle is the early onset of transition although there is no change in the physical mechanism.

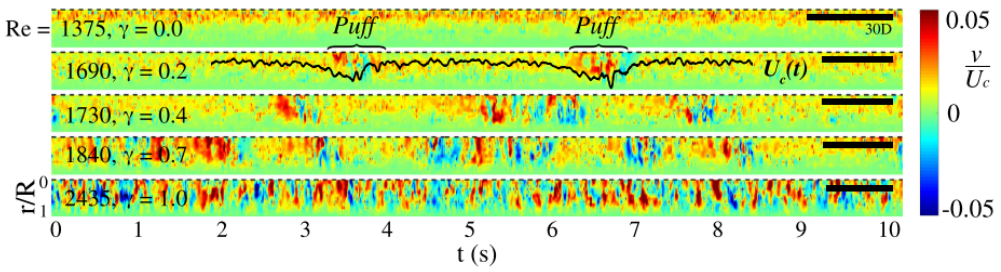

Figure 2.20: Intermittency of flow obtained from pressure signal at different Reynolds number for ϕ = 1%. Only the top half of the pipe is shown. The radial direction is normalized with pipe radius and the radial velocity with centerline velocity. Figure reproduced from Hogendoorn et al. [15]

But the same cannot be said for case of ϕ = 14% where distinct structures can be observed for Re = 760 throughout the pipe section. These fluctuations grow with increasing Reynolds number suggesting a different mechanism for transition to turbulence. Here the intermittency parameter only suggests the relative position between laminar and turbulent friction factor curves. The nature of transition is different for the two particle concentrations suggesting a gradual change in transition behaviour. Two mechanisms are hypothesized to explain the transition behaviour: (a) puff splitting and (b) local disturbance by particles triggering super-critical transition.

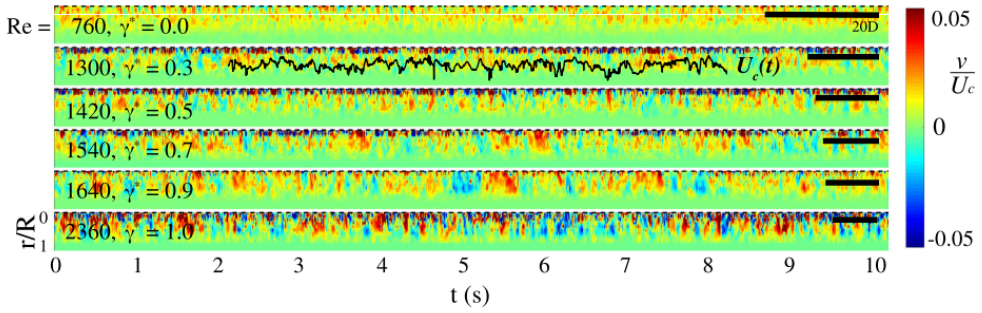

Figure 2.21: Radial velocity data obtained from pressure signal at different Reynolds number for ϕ = 14%. Figure reproduced from Hogendoorn et al. [15]

2.2. Gaps in literature and goals of current thesis

The research in transition on single phase flows is extensive and there is agreement on the mechanism involved in transition to turbulence. The same cannot be said of the findings for multi-phase flows. One of the problems is the disturbance induced by the particles on the flow field. Thus different parameters have been used to characterize transition. Also very limited experimental evidence is available in literature that goes into detail on using different particle sizes to understand its impact on the flow. The current research, as mentioned before, will be building on top of the experiments conducted by Hogendoorn and Poelma [15]. The effect of particle size will be studied using particles of different diameters such that different diameter ratios between the particle and pipe are obtained. Also some of the gaps in literature will be addressed with the experiments planned.

- Different parameters have been used to characterize the point of transition like spectrum pressure fluctuation [10], [14]; RMS value of streamwise velocity fluctuations [12]; energy of streamwise vortices [13]; friction factor [15], [6] with some contradicting results for variation of transition Reynolds number for different particle concentrations. Therefore further experimental evidence is required to come to a consensus on the point of transition. The current work will compare criteria based on pressure drop measurements.

- The effect of particle concentration on the transition on perturbed and unperturbed flow will be analyzed to understand the transition as particle induced turbulence plays an important role in the nature of transition to turbulent regime.

3

Experimental setup and methodology

The goal of this work is to study transition behavior of neutrally buoyant particles of different sizes and volume fractions. The study is primarily based on pressure drop measurements over a fixed distance. The current chapter aims to elucidate on the components used for measurement, calibration of pressure sensors and post processing to obtain the desired results.

3.1. Preliminary experimental setup

The current section details the preliminary experimental setup built to study the transition behavior. This setup is built to study transition in single phase flows using the water. The primary motivation of the setup is to ensure proper functioning of the apparatus used and verify the transition of single phase flow with the perturbation mechanism. The schematic of the experimental setup is displayed below in figure 3.1. The individual components are annotated for better clarity.

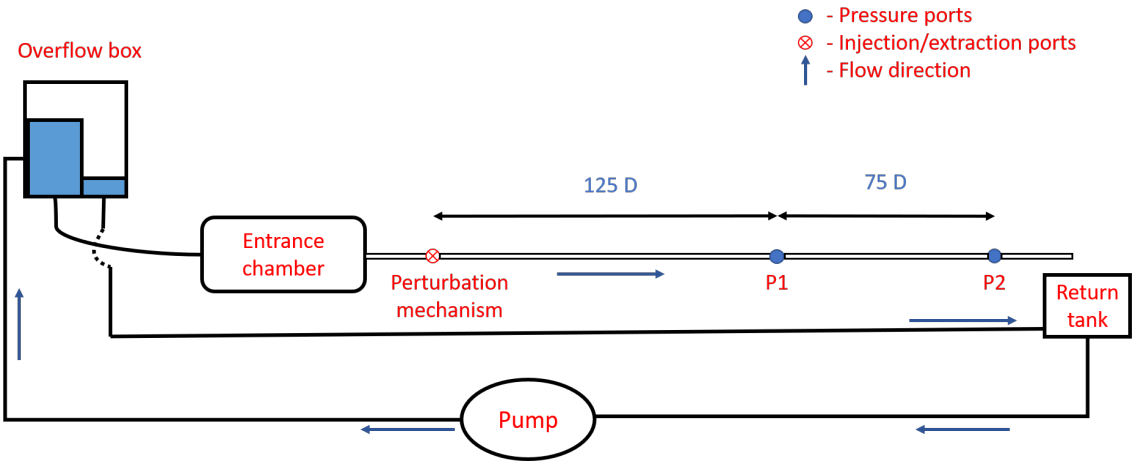

Figure 3.1: Schematic of the preliminary experimental setup

The setup shown above is not used to perform the experiments with particle laden flows due to the limitations of the pump and the available hydrostatic head. The maximum Reynolds number achieved with the setup is Re ≈ 3300. However, this facilitates testing the functioning of pressure sensors and the perturbation mechanism. The perturbation mechanism is tuned to trigger transition at Re ≈ 2000 and the flow becoming fully turbulent at Re ≈ 3000. The experiments are performed only with water as addition of glycerine increases the viscosity and thereby reducing the range of Reynolds numbers the setup can be operated. Furthermore, the setup uses only a single pressure sensor across 75 pipe diameters as the motivation is to validate the setup and the components using the Moody diagram. For this purpose, measuring the average pressure drop is relevant.

The experimental setup is designed in such a way that transition regime is studied based on pressure drop measurements. The average pressure drop is used to calculate friction factor and using which Moody plots are obtained to study the transition behavior. For this reason, pressure drop measurements requires the flow to be free from large scale fluctuations. This is achieved by using a gravity driven setup using an overflow box where a constant head is maintained. The overflow box is connected to the pipes via an entrance chamber which breaks down large scale disturbances. The connections between different pipe segments are machined from PMMA blocks, thereby avoiding disturbances created in these sections. These connecting pieces are in turn used as pressure ports and also for perturbation mechanism. The flow is perturbed by a zero mass flux injection/extraction mechanism to trigger transition. The flow is collected in a return tank which is then connected back to the pump for circulation. The mass flow rate of the system is measured by collecting water in a beaker for recorded time interval. The following subsections explain the components shown in figure 3.1 in more detail.

3.1.1. Pipes

The pipes used for the experimental setup are made of PMMA (Poly methyl methacrylate). The pipes have an inner diameter of 20 mm while the outer diameter is 30 mm. The total length required is *5 m* which included the required development length and length of pipe sections required for measuring pressure drop. A total of 10 pipes (each pipe is 2 m long) were procured and the pipes having the minimum variation in its inner and outer diameters were chosen for the setup. The inner and outer diameter is measured using a vernier caliper at different orientations at the end sections of the pipes. The pipes are also placed in such a way that the difference between the diameter of subsequent pipe sections are minimal. The uncertainty in the pipe diameters are characterized and is shown in figure 3.2. The chosen pipes have internal diameters within [19.9, 20.1]. Each individual marker in the figure represents a single measurement made at one end of a pipe. Furthermore, the pipes are selected only if both the ends of the pipe have internal and external in the aforementioned range.

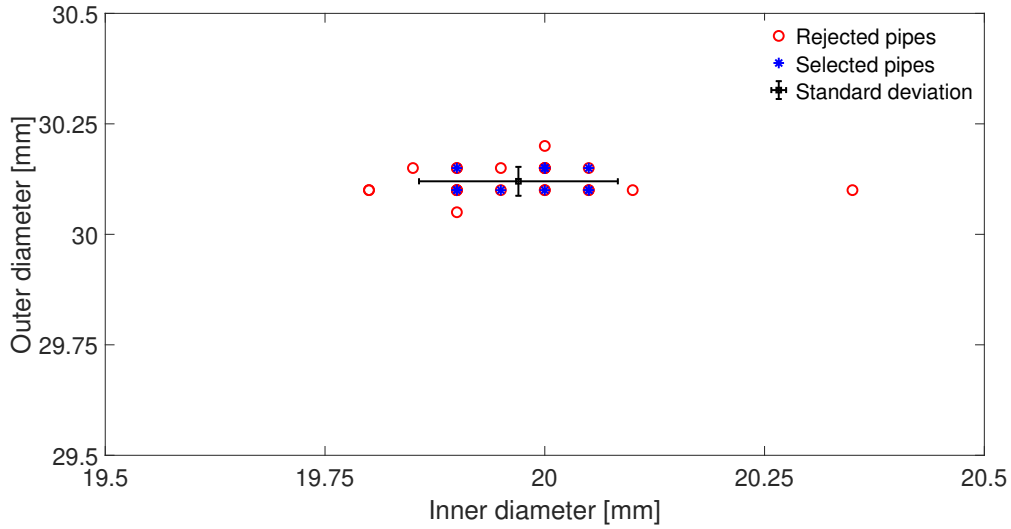

Figure 3.2: Criterion for selecting the pipes for the experiment. The pipes are selected if the variation in pipe inner diameter is ± 0.1mm resulting in variation in D/d of 0.15

3.1.2. Overflow box

The primary advantage of using a gravity driven setup is that periodic large scale fluctuations due to pump are minimised. The overflow box is designed in such a way that a constant head is maintained and the overflow section directly connected to the return tank. The overflow box measured *245 mm* × *150 mm* × *200 mm* in dimensions and is made of PMMA plastic. The section that maintains constant head is *120 mm* high and holds a total volume of *2.7 L*. The box is closed on top in order to minimise evaporation of water. The water is fed into and drawn from the box through holes with diameter of *12 mm* through brass hose nozzles. The figure 3.3 shows the overflow box used in the setup.

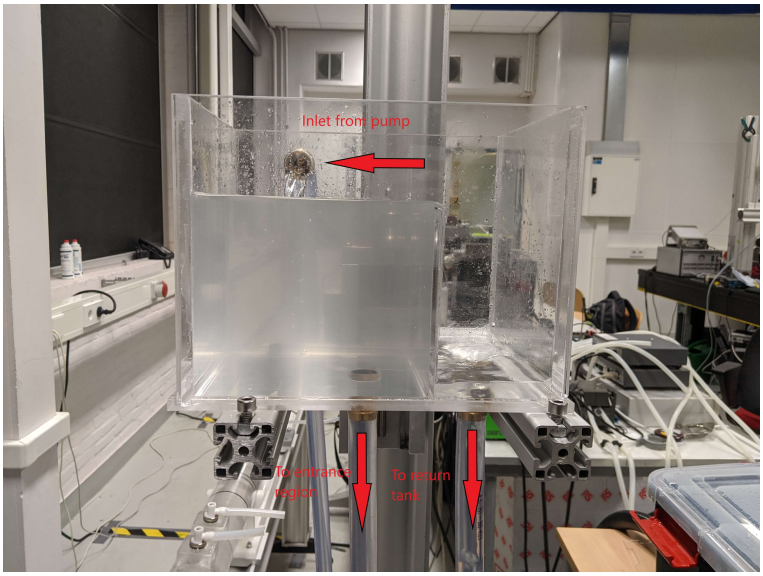

Figure 3.3: Overflow box to maintain a constant head for the flow. The overflow section is connected back to the return tank

3.1.3. Entrance chamber

The entrance chamber is used to break down the eddies to smaller length scales and also smoothly transition the flow to the pipe. Also the larger diameter of the chamber in comparison to the pipe increases viscous dissipation of eddies and thus minimising the fluctuations further. The entrance region is shown in figure 3.4. Despite the use of overflow box, the eddies and disturbances needed to be reduced further and is done by using a series of flow conditioners.

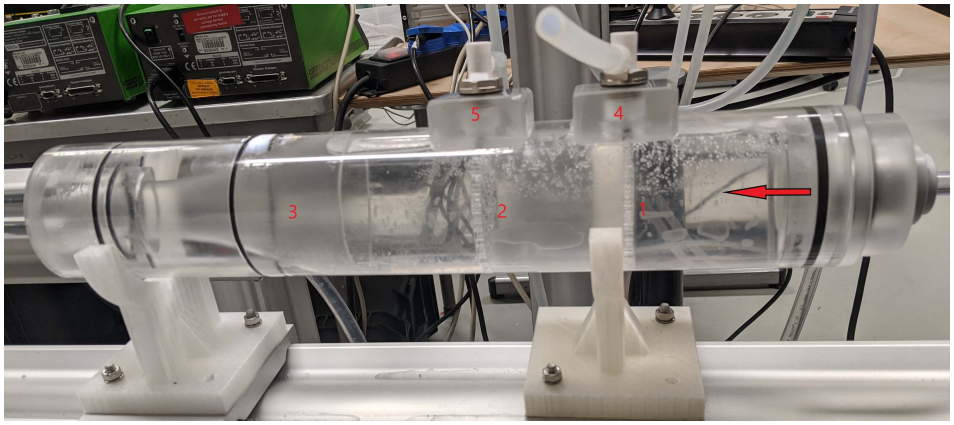

Figure 3.4: Entrance chamber with the components annotated as follows (1),(2) show the flow conditioners used to the break down the eddies to smaller dimensions (3) contraction region to transition the flow from the entrance region to the pipe (4),(5) are air vents to remove air bubbles trapped in the entrance chamber. The arrow indicates the direction of flow

In order to break down the eddies two flow conditioners are used with disks of 60 mm outer diameter as shown in figure 3.5. The first flow conditioner has no holes in the central region in order to break down the jet of fluid coming through the pipe from the overflow box. The holes have a diameter of 5 mm and break down eddies to the length-scale of diameter of the holes. The flow is passes through a contraction before entering the pipe. The contraction (labelled 3 in figure 3.4) has a smooth profile to avoid flow separation when the pipe diameter changes from 60 mm to 20 mm. The profile of the contraction is obtained from Draad et. al. [31] which minimises the velocity gradients in the streamwise direction. Two air vents are attached to the top of the entrance chamber in order to remove air bubbles that would be trapped in the chamber otherwise. The entrance chamber is made leak-proof by using O-rings made of nitrile rubber.

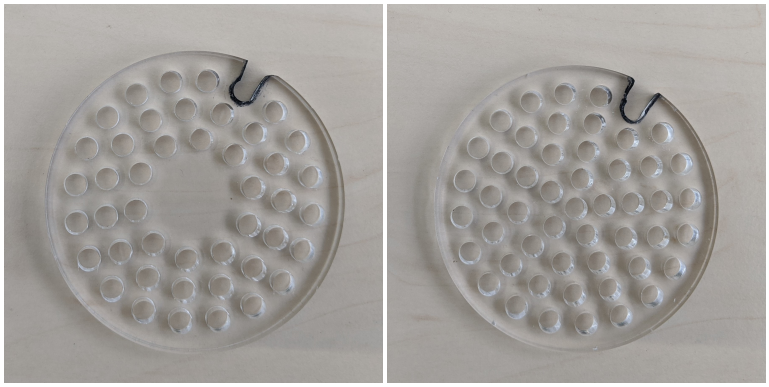

Figure 3.5: Flow conditioner used in the entrance region. The first flow conditioner does not have holes in the central region to break the jet. The flow conditioner placed downstream has uniform distribution of holes to break eddies to smaller dimensions

3.1.4. Perturbation mechanism

The perturbation mechanism is used to trigger puffs which in turn triggers an early sub-critical transition. The mechanism uses an injection/extraction mechanism with zero net mass flux added/removed from the system. This is made possible by the use of a DC motor controlled by a motor controller. The motor drives a piston attached to a linear guide using a timing belt, while an encoder measures the the speed of rotation. The figure 3.6 shows the perturbation mechanism used for the current study. Different velocity profiles can be given to the motor which will be discussed in section 3.3.3. Water is injected and extracted through silicone tubes connected to the piston ports. The tubes are connected to the pipe by means of a coupling made from PMMA plastic. Water is injected/extracted through holes 2 mm in diameter for a pre-determined amount of time. The duration of perturbation is also based on literature as discussed in section 3.3.3.

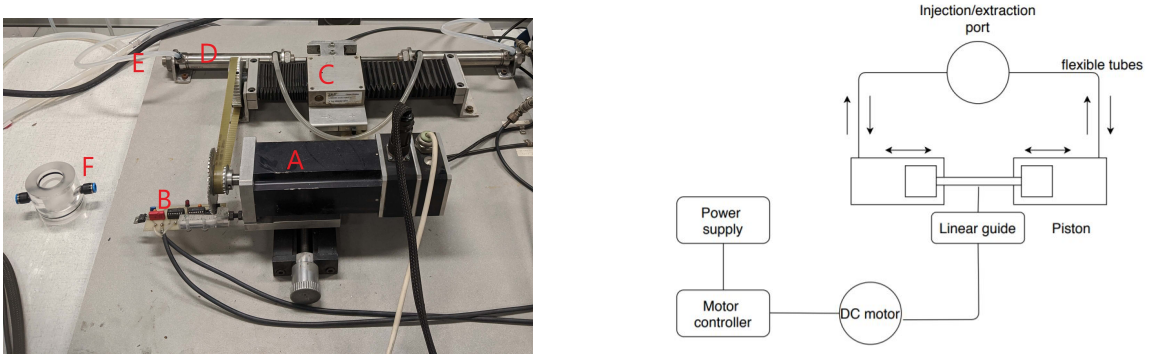

Figure 3.6: (a) shows the perturbation mechanism with individual parts annotated: (A) DC motor (B) Toothed wheel and encoder (C) Linear guide connected to timing belt (D) piston used for injecting/extracting fluid (E) tubes connecting the piston to the port (F) Injection/extraction ports (b) shows the schematic diagram of the mechanism with the arrow marks indicating the direction of motion/fluid flow

3.1.5. Pressure sensor

As mentioned above, only one differential pressure sensor is used to obtained the average pressure drop in the pipe. The pressure sensor measures the pressure drop across 75 pipe diameters. The typical length scale of a turbulent puff is reported to be 20 - 30D long [32]. Therefore, the pressure ports are placed 75 D apart in order to capture multiple puffs to represent the average pressure drop. Furthermore, the upper limit of this distance is determined by the rating of the membrane used along with the dynamic range capable by the demodulator. A Validyne DP 45 pressure sensor with *'14* stainless steel membrane is used for the experiments. The membrane is rated to measure pressure drop up to 225 Pa. The sensor is connected to a CD-15 demodulator to provide a DC output which is then converted to the relevant pressure drop reading. Section 3.2.2 explains the construction and working of the sensor and demodulator in detail.

3.1.6. Pump

The setup uses two *Watson-Marlow 505 Du* pumps to provide the required mass flux. The pumps operate by peristaltic compression and expansion of the flexible tubes passing through a set of 6 rollers. It can circulate fluid in tubes of bore diameter upto 8 mm. The flexible tubes used for the experiments have inner and outer diameter of *8 mm* and *12 mm* respectively. The maximum rotational speed of the rollers is 220 rpm. Furthermore, the pump supports Y-type configuration of tubes wherein two flexible tubes could pass through the rollers and thereby increasing the mass flux provided by the pump. Two such pumps are used in parallel to increase the maximum volume flow rate to *4.2* liters per min.

3.2. Final experimental setup

The current section will explain the construction and the components used for the experimental setup used to conduct experiments with glycerine and particle laden flows. The final setup shares most of the individual components used for the preliminary setup as seen in figure 3.7. The setup employs a more powerful pump and flexible tubes of higher diameter to reduce friction. The changes enable a higher Reynolds number when particles are added. The setup also uses an additional pressure sensor to measure pressure drop over 10 pipe diameters to record the intermittent structures. The working of the pressure sensor and the additional parts used in the setup are explained below.

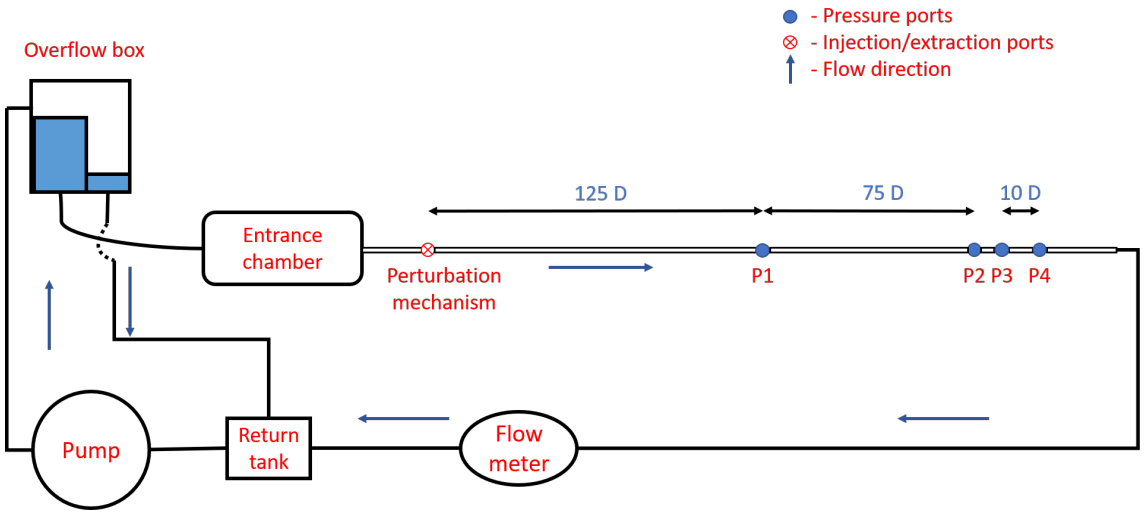

Figure 3.7: Schematic of the experimental setup used for single phase (with glycerol-water mixture) and multi-phase experiments

3.2.1. Overflow box

The overflow box is modified to accomodate the change in the size of flexible tubes connecting the box to the pipes and the return tank. The overflow box measures *260 mm* × *175 mm* × *200 mm* in dimensions and is made of PMMA plastic. The box maintains constant head of *135 mm* and can hold a net volume of *3.78 L*. The box is also closed on top in order to minimise evaporation of water. A steel mesh is used to reduce fluctuation in head when water falls directly in section where a constant head is maintained. The water is fed into and drawn from the box through holes with diameter of *20 mm* through brass hose nozzles.

3.2.2. Pressure sensor

The experimental setup employes two different pressure sensors (Validyne DP 45) to record pressure drop across streamwise distances. The first sensor is used to record pressure drop a distance of 75 diameters to represent the average pressure occurring in the pipe. This sensor has a *'20* diaphragm which can measure pressures upto 860 Pa. The second sensor is used to measure the drop in pressure over a distance of 10 pipe diameters to track turbulent structures like puffs and slugs. This sensor uses a *'14* diphragm which has can measure pressure upto 225 Pa.

The current setup uses differential pressure sensors based on variable reluctance with a magnetically permeable stainless steel diaphragm clamped between between two blocks of stainless steel. E-shaped cores are

embedded in the each block. In the undeflected condition, the plate is equidistant from both the coils (0.005 inch) providing equal reluctance. The magnetic reluctance changes when the diaphragm is deflected towards one side due to pressure difference and thereby resulting in an electrical output. The transducer is connected to an AC bridge circuit in order to take advantage of the inductance variations in the coils. The coils form one half of the bridge and the center tapped secondary of the carrier supply transformer (carrier demodulator) forms the other half. The electrical output of this bridge circuit is an AC signal whose phase depends on the direction of diaphragm displacement. When the diaphragm is in its undeflected (zero) position, the bridge output is at its minimum. Since the diaphragm displacement is linear with pressure applied, the bridge output is also linear with pressure. If the diaphragm is displaced in the opposite direction, the bridge output is again linear with pressure.

A CD-15 basic sine wave carrier demodulator that operates with variable reluctance transducers is used to provide steady DC output signal. A 5 kHz sine wave excitation is applied to the two inductance ratio arms of the transducer and the output is demodulated and amplified. The figure 3.8 shows the pressure sensor used to perform pressure drop measurements.

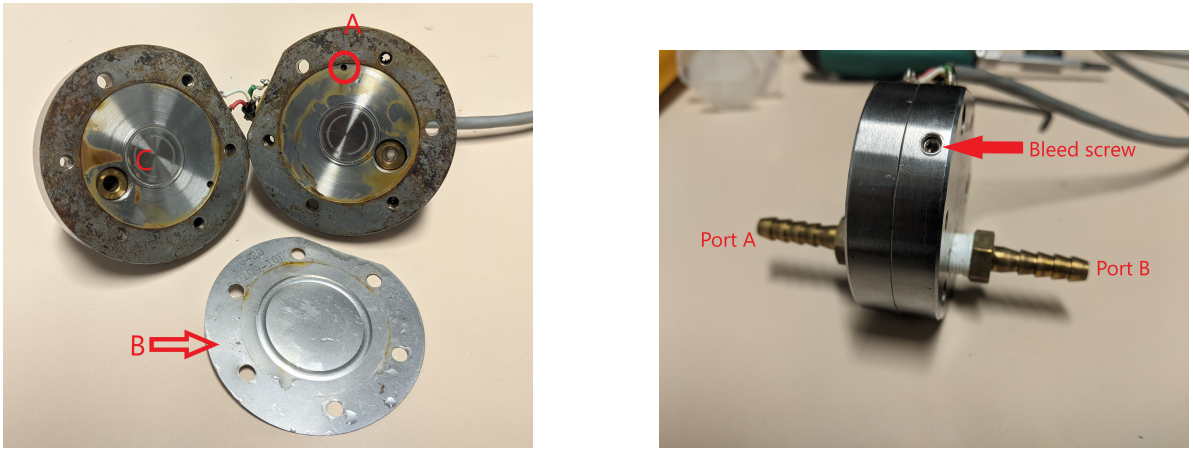

Figure 3.8: (a) pressure sensor and its components annotated A: Bleed holes, B: Flexible diaphragm and C: E-shaped cores (b) Pressure drop measured as pressure difference between ports A and B while bleed screw is used to remove air from the sensor

3.2.3. Pump

Preliminary calculations indicated the maximum flow rate required for the experimental campaign to be *8 L/min.* This is provided by a progressive cavity pump from MONO. The pump has a capacity upto *3750 L/min* with capability to operate at a peak pressure of 24 bar. It is operable between a temperature of $-10°C$ to $100°C$ although the typical operating temperature ranges from $20°C$ to $27°C$. The motor is coupled with a frequency controller to operate the pump at different flow rates.

3.2.4. Flow meter

An Optimass 7050c is used to measure the volume flow rate of the flow. It uses Coriolis forces to measure the flow rate. A titanium measuring tube is oscillated at a constant frequency and any fluid passing through the tube will change the frequency. This change in oscillation amplitude and frequency is measured by sensors housed in stainless steel housing is used to calculate the density and mass flow rate of the flow. The figure 3.9 shows the flow meter used in the experimental setup. The measuring tube has an internal diameter of 15 mm and a total length of 450 mm. The flow meter is accurate upto 1 % of the measured value, the repeatability is rated as 0.005 % including hysteresis, linearity and zero stability. The density measurements are accurate upto $\pm 2 kg/m^3$ while it can measure densities from $500 - 2000 kg/m^3$.

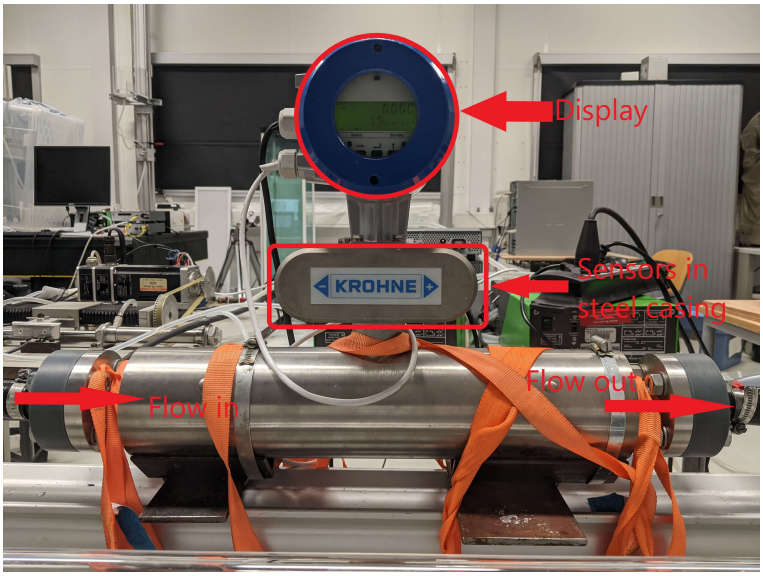

Figure 3.9: Flow meter used for the experiment. The fluid enters from left and the measured values are displayed in the screen

3.2.5. Return tank

The return tank is used for two purposes: addition/removal of suspension or particles and act as a reservoir for the pump to draw flow from. The tank is made out of plastic and measures $350 \times 545 \times 270\ mm$ in dimensions. The lid of the tank has a hole to accommodate the tube from the overflow section of the overflow box.

3.3. Methodology

The current section will elucidate the methods employed and processes followed to take the pressure drop measurements across the pipe. These include the calibration of equipment, characterization of of particles and the suspension.

3.3.1. Pressure measurement

As mentioned above, the transition is studied by recording pressure drop over a fixed distance. Therefore, the protocol followed in recording it should be robust for the entire range of measurement. The pressure drop in the laminar and turbulent regime is rather stable and is less prone to fluctuations. Therefore, the duration of measurement does not play a significant role. Also, the higher value of pressure drop in turbulent regime ensured the effects of pressure fluctuation are minimal. In the transition regime, particularly for intermittency less than 25 %, the pressure measurement needs to be long enough to capture sufficient number of puffs such that the repeatability error is minimised. For the reasons mentioned above, a small study is conducted to identify the measurement time required for measuring pressure drop in the transition regime repeatably.

The pressure drop measurements are performed for different time duration and is repeated 20 times for each measurement time while keeping all the other parameters constant. The experiment is conducted at an intermittency of 15 % and at a Reynolds number of 2200. The mean value of pressure drop measurements are calculated and compared to study its repeatability. It is to be noted that the pressure sensor is calibrated upto 300 Pa when this study is performed. This is relevant because the accuracy of the sensor is expressed as $\pm\ 0.5\%$ of full scale reading. This results in an accuracy of $\pm$ 1.5 Pa.

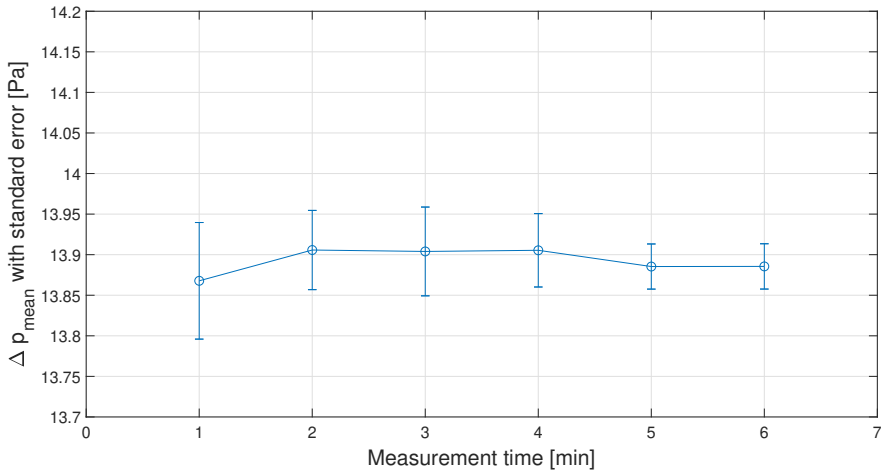

Figure 3.10: Mean value of the pressure drop measurements for a given measurement time with standard error.

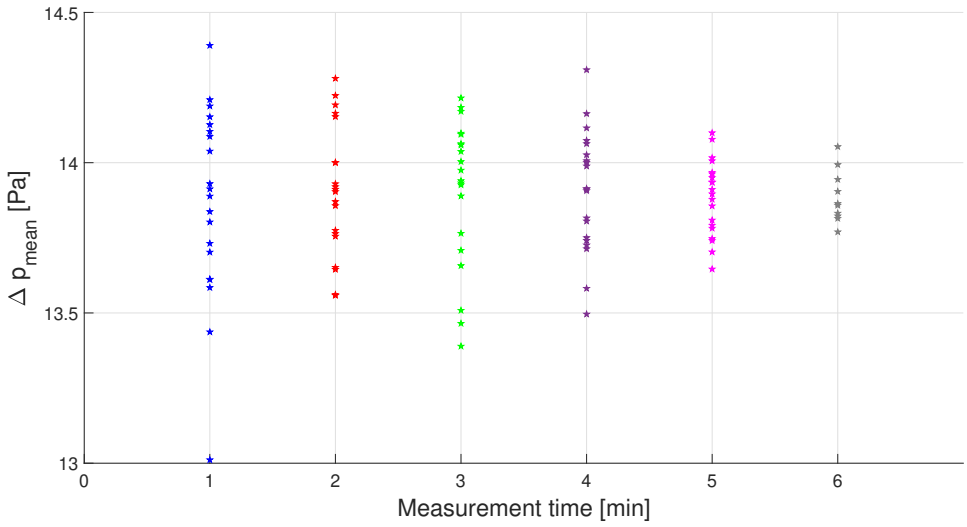

Figure 3.11: Mean pressure drop of individual measurements for different measurement times.

It is clear from figure 3.11 that the error reduces as the pressure drop is measured over a longer duration of time. While the variation in mean values of pressure drop is within the uncertainty of the sensor for all the measurement times, a variation of 0.5 Pa is considered desirable. This condition is satisfied when the pressure drop is recorded for more than 5 minutes. This condition is important for flows with low particle concentration and at low intermittency as an error of 1 Pa can shift the point by 5-8 % in the Moody chart. Thus, a measurement duration of 5 minutes is used for the transition regime.

3.3.2. Particle size characterization

The particles used for the experiment is procured from *Synthos B.V.* and is found to be poly-disperse in shape and size. Therefore, in order to reduce the variation in diameter of the particles, they are sieved for 4 hours before using them in the experiment. A combination of two sieves are used to filter the particles that will be used for the experiment. The sieves have circular pores with diameters of 1.3 and 1.6 mm respectively. A small study is carried out to find the average particle diameter. A more detailed report of this study is given in appendix A on how the diameter of particle is measured.

3.3.3. Perturbation mechanism parameters

Because the study uses an active perturbation mechanism, it is imperative to find the desired range of values for those parameters. The perturbation mechanism has many parameters that can be varied like perturbation amplitude, duration and frequency. As explained in section 2.1.1, there is an optimum range of parameters to work in, outside of which, it becomes ineffective to use or produce undesirable results. A brief study is conducted for determining the perturbation amplitude that can trigger puffs for different Reynolds numbers. The perturbation amplitude is described in equation 3.1.

$$A = \frac{\Phi_{inj}}{\Phi_{flow}} \tag{3.1}$$

The amplitude of perturbation is varied by changing the mass flow rate of injection/extraction by varying the speed of rotation of the DC motor. This exercise is performed at different Reynolds numbers and thus the minimum amplitude of perturbation can be identified to generate puffs.

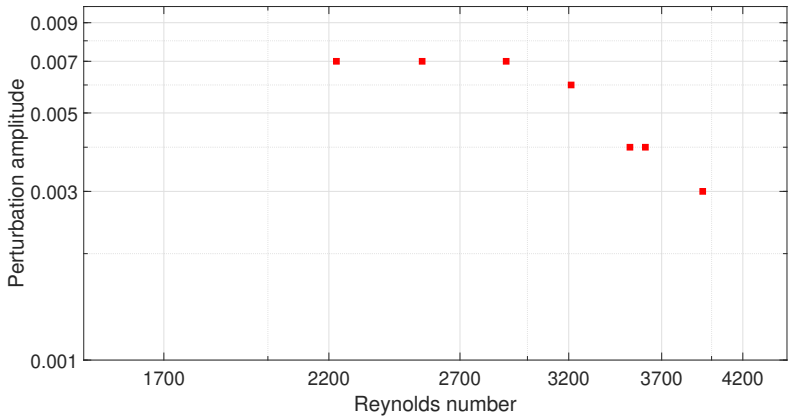

Figure 3.12: Minimum amplitude of perturbation required to trigger puffs plotted for different Reynolds numbers

The figure 3.12 shows the results from the study. Turbulent puffs are not observed for Reynolds number less than 2000 for an amplitude of 0.1. The study primarily focused on the ability of the system to generate turbulent puffs during a single instance of injection/extraction. The minimum amplitude that trigger puffs for the lowest Reynolds number is used for the entire experimental campaign. The flow is perturbed at a frequency of 0.15 Hz. This is decided by determining the desired Reynolds number at which the flow needed to fully turbulent. For the current work, different perturbation frequencies (0.03 Hz - 0.22 Hz) are used at a Reynolds number of 3000. It is found that the flow becomes turbulent at Re $\approx$ 3000 when the perturbation frequency of greater than or equal to 0.15 Hz. Any higher frequency does not make meaningful difference to the result.

The duration of perturbation is decided based on evidence from the literature. The study for Mullin et. al. [8] showed that the duration of perturbation is required to be more than 10 non dimensional units of time for it to be independent of perturbation amplitude. The duration and amplitude of perturbation is influenced by another factor. The process of injecting/extracting fluid generated a pressure disturbance that travels through the tube walls and is recorded by the sensor. These disturbances are higher for higher perturbation amplitude and lower duration of perturbation. Therefore, the duration of perturbation is fixed at 10 non-dimensionalized time units.

Finally, a sinusoidal velocity profile, as described in equation 3.2, is used for perturbing the flow. Different functions like top hat, saw-tooth, triangular and sinusoidal waveforms are available in the software. The sinusoidal waveform is used to minimise any steep gradients in the profile. It is important because any steep gradient in velocity will induce a jerk in the motion of the piston and thereby creating an undesirable disturbance while measuring pressure drop.

$$v(t) = \frac{v_{max}}{2}\left[1 + sin\left(\frac{2\pi t}{T} - \frac{\pi}{2}\right)\right] \tag{3.2}$$

In this equation, T is the total time period of the signal and v_{max} is the maximum velocity.

3.3.4. Adjusting fluid density

The particles cannot be used directly in water because the density of the particles is higher than that of water. Therefore, glycerine (*87 %* pure) is mixed with water to obtain a neutrally buoyant solution. The density of particles is estimated using a simple experiment wherein particles are suspended in separate mixtures containing different proportions of glycerol-water mixtures. The ratio of height of particles that float to that of those that sink is used to obtain an estimate of the average density of the particles. This is explained in more detail in Appendix C. The density of glycerine and the glycerine-water mixtures are measured using *ANTON PAAR DMA 5000* density meter. It measures the density of the fluid using their patented pulsed-excitation method. The equipment has an accuracy of 0.007 kg/m^3, while the repeatability and reproducibility are 0.001 kg/m^3 and 0.005 kg/m^3 respectively.

While the experiment mentioned in Appendix C provided an estimate for the mean density of the particles, finer adjustments are required for each particle concentrations when performing the experiments. It is achieved by adding water or glycerol based on the requirement. The particles are added to the system and soaked overnight. Water or glycerol is added based on the need and the system is run at high Reynolds number to facilitate thorough mixing of suspension. Once the suspension is well mixed, the flow is stopped and the particles are monitored for 4 minutes. The time scale of observation is greater than the advection time scale of the flow. If the particles do not rise/settle down more than the pipe radius, the suspension is considered neutrally buoyant.

4

Results and discussion

The current section presents the results from the experiments performed in the pipe. The chapter is divided into four sections: Transition in single phase flows, Transition in multi-phase flows, study of intermittency and finally critical Reynolds number. The section 4.1 describes the experiments performed to validate the setup with literature. Later, section 4.2 explains the results obtained from experiments performed using the particles. The aforementioned explains transition by using Moody diagrams. Section 4.3 explains about study of intermittency using instantaneous time series of pressure drop. The final section attempts to study the transitional Reynolds number obtained using the Moody plot and compare different criteria used in literature.

4.1. Transition in single phase flows

The experiments for single phase flow are performed to validate the setup. A mixture of water and glycerol is used for this purpose as the same is used for multi-phase experiments. The properties like viscosity and density are obtained from the literature [33]. The density and viscosity of the mixture is adjusted based on mass fraction of glycerol and temperature. The equations describing the adjusted viscosity and density is explained in Appendix F.

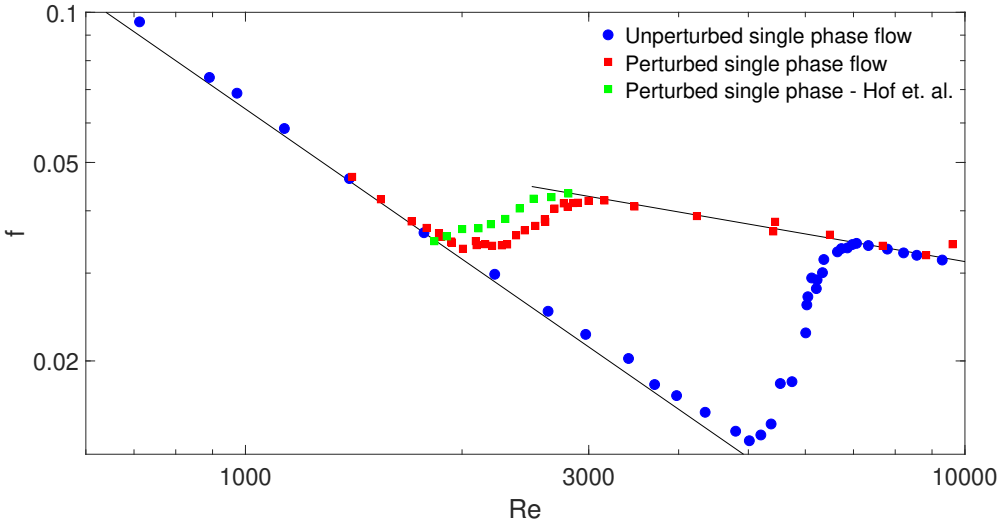

Figure 4.1: Moody chart for single phase flow used to validate the experimental setup. The results from perturbation mechanism is validated with Hof et. al. [16]. Flow becomes intermittent for Re ≈ 2000 and 5100 for perturbed and unperturbed condition

Figure 4.1 shows the Moody diagram for single phase flows. The friction factor at Re ≈ 700 for unperturbed flow is slightly higher than the theoretical value. This can be explained by the uncertainty of the

pressure sensor whose accuracy corresponds to ± 1.5 Pa. This is significant because the pressure drop for the aforementioned Re ≈ $\mathcal{O}$(10 Pa). Furthermore, the friction factor is higher than the theoretical value for Re > 4000 because of the insufficient development length. The entrance length provided for the current setup ensured fully developed laminar flow up-to Re ≈ 2200. The flow is fully developed for Re > 2200 because of the entrance chamber, where the disturbances are minimized by viscous dissipation. Equation 4.1 provides the correlation between the entrance length required for flow to develop as a function of Reynolds number [34].

$$\frac{L_{entry}}{D} = \left[(0.619)^{1.6} + (0.0567\ Re)^{1.6} \right]^{\frac{1}{1.6}} \tag{4.1}$$

The use of entrance region helps in development of flow by minimising disturbances. The first inference to be drawn from the figure is the point of transition without the use of perturbation mechanism. The pressure drop is measured for a duration of 2 minutes when the flow is completely laminar or turbulent while the measurement is done for 5 minutes when the flow becomes intermittent. The pressure drop is measured for a longer duration to minimize variation in measured value. This is explained in more detail in section 3.3.1. The flow becomes unstable at Re ≈ 5000, indicating that the setup is free from any inherent disturbance for Re ≤ 5000. The flow starts to become intermittent from Re = 5100 with turbulent puffs interspersed in otherwise laminar flow. The intermittency increases and the flow becomes turbulent at Re = 7000. The experiment is carried out till the flow reached Re = 9600 where the friction factor matched with the Blasius correlation.

The flow is perturbed with the active perturbation mechanism described in section 3.1.4. The parameters are based on the experiments detailed in section 3.3.3. The perturbation amplitude is set at *0.007* while the perturbation duration and frequency are *1.5 s* and *0.15 Hz* respectively. The perturbations are ineffective for Re < 1800 as any disturbance generated in the flow is re-laminarized. When the flow is perturbed, it becomes unstable at Re ≈ 2000. The flow becomes completely turbulent at Re ≈ 2900. The measurement duration of pressure drop is similar to the aforementioned unperturbed conditions. The transition curve agreed well with literature [16] wherein an injection mechanism was used to perturb the flow. The experiments with the perturbed flow is continued till Re = 9500 to compare with the unperturbed flow. These results for single phase flows validates the setup regarding the stability and the perturbation mechanism and also acts as the baseline case with which the results for multi-phase flows will be compared.

4.2. Transition in multi-phase flows

Once the single phase characteristics are established, the particles are added to study its impact on transition. The particles concentration studied in the experiments ranged from 0.2 % to 25 % by weight. The use of an active perturbation mechanism enabled the experiments to be performed with and without perturbation simultaneously. The particles used for the experiment are made of Polystyrene and measured *1.3 mm* in diameter resulting in D/d = 15.4. The estimation of particle diameter is explained in detail in Appendix B. Water - glycerol mixture is used to make the suspension neutrally buoyant. As mentioned in section 3.3.4, the density had to be adjusted for each particle concentration by adding water or glycerol as per the requirement. With the addition of the particles, the change in effective viscosity of the suspension is accomodated. This is performed using Eiler's viscosity correction as given in 4.2 [35].

$$\frac{\mu_{adj}}{\mu_0} = \left(1 + 1.25\frac{\phi}{1-\phi/0.64}\right)^2 \tag{4.2}$$

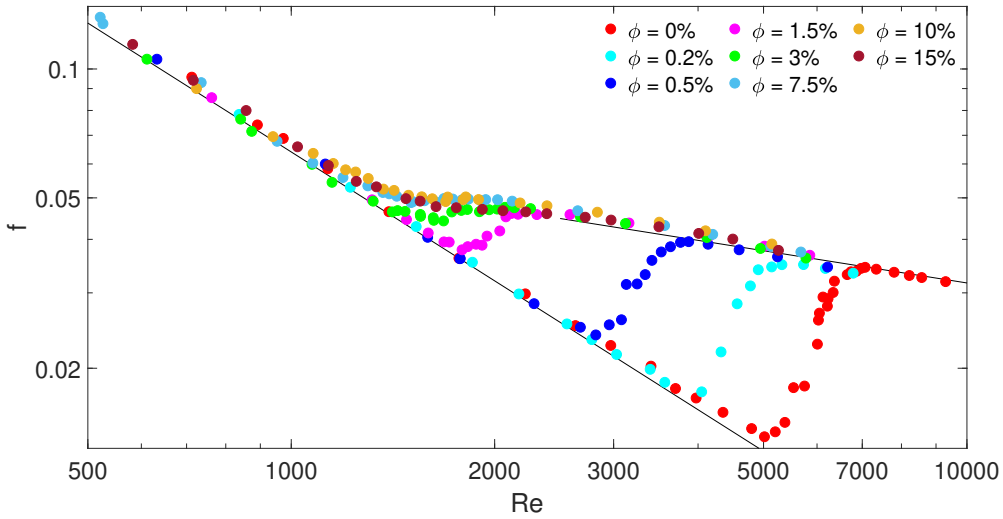

Figure 4.2: Transition behavior of unperturbed particle laden flow studied using the moody chart. Flow deviates from laminar regime at lower Re for increasing ϕ. Sub-critical transition is observed for $\phi \leq 1.5$ % while super-critical transition behavior is observed for $\phi \geq 3$ %. The Moody chart does not show $\phi = 0.75$ %, 1 %, 5 %, 25 % as they display similar transition behavior to other ϕ

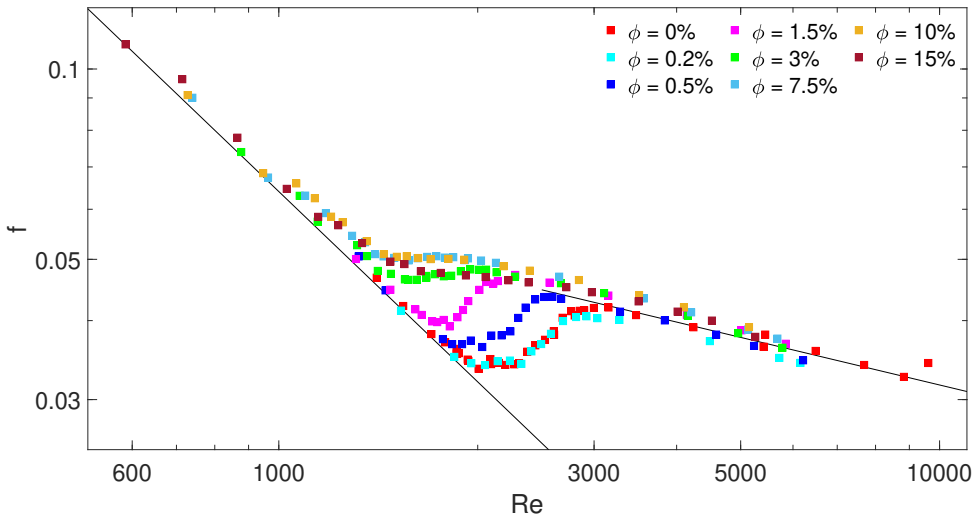

Figure 4.3: Transition behavior of perturbed particle laden flow studied using the moody chart. Sub-critical transition is observed for $\phi \leq 1.5$ %. Transition behavior is unaffected by perturbation mechanism for $\phi \geq 1.5$ % while super-critical transition is observed only when $\phi \geq 3$ %. The Moody chart does not show $\phi = 0.75$ %, 1 %, 5 %, 25 % as they display similar transition behavior to other ϕ

It is prudent to understand the transition behavior by comparing the Moody diagrams for unperturbed and perturbed condition which are plotted in figures 4.2 and 4.3 respectively. The Moody diagrams comprising all the mass fractions are provided in Appendix G as certain plots are omitted in figures 4.2 and 4.3 for better understanding. Furthermore, important characteristics of the transition behavior observed in figure 4.2 and 4.3 is tabulated in Table 4.1.

The first particle concentration analyzed is $\phi = 0.2$ %. It can be seen from figure 4.2, that addition of particles makes the flow unstable. The transition is triggered earlier compared to single phase flow. While the flow becomes turbulent earlier, the mechanism is similar to that of transition behavior in single phase flows. However, it can be seen from figure 4.3, perturbing the flow at $\phi = 0.2$% makes no difference to the transition behavior. This can be explained by the fact that the addition of particles, while introducing additional disturbance, is not strong enough to create additional disturbance in addition to the perturbation mechanism to

trigger an earlier transition.

Further addition of particles (ϕ = 0.5%, ϕ = 0.75% and ϕ = 1%) triggers an earlier transition for perturbed and unperturbed condition. This indicates that the disturbances introduced by the particles are strong enough to supplement the perturbation mechanism. Also, the critical Reynolds number is different for perturbed and unperturbed transition meaning that the presence of particles merely adds turbulence to the flow. For the aforementioned particle concentrations, the flow exhibits intermittent behavior and distinct puff-like structures are visible. These structures are discussed more in detail in section 4.3.

Interestingly, the transition behavior of the suspension is identical for perturbed and unperturbed conditions for ϕ = 1.5 %. The flow shows intermittent behavior at Re ≈ 1800 irrespective of the application of external perturbation. This suggested that the disturbance created by the particles are qualitatively greater or equal to the external perturbations and therefore the transition behavior is unaffected by perturbation mechanism. It should be noted that, despite the domination of particle induced fluctuations, the transition behavior is similar to traditional sub-critical transition.

The effect of particle induced disturbance is more dominant for higher particle concentrations ($\phi > 3\%$). Apart from the perturbation mechanism being ineffective in making a difference in transition behavior, the flow does not display spatio-temporal intermittency. This suggests that the disturbance increases globally as Re increases instead of appearance of puffs when the flow deviates from laminar state. This difference in behavior will be explained in further detail in section 4.3.

S.No	**Particle Concentration** (ϕ) [%]	**Nature of transition**	**Effect of perturbation mechanism**	**Additional characteristics**
1	0	Sub-critical	Earlier onset of transition when using perturbation mechanism compared to unperturbed flow	
2	0.2	Sub-critical	Earlier onset of transition when using perturbation mechanism compared to unperturbed flow	Transition behavior of perturbed flow identical single phase perturbed flow
3	0.5, 0.75, 1	Sub-critical	Earlier onset of transition when using perturbation mechanism compared to unperturbed flow	
4	1.5	Sub-critical	Perturbation mechanism did not affect transition behavior	Intermittent structures with similar length-scales observed for perturbed and unperturbed flow
5	3, 5, 7.5, 10	Super-critical	Perturbation mechanism did not affect transition behavior	
6	15, 25	Super-critical	Perturbation mechanism did not affect transition behavior	Friction factor reduced monotonically with Re

Table 4.1: Summary of observations made on the transition behavior for different particle concentrations using the Moody chart. The table groups particle concentrations based on their transition behavior

Another important characteristic is that the friction factor is over-predicted in turbulent regime for all the volume fractions displaying super-critical transition behavior. This can be explained by the additional friction generated by the particles on top of the fluid-particle interaction. Equation 4.3 describes the additional friction recorded in the flow for different particle concentrations. Figure 4.4 shows this behavior by plotting the deviation of friction factor for all particle concentrations. The Reynolds number for the points plotted in the figure ranged from 3100 to 3600 and the flow is turbulent for all particle concentrations. As the flow is pressure driven, Reynolds number cannot be matched for different particle concentrations. The friction factor is over-predicted for particle laden flows and the margin of over-prediction increases up to ϕ = 10 %. This additional friction is the result of the presence of particles as the increase in viscosity caused by the particles are accounted by equation 4.2. The under-prediction of friction factor for ϕ = 0.2 % and ϕ = 0.5 % are attributed to the measurement uncertainties as indicated by the error-bars. The additional friction in the flow reduces for higher particle concentrations indicating reduced drag due to presence of the particles. The friction factor for ϕ = 25 % matched the value calculated using the Blasius correlation and therefore matches with the single phase flow. It is also important to note that the friction factor decreases monotonically with

Reynolds number for $\phi \geq 15$ %. This indicates that the monotonic behavior of the friction factor is the result of drag reduction observed for high particle concentrations.

The trend is similar to the behavior observed in figure 2.18(c) where friction factor is plotted at Re = 3500 for all particle concentrations [14]. The friction factor was over-predicted for flows where sub-critical transition was observed. Furthermore, the over-prediction in friction factor was significantly higher than the values reported in figure 4.4. Similar behavior could be observed from the experiments performed by Hogendoorn et al. This behavior can be observed in figure 2.19a. These deviations in behavior can be attributed to the difference in the particle sizes. The current work studies particles with $D/d = 15.4$ while the experiments performed by Agarwal et al. and Hogendoorn et al used particles with $D/d = 20$ and $D/d = 19.6$ respectively.

$$f_{add} = \frac{f_{actual} - f_{blasius}}{f_{blasius}} \tag{4.3}$$

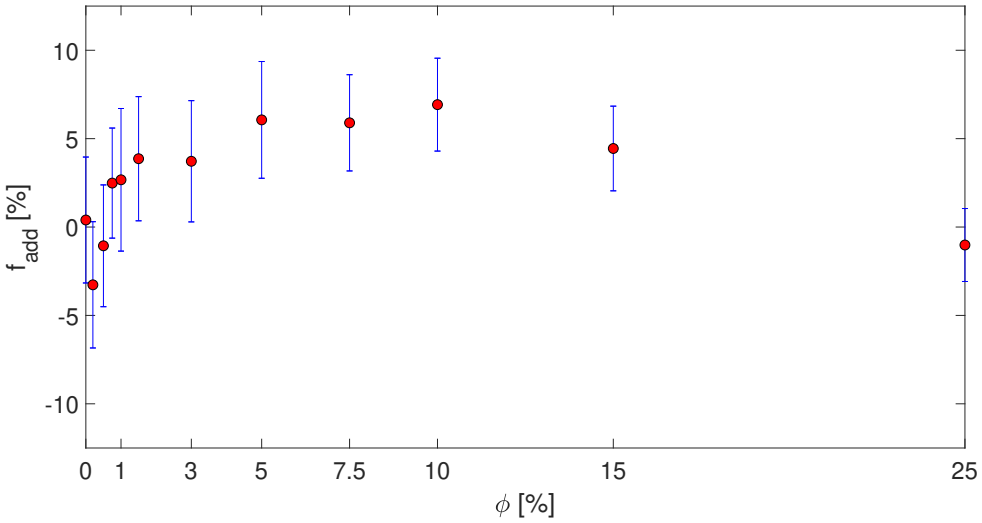

Figure 4.4: Additional friction due to presence of particles in the suspension for different ϕ. Re is maintained in the range of 3100 - 3600

4.3. Study of intermittency

As the overall behavior of the flow is studied in response to addition of particles in the previous section, the current section focuses on the spatio-temporal intermittency in particle laden flows. This study reveals some of the finer details of transition and their changes when particles are added.

In order to study intermittency, the time series of pressure drop data will be analyzed for different particle concentrations. The pressure drop is recorded for a distance of 10 pipe diameters in order to record turbulent characteristics of the flow. The pressure drop is recorded over a duration of 30 minutes in order to collect sufficient number of puffs. The mean value of the pressure drop is subtracted from the data as the primary objective of the section is to illustrate the impact of particles with pressure fluctuations. This study is performed at an intermittency of 10% – 20% to understand the mechanisms driving the transition. Signal conditioning is also performed to reduce noise and therefore have a clear understanding of the data. A hanning window of length 25 data points is used to reduce noise. The window used to perform the convolution is shown in figure 4.5.

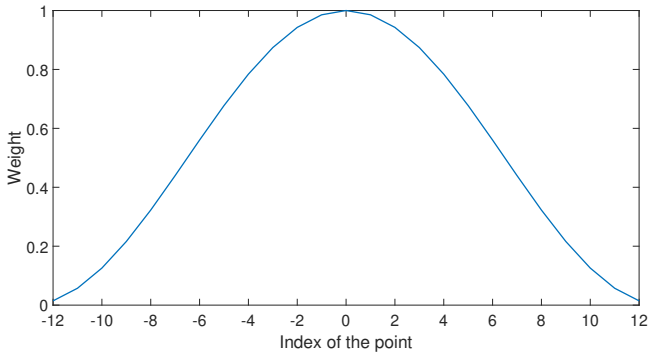

Figure 4.5: Hanning window used to smoothen the time series of pressure drop signal. The index 0 corresponds to the point to which the filter is used. 12 points before and after the index '0' is weighted according to the filter where index '0' corresponded to the point to which the filter is applied

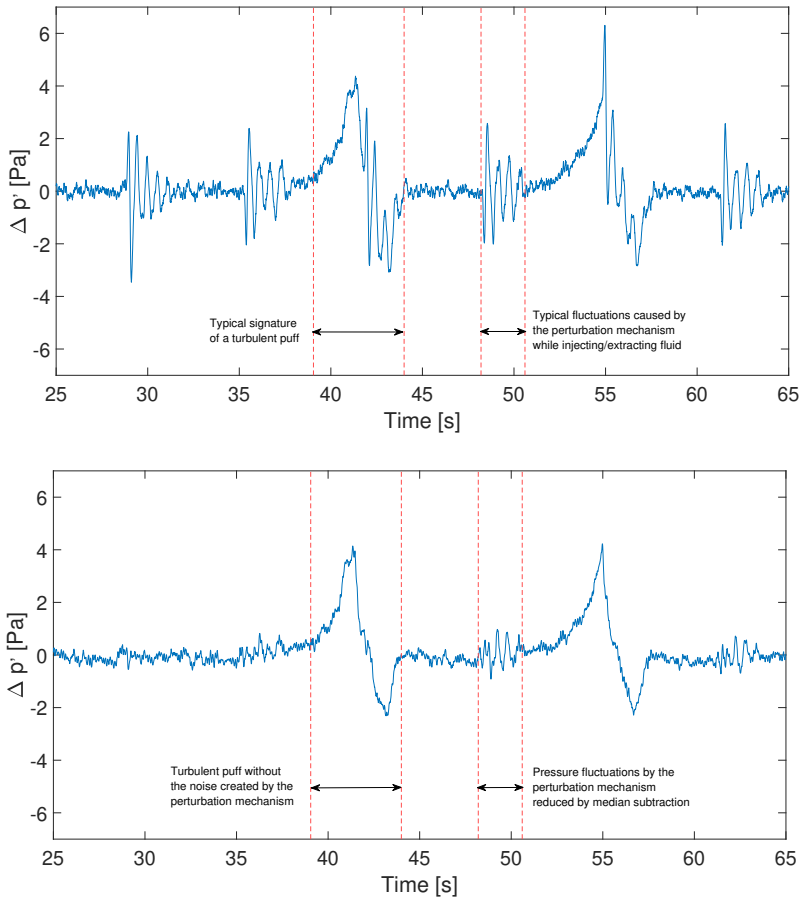

Figure 4.6: (a) Pressure drop time series data recorded across 10D showing typical puff signatures along with the fluctuations caused by the perturbation mechanism (b) Pressure drop conditioned by subtracting the median signal of pressure fluctuations caused by the perturbation mechanism. This removes most of the noise and thereby indicating the physical phenomena with better clarity

The pressure drop data contains the noise created by the perturbation mechanism. Figure 4.6 shows the pressure fluctuations caused by the perturbation mechanism. While any physical disturbance requires a finite time to advect from the point of perturbation to the pressure sensors, the aforementioned fluctuations were recorded at the same instant as the perturbation mechanism is active. This suggests that these fluctuations are caused by the physical vibrations caused by the process of injection/extraction, which travels through the tube walls at the speed of sound. In order to remove these fluctuations from the data, the signal

is divided into two parts and the individual pressure fluctuations caused by the perturbation mechanism is collected and the median of these fluctuations is calculated. This procedure is performed for both halves of the signal and is shown in figure 4.7. Finally, this median pressure fluctuation is subtracted from the signal. The signal is divided into two halves because it was found that the pressure fluctuations caused by the perturbation mechanism had small differences between the two parts of the signal.

An arbitrary segment for a finite time is used to represent the pressure drop data as the there are no qualitative differences in the length scales and time scales of any physical phenomena. The pressure drop data corresponds to perturbed condition with the perturbation parameters unchanged from the experiments conducted to obtain the Moody plots.

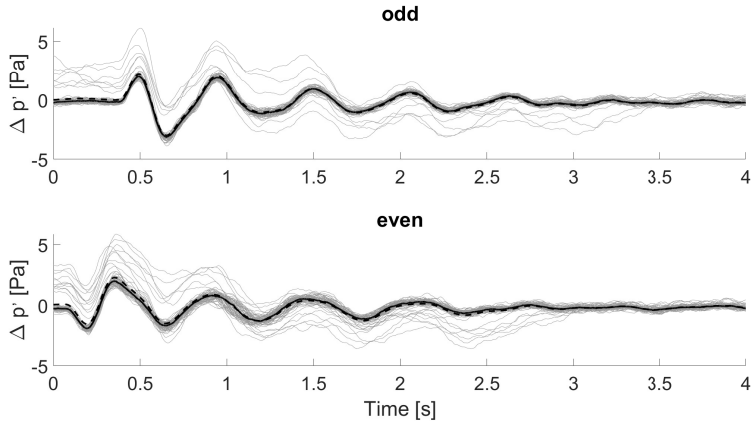

(a) Median signal of pressure fluctuations caused by the perturbation mechanism from (a) *t = 0 s* to *900 s*

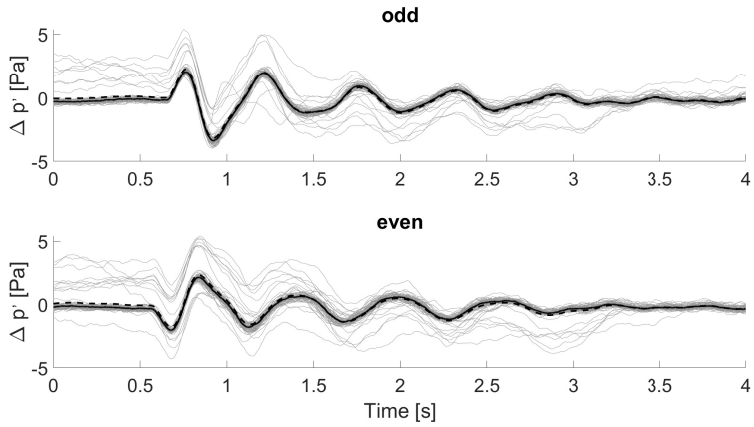

(b) Median signal of pressure fluctuations caused by the perturbation mechanism from (a) *t = 901 s* to *1800 s*

Figure 4.7: Grey solid lines indicate the time series data individual perturbations while the black solid line represents the mean fluctuation and the black dotted line representing median fluctuation caused by the perturbation mechanism

Figure 4.8a shows the pressure drop time series data for particle volume concentration of 0.5%. The time is non-dimensionalized using the bulk velocity of the fluid and pipe diameter as given in equation 4.4. The current data is recorded for Re = 2032 and it corresponds to an intermittency of 10.6 %. Different signatures can be seen in the figure including the pressure fluctuation due to the perturbation mechanism and the turbulent puffs. The flow displays spatio-temporal intermittency as evidenced by appearance of occasional puffs. This is also in line with the Moody plot for ϕ = 0.5%, as the transition is sub-critical in nature. The figure also indicates the length of the typical puff observed in the flow. The length of puffs shown in the figure is found to be consistent across the entire time series and also with the length scales reported in literature. A total of 38 puffs were recorded in the entire duration of this measurement. Figure 4.8b shows a typical turbulent puff recorded for ϕ = 0.5%. The average length of the puffs are estimated to be 34 D. The pressure drop increases to a maximum of 3.42 Pa as it crossed the first pressure sensor while a mean sub-laminar pressure drop 2.46 pa is recorded as the puffs advects past the second pressure sensor. The unperturbed flow remained

laminar for $\phi = 0.5\%$ for the Reynolds number at which the current data is recorded. This further reinforces the fact that the transition is influenced by external perturbation rather than the disturbances induced by the particles.

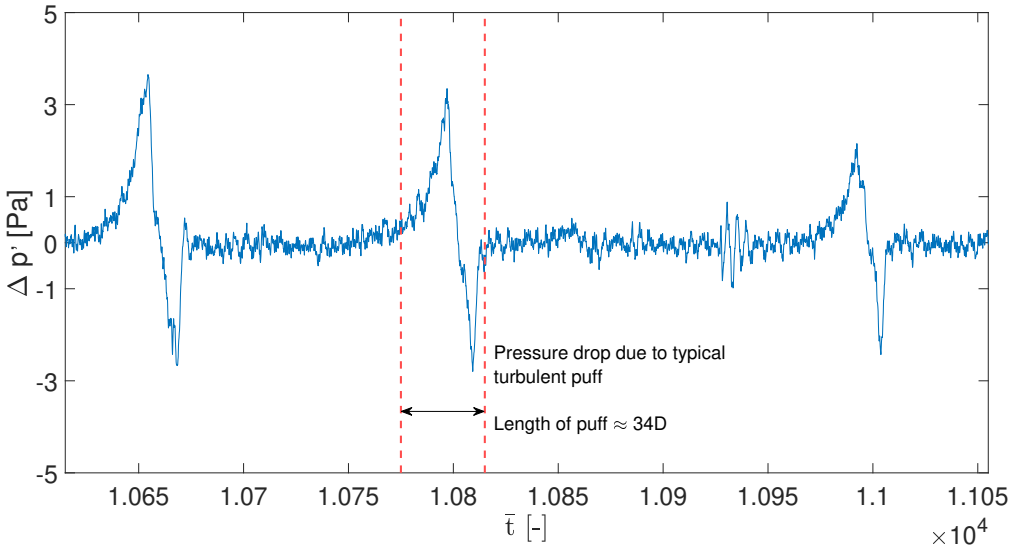

(a) Pressure drop time series indicating the pressure fluctuations ($\Delta p'$) due to the perturbation mechanism and the puffs. The flow corresponds to particle concentrations of $\phi = 0.5\%$ shows spatio-temporal intermittency while the transition is sub-critical

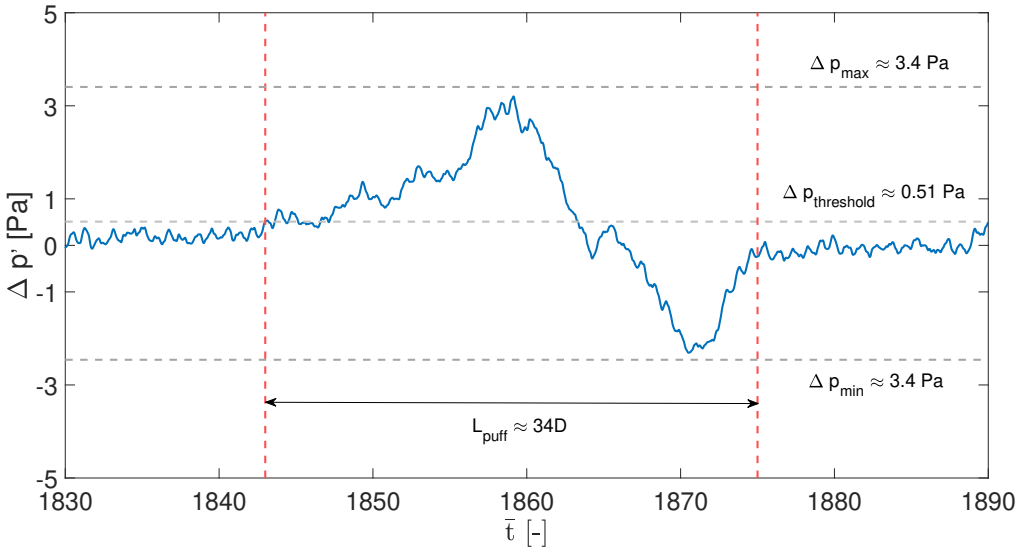

(b) Pressure drop in a typical turbulent puff. The flow corresponds to particle concentrations of $\phi = 0.5\%$. The threshold for identifying a puff is shown along with the maximum and minimum pressure drop observed in puffs. The maximum and minimum pressure drop in the puffs are calculated based on statistics collected for all the puffs

Figure 4.8: (a) Arbitrary segment of time series of pressure fluctuations ($\Delta p'$) recorded to obtain statistical information of puffs (b) Typical structure of a turbulent puff

It is important to analyse Figure 4.9 and Figure 4.10 together to understand the impact of particles on the pressure fluctuations. Figure 4.9 shows the pressure drop recorded for perturbed flow with particle concentration of $\phi = 1.5\%$. The flow displays intermittent behavior similar to the case of $\phi = 0.5\%$ alongside other fluctuations. These intermittent puff-like structures displays similar length-scales as mentioned previously. However, the length-scale of puffs recorded for $\phi = 1.5\%$ are slightly lesser than those recorded for $\phi = 0.5\%$ and shows greater variation within the duration of measurement. This suggests potential interaction between the turbulent puffs and the particles advecting through them. However, flow visualization is required to confirm this hypothesis. A total of 93 incidents of pressure fluctuations were recorded during the measurement.

The length of turbulent puffs is measured when pressure fluctuations crossed a threshold of *0.43 Pa*. The puffs have a maximum pressure drop of *2.88 Pa* and a sub-laminar pressure drop of *1.63 Pa*. The values of maximum and sub-laminar pressure drop for puffs recorded for $\phi = 1.5\%$ is less than the corresponding values calculated for $\phi = 0.5\%$. This can also be attributed to the interaction of particles and turbulent puffs. The pressure drop signal also shows other fluctuations that are caused by the particles. These disturbances are markedly different to the typical signature of a turbulent puff. Furthermore, these signatures do not correspond to decaying puffs as the probability of survival of a turbulent puff is close to 96 % for non dimensional time of 250 [5]. The puffs are recorded for $\phi = 1.5$ % and Re = 1924 and they crossed the pressure sensors at $\bar{t} \approx 210$. Equation 4.4 formulates the non-dimensional time used above.

$$\bar{t} = \frac{ut}{D} \tag{4.4}$$

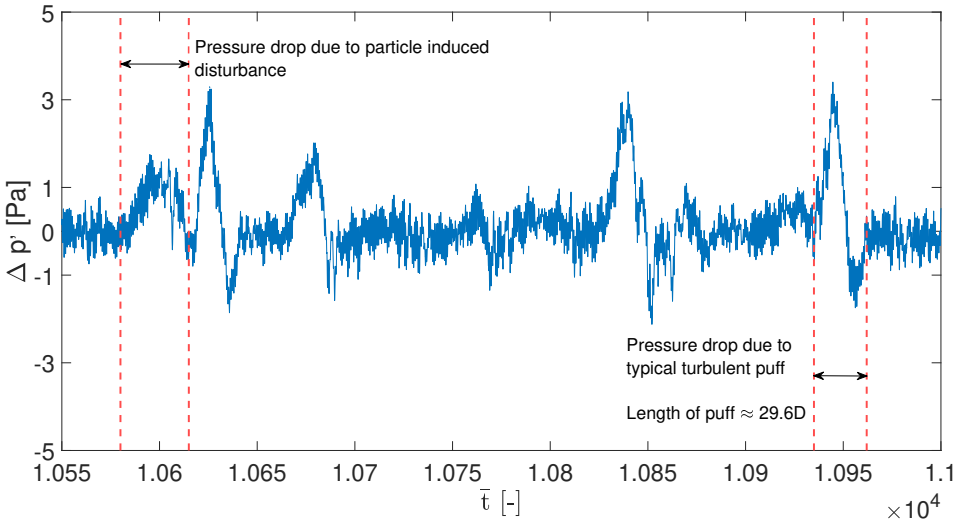

Figure 4.9: Pressure drop time series indicating the pressure fluctuations ($\Delta p'$) due to the perturbation mechanism and the puffs. The flow which corresponds to particle concentrations of $\phi = 1.5\%$ shows spatio-temporal intermittency as well as fluctuations due to presence of particles

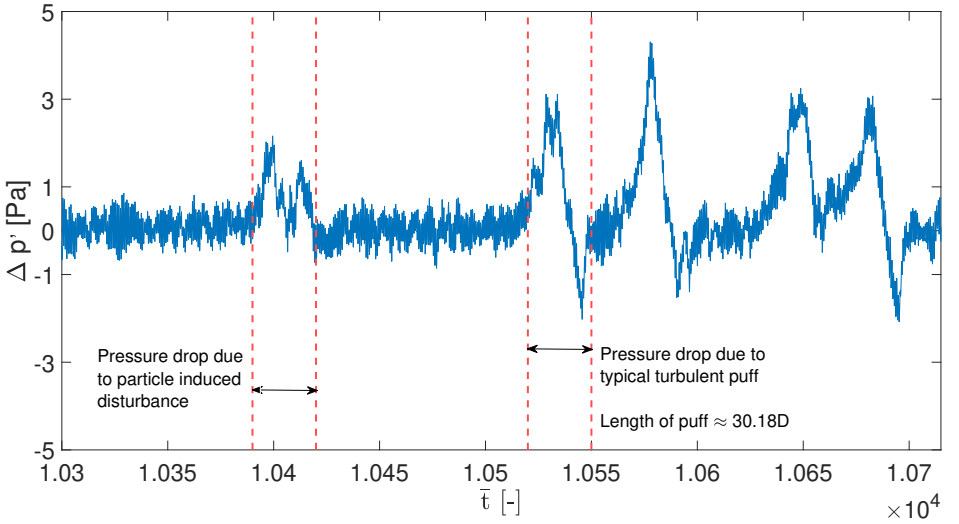

Figure 4.10: Pressure drop time series recorded across 10 D indicating the pressure fluctuations ($\Delta p'$). The flow corresponds to particle concentrations of $\phi = 1.5\%$ shows spatio-temporal intermittency as well as fluctuations due to presence of particles. This indicates that the particles have similar impact on transition as evidenced by data from the Moody diagrams

Figure 4.10 shows the pressure drop time series for unperturbed flow and it is clear that the flow displays intermittent behavior similar to perturbed condition even in the absence of external perturbation. This indicates that the particle concentration is large enough that the disturbance created in the flow by particles and the perturbation mechanism are qualitatively similar. This provides further evidence that the particle induced disturbance is qualitatively similar to external perturbation in addition to the Moody diagrams. While the length-scale, maximum and sub-laminar pressure drop is different from $\phi = 0.5$ %, the structure of turbulent puffs observed for $\phi = 1.5$ % is similar to figure 4.8b.

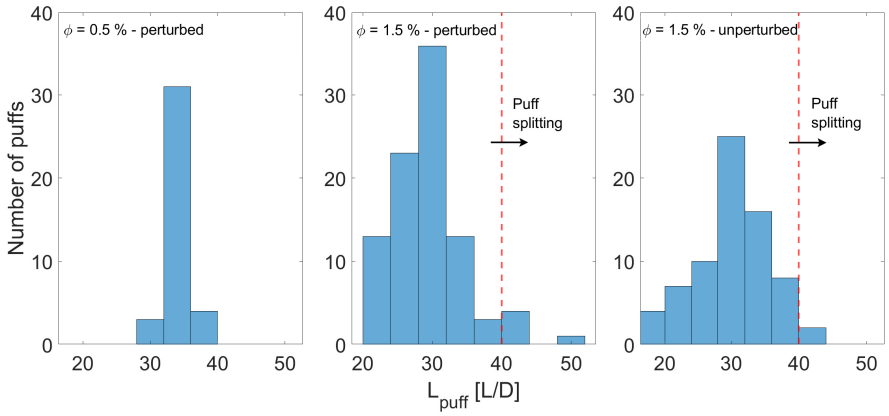

Figure 4.11: Comparison of length-scales of puffs recorded for $\phi = 0.5$ % and $\phi = 1.5$ %. The length-scales of the puffs are higher and showed lower variation for lower particle concentrations. The length-scales for puffs are similar for perturbed and unperturbed cases for $\phi = 1.5$ %

Figure 4.11 shows the typical length-scale of the puffs recorded for different particle concentrations. It can be seen that the puffs recorded for $\phi = 0.5$ % shows lower variation in the length-scale of puffs compared to $\phi = 1.5$ %. Furthermore, the fact that similar length-scales and its variation being observed for perturbed and unperturbed condition indicates that the intermittency is caused by the particles and the perturbation mechanism does not have any impact in transition. Puff splitting is also observed for $\phi = 1.5$ % which are characterized by $L_{puff} \geq 40$ D. This is the result of operating at a higher intermittency compared to $\phi = 0.5$ %. One such splitting event is shown in figure H.1 in Appendix H.

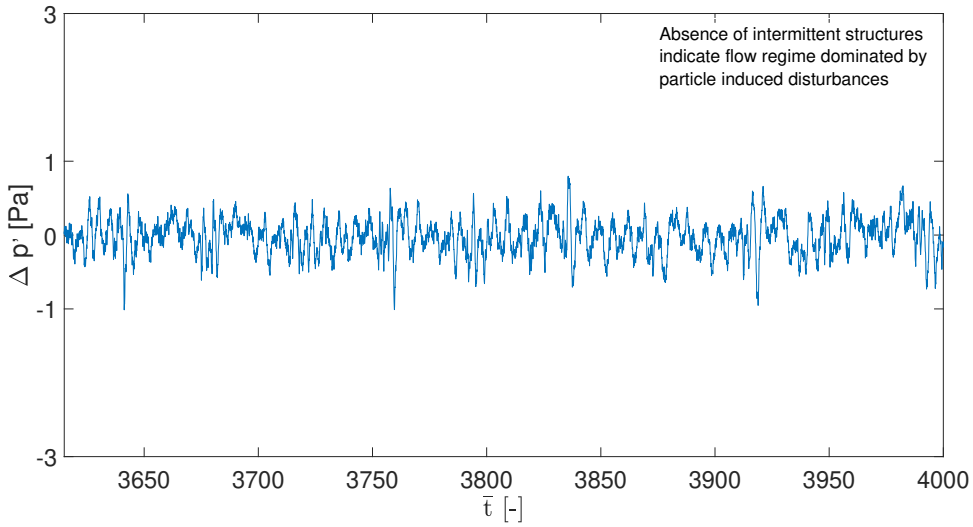

Figure 4.12: Pressure drop time series recorded across 10 D indicating the pressure fluctuations ($\Delta p'$). The flow corresponds to particle concentrations of $\phi = 7.5$% shows no spatio-temporal intermittency. This indicates that the particles induced disturbance dominates transition behavior as evidenced by data from the Moody diagrams

Figure 4.12 shows the pressure fluctuations for $\phi = 7.5\%$. A significant difference that can be observed is that, there is no spatio-temporal intermittency in the flow. The flow is devoid of turbulent puff-like structures and the particle induced fluctuations. This indicates that the fluctuations are global in nature and that the transition is driven by the particle induced disturbances. Furthermore, it is important to understand that the trend of growing global fluctuations was first observed for $\phi = 3\%$ upto $\phi = 15\%$. This is relevant because, the friction factor monotonically decreased only for $\phi = 15\%$, while there is a local minima for other particle concentrations analyzed. This indicates that the monotonic behavior is perhaps due to the drag reduction in addition to fluctuations induced by the particles. This further points out that, at high particle concentrations, the additional friction generated due to the presence of the particles dominate the small scale fluctuations created by the advection of particles through the flow.

4.4. critical Reynolds number

The final section collates data from the Moody diagrams and the pressure fluctuations to analyze some of the transition criteria discussed in section 2.1.2. Since the current work uses only pressure drop based measurements, the pressure fluctuations and deviation of friction factor from the Poiseuille line in the Moody diagram will be used to compare results.

The figure 4.13 shows the mean pressure fluctuations at different Re for different particle concentrations. The pressure fluctuations shown in the figure are obtained by calculating the standard deviation of the pressure drop measured across 10D. The plot compares trend in the mean pressure fluctuations for different particle concentrations to correlate it with the behavior observed in the Moody plots.

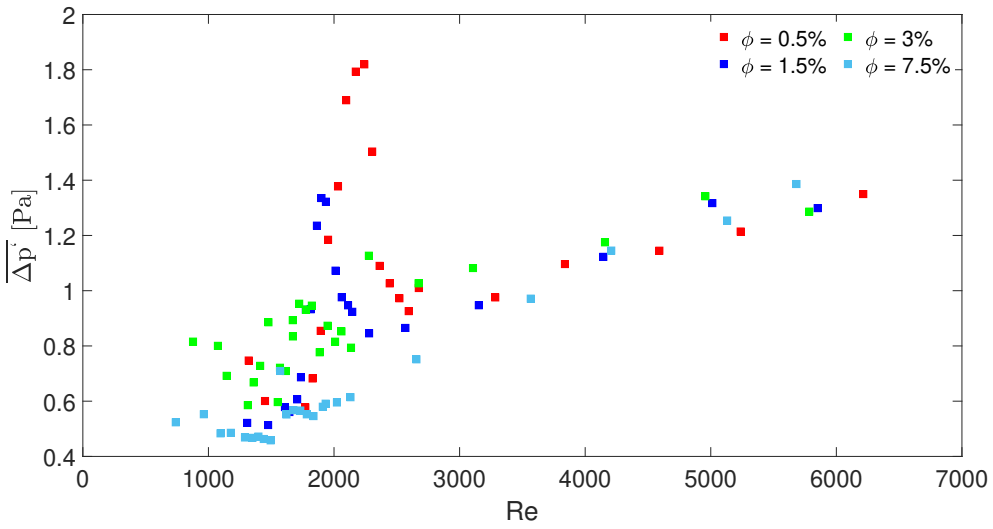

Figure 4.13: Pressure fluctuations (calculated as standard deviation of pressure drop across 10D) plotted for different Reynolds number and particle concentrations. The sudden increase in pressure fluctuations indicate intermittent behavior of the flow

The pressure fluctuations shown here are not normalized and therefore the fluctuations generally increases due to increase in mean pressure drop and uncertainty of the measurement system. The particle concentrations of $\phi = 0.5\%$, $\phi = 1\%$ and $\phi = 1.5\%$ displays sub-critical transition behavior as evident from the Moody diagram in figure 4.3. This is indicated as the sudden increase in the pressure fluctuations in the flow. This can be explained by the intermittent behavior of the flow as the flow regime alternates between laminar and turbulent states. As the intermittency increases, the flow is predominantly covered by turbulent puffs while there are small regions of laminar flow. This reduces the pressure fluctuations which can be seen in the figure. Once the flow becomes completely turbulent the pressure fluctuations increases gradually for the reasons mentioned previously. It can also be seen from the figure that the pressure fluctuations show no visible spike for particle concentrations $\phi = 3\%$ and $\phi = 7.5\%$. The fluctuations increase monotonically as the Reynolds number increase. This provides further evidence to the fact the flow regime displayed no spatio-temporal intermittency.

Another important observation to be made is the reduction in the maximum value of pressure fluctuations for increasing particle concentration. The onset of transition occurs at lower Re for increasing ϕ. This results in lower magnitude of pressure drop and consequently the magnitude of the pressure fluctuations also reduced. It should also be understood that the pressure fluctuations rise at the onset of turbulence. The peak value of the pressure fluctuations corresponds to the Reynolds number where the intermittency is approximately 25%. Therefore, the critical Reynolds number should be identified based on the point where the pressure fluctuations increases sharply and not the point where it reaches its maximum value.

Figure 4.13 aims to compare the transition criteria used by Matas et al [10]. The study used pressure spectrum to identify spikes in low frequencies indicating intermittent behavior of the flow. The critical Reynolds number calculated using pressure spectrum yielded a decreasing Re_c up to $\phi = 10$ % after which Re_c remained unchanged. The transition behavior shown in figure 4.14 is compared with results obtained by Matas et al for $D/d = 16$. The current findings are in agreement with the observations made by Matas et al. for low particle ($\phi \leq 1.5\%$) concentrations where sub-critical transition is observed. However, it is evident from figure 4.13 that Re_c cannot be computed from the pressure fluctuations or the pressure spectrum directly, as super-critical transition is observed when ϕ is increased. This suggests that the criterion is not applicable to high particle concentrations where there is no intermittent behavior.

The next analysis is based on Moody diagram wherein the flow is considered to be in transition regime when the friction factor is more than 10 % higher than the value corresponding to Poiseuille line ($f \geq 1.1\ f_{lam}$). This criteria is based on the evidence that the flow remains free from fluctuations in laminar regime and therefore friction factor falling on the Poiseuille line. Consequently, as the flow becomes intermittent, the friction factor increases and thus deviating from the Poiseuille line. Figure 4.14 shows the variation of critical Reynolds number for different particle concentrations for perturbed and unperturbed flow. It can be observed that the difference in Re_c for perturbed and unperturbed condition becomes insignificant at higher particle concentrations. This is demonstrated using the Moody diagrams and is explained using the pressure fluctuations in section 4.3.

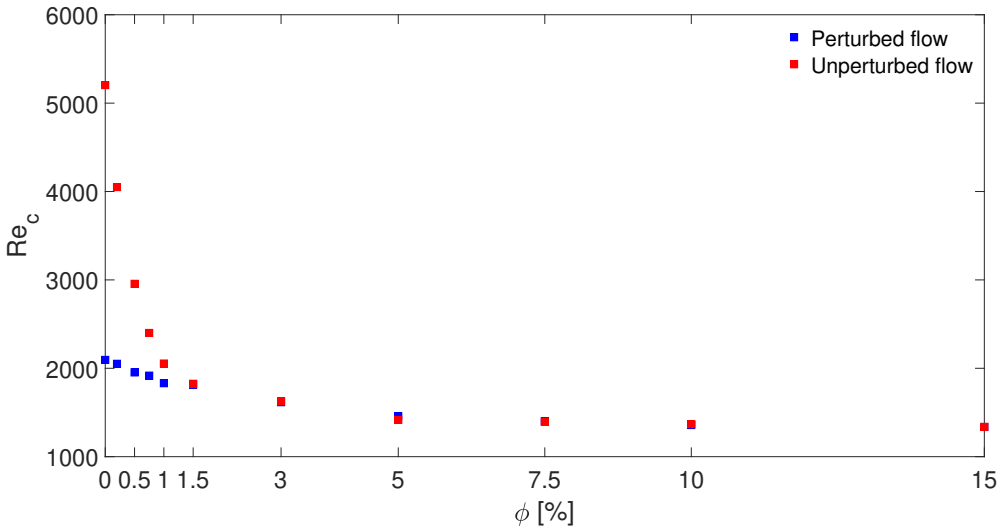

Figure 4.14: critical Reynolds number for different particle concentrations for perturbed and unperturbed condition. The transition becomes similar for higher particle concentrations indicating particle induced transition

This transition behavior can be compared to results obtained by Agarwal et al [14]. where the effect of particles with D/d = 19.6 was studied. The critical Reynolds number (adjusted for particle concentration) decreased as the particle concentration is increased and this behavior is in line with the findings from the current work. However, the transition criterion used by Agarwal et al. suffers from the same pitfalls as the criterion used by Matas et al [10]. The study conducted by Agarwal et al used the pressure fluctuations normalized with the standard deviation due to background noise. This is similar to the parameter shown in figure 4.13 and therefore has the same shortcomings. The pressure fluctuations increases smoothly for high

particle concentrations without a significant peak. As the criterion used the inflection point in the pressure fluctuations to determine the critical Reynolds number, it makes estimation of Re_c difficult for high particle concentrations where pressure fluctuations increased gradually.

The criterion used in the current work do not have the aforementioned shortcomings. The critical Reynolds number shown in figure 4.14 matches with the point where the flow displayed spatio-temporal intermittency for $\phi \leq 1.5\%$. This indicates that the criteria can estimate the point of transition when it is sub-critical. The criteria is not straightforward for $\phi \geq 3\%$ as there is no intermittency. However, the criteria holds good as the transition is driven by particle induced disturbances and additional friction generated by the particles. While this criterion is arbitrary in nature, it indicates the point where the flow deviates from laminar behavior. This is important because criteria using pressure spectrum cannot detect the point where the flow deviates from laminar regime when the transition becomes super-critical. It is also important to understand that D/d affects the onset of transition and the ϕ where transition becomes super-critical. Therefore, other D/d ratios need to be analyzed to ascertain the validity of the criteria. Furthermore, scaling laws will be required to understand and predict the transition behavior by formulating an expression relating f, D/d, ϕ and Re.

5

Conclusions and recommendations

The current chapter summarizes the experimental setup used for the experimental campaign along with the methodologies used for the measurements. The chapter further details the conclusions drawn from the results of the experiments conducted. Finally, some recommendations for future research are suggested at the end of the chapter.

5.1. Summary and conclusions

The experimental setup was constructed to study the impact of particles on transition in pipe flow. Pressure drop measurements were used to analyze the transition behavior with the help of Moody charts. The flow was perturbed by an active mechanism where the amplitude and frequency of perturbation could be controlled individually. The perturbation mechanism used in the setup was zero net mass injection/extraction mechanism where jet of the fluid was injected and extracted. The single phase measurement was performed with water-glycerol mixture where the setup was validated up to Re ≈ 9600. Polystyrene particles with a mean diameter of 1.3 mm (*D/d =15.4*) were used for the multi-phase experiments. The particle concentrations that were studied ranged from ϕ = 0.2% to ϕ = 25%. The measurements were used to plot Moody diagrams for perturbed and unperturbed condition. Finally the transition Reynolds number was estimated using two different criteria and was compared against each other.

The results from the measurements for single phase flow validates the apparatus used for the experiment. The parameters used for the perturbation mechanism triggers transition at $Re \approx 2000$ while the flow becomes fully turbulent at $Re \approx 3000$. The parameters like perturbation amplitude and frequency used for this particular case is used for multi-phase experiments as well. Results from the Moody diagrams indicates that the transition is sub-critical for particle concentrations up to ϕ = 1.5%. However the transition behavior for ϕ = 1.5% is identical for perturbed and unperturbed condition. Furthermore, the transition is triggered earlier as the particle concentration is increased. The flow displays super-critical transition behavior for $\phi \geq 3\%$ where the fluctuations increases globally as the Reynolds number increases and the flow becomes turbulent. The transition is triggered earlier for increasing particle concentration until ϕ = 10% after which the friction factor deviates from the Poiseuille line at similar Reynolds numbers. It should be noted that, while super-critical transition is observed for $\phi \geq 3\%$, the friction factor decreases monotonically only for $\phi \geq 15\%$.

Intermittent structures are observed for ϕ = 0.5% and ϕ = 1.5% in the time series of pressure drop recorded for 10D. These structures are also observed for unperturbed flow in case of ϕ = 1.5% providing evidence for the identical transition behavior seen in the Moody diagram. No such behavior is observed for ϕ = 7.5% where the fluctuations seems to increase globally as Re increases. The length-scales of turbulent puffs are compared for ϕ = 0 % and ϕ = 0.5 %. The puffs are shorter and less intense for ϕ = 0.5 % suggesting interaction between the particles and the puffs. There are no differences in the length-scales for perturbed and unperturbed cases. Puffs splitting is observed for ϕ = 1.5 % which is indicated by $L_{puff} > 40$D.

The pressure fluctuations ($\overline{\Delta p'}$) are plotted as function of Reynolds number for different particle concentrations. It is estimated by calculating the standard deviation of pressure drop measured across 10D. A

sudden spike in $\overline{\Delta p'}$ is observed for cases of sub-critical transition which is explained by the fact that the flow alternates between laminar and turbulent states. The peak of $\overline{\Delta p'}$ corresponds to an intermittency of 15%. This behavior is absent for $\phi \geq 3\%$, where $\overline{\Delta p'}$ increases gradually as the flow deviates from laminar state. The transition Reynolds number is difficult to identify using the pressure fluctuations as there is no peak in the pressure fluctuations when the transition is super-critical. it is for this reason, the criteria using pressure fluctuations or pressure spectrum cannot be used determine transition Reynolds number for all particle concentrations. When the transition Reynolds number is calculated based on the friction factor, it matches with the points where the flow becomes intermittent. At high particle concentrations the friction factor deviates from the Poiseuille line in the Moody chart due to added friction by the particles. Therefore, the criteria holds good for the super-critical transition as the behavior shifts towards particle induced disturbances. However, this needs to be revisited for particles with different *D*/*d* ratios as the behavior was different for different *D*/*d* ratios.

5.2. Recommendations

The current work focused on performing multiphase experiments with a single *D*/*d* to understand the transition behavior. Further research must be performed to gain more understanding on this topic. Some recommendations based on the gaps found in the current research are given below.

The current work studied the impact of particles of diameter $\approx$ 1.3 mm and thus yielding a single *D*/*d* ratio. In order to understand the impact of particle in transition behavior, it is imperative to vary ϕ and *D*/*d*. This is particularly important as the particles disturb the flow with its wake as it gets advected. The particles can add additional friction to the flow and also can dampen some of the fluctuations in the flow depending on the size and concentration. Secondly, the transition behavior can be classified into four separate conditions: (a) Particles triggering earlier sub-critical transition when the flow was perturbed externally, (b) Sub-critical transition triggered by the particles without the use of perturbation mechanism, (c) Super-critical transition triggered by the particles with the friction factor decreasing non-monotonically, (d) Super-critical transition triggered by the particles with the friction factor decreasing monotonically. These regimes can be better understood by investigating with measurement techniques like Ultrasound Image Velocimetry (UIV), Magnetic Resonance Velocimetry (MRV) in conjunction with the data obtained from the pressure drop measurements. Furthermore, the puff statistics can be collected for more particle concentrations to study its effect on the length-scales and intensities of turbulent puffs. This will shed light on the reduction in length-scale and intensity of turbulent puffs observed in current study. Finally, puff statistics can be collected for longer duration and at different *L*/*D* to understand the impact of particle size and concentration on phenomena lie puff decay and puff splitting. This can provide additional insight into transition behavior as puff splitting is observed at lower Re in the current study when compared with results from literature.

A

Calibration of pressure sensor

As mentioned previously, two different pressure sensors were used to measure pressure drop in the flow. The pressure drop was calculated based on the voltage output resulting from the change in inductance in the coils. Therefore the calibration process of the sensors included comparing the voltage output from the demodulator to a known value. In order to achieve this, one end of the pressure sensor was connected to a pressure source (syringe) and one end of a manometer. The other end of the sensor and the manometer were exposed to atmosphere. This implied that the measured pressure is the pressure difference between the pressure applied through the syringe and the atmosphere. The pressure applied through the syringe increases the water level in the manometer. This rise is water level leads to increase in hydrostatic pressure which is also measured by the pressure sensor. The output of the demodulator was connected to a digital multimeter. The equipment used for calibration can be seen in figure A.1. The components are annotated and their purpose is explained for better clarity.

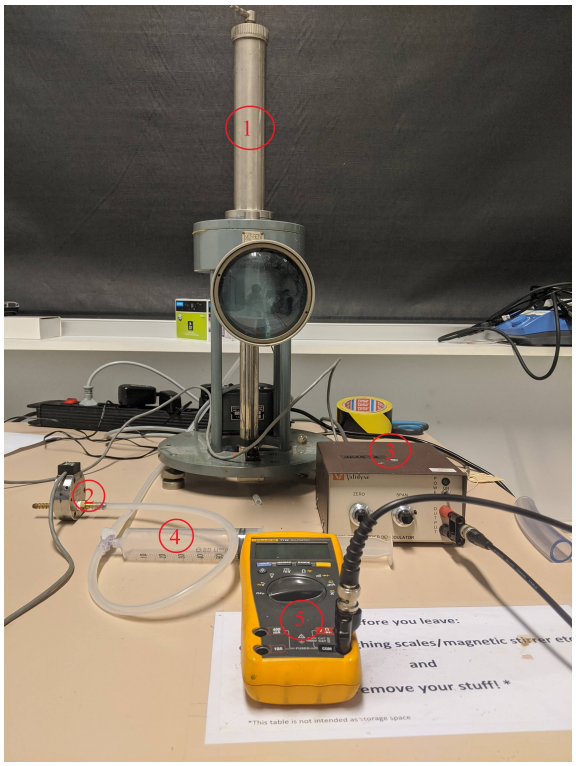

Figure A.1: Setup used for calibrating the pressure sensors. (1) Manometer with manual readout through the magnifying lens in the front (2) Pressure sensor to be calibrated (3) CD-15 demodulator used to convert the signals from the sensor to DC output (4) Syringe used to apply pressure drop to the positive side of the sensor and manometer (5) Multimeter used to record voltage readings from the demodulator

The level of the manometer reading was ensured to be zero along with the voltage output when no pressure was applied through the syringe. At this point the span was also set to zero. Then, pressure was applied through the syringe to the desired maximum pressure. The maximum pressure was estimated using preliminary calculations made using the measurement plan drawn up before starting the experiments. At this point the span was set to get *10 V* in the multimeter. After this step the zero value and the voltage at the maximum pressure was ensured to remain with 0 - 10 V by adjusting the knobs *zero* and *span* while varying the pressure applied through the syringe. Once this step was performed, the pressure was slowly increased in steps and the corresponding voltage values were recorded. A linear relationship is expected between the applied pressure and voltage and the the plots shown in figure A.2 indicate the same.

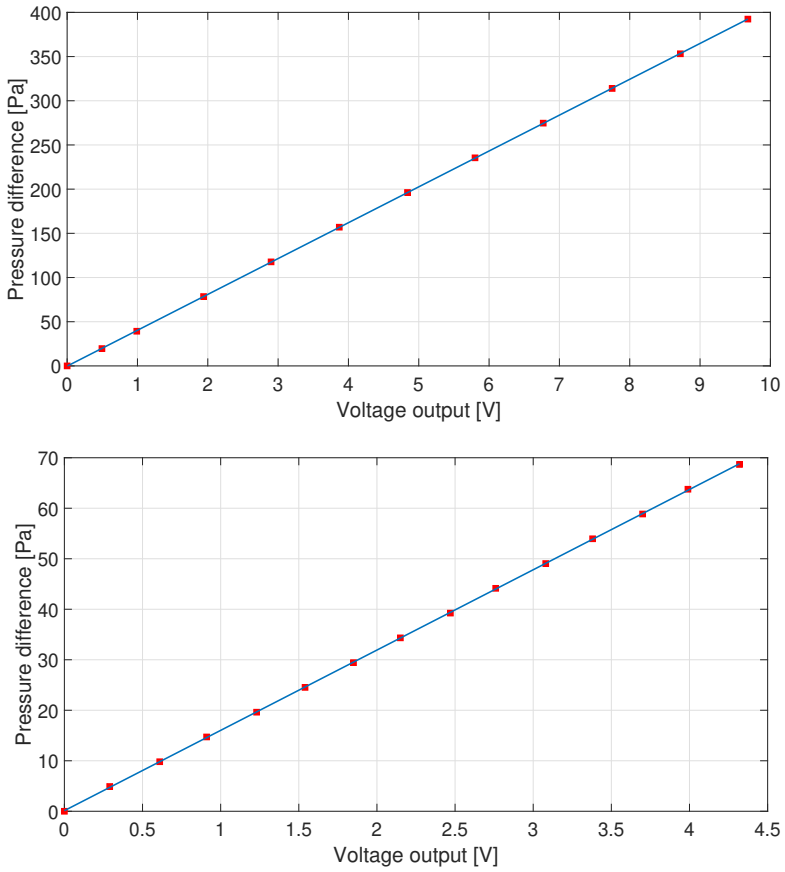

Figure A.2: (a)Calibration curve of DP 45-*'20* used to measure pressure drop across 75D. The sensor was calibrated up to 400 Pa (b) Calibration curve of DP 45-*'14* used to measure pressure drop across 10D. The sensor was calibrated up to 70 Pa

B

Particle size characterization

The experiments made use of polystyrene (Synthos) particles with an average diameter of *1.3 mm*. It was important that the particle diameter was characterized because the primary objective of this thesis is to understand the impact of particle size and concentration on the transition behaviour. Therefore, the diameter of select number of particles was measured by taking images of particles using a camera. The camera used for this purpose was a sCMOS camera from LaVision. The sensor has *2560 X 2160* pixels in total and each measuring *6.5 μm X 6.5 μm*. The lens used for capturing the images is *NIKKOR - Z 105 mm*. Before taking images of the particles, it was imperative that the image from the camera was calibrated against a reference. For this purpose, a calibration sheet with markings of known dimensions was used. The figure B.1a shows the calibration sheet placed on a petri dish.

(a) Petri dish used for calibrating the camera before taking images of the particles

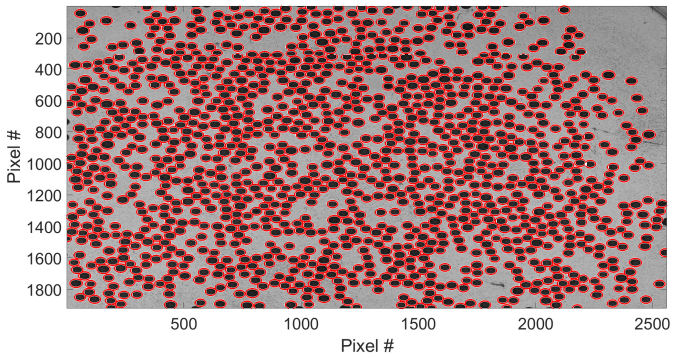

(b) Raw image with the particles identified using Matlab code showing the average number of particles used for the experiment

Figure B.1: (a) Calibrations sheet with markers used before taking images of the particles (b) Typical sample size of particles used for each image. 12 sucj samples were used to obtain the particle size distribution

The calibration sheet was marked with crosses that are *5 mm* apart. The calibration sheet was imaged in order to the calculate the magnification of the lens. The number of pixels between the markers in the calibration sheet was found to be 183. Using equation B.1, the magnification was calculated to be *0.238*. The focal length and *f#* were decided in order to have maximum resolution when imaging the particles. The parameters used during calibration yielded a resolution of *47.5* pixels per particle where the average particle diameter was estimated to be *1.3 mm*.

$$M = \frac{Pixel\ size\ in\ sensor}{Pixel\ size\ in\ image} \tag{B.1}$$

Once the lens is calibrated, the calibration sheet is removed and particles are added such that there is no overlapping between them. A total of 12 sets of particles are imaged to achieve convergence. The particles are taken after manually mixing the particles in order to avoid any bias. Before adding to the petri dish, the

particles sieved using sieves of diameters *1.2 mm* and *1.6 mm* to remove very large/small particles. The figure B.1b shows the average number of particles imaged in each set.
The imaged particles were then identified using matlab based on the difference in intensity in the image. The diffraction diameter was calculated based on equation B.2.

$$D_{diff} = 2.44\lambda f_{\#}(M+1) \tag{B.2}$$

The figure B.2 shows the average particle diameter in the form of a gaussian. The mean particle diameter was calculated to be *1.31 mm*. The skew towards higher diameter could be explained due to the use of the dimensions of the available sieves.

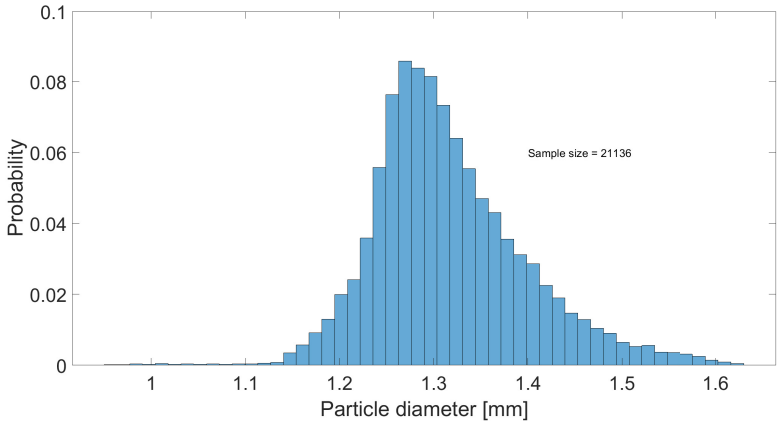

Figure B.2: Particle size distribution indicating the average particle diameter and the total number of particles used for this study. The mean particle diameter was found to be 1.31 mm

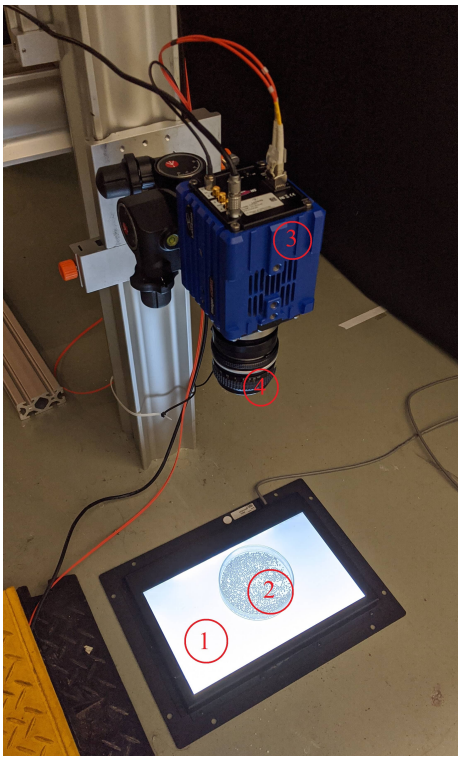

Figure B.3: Calibration setup used for the study (1) LED for backlight (2) Particles in the petri dish to be imaged (3) Camera from LaVision with a CMOS sensor (4) NIKKOR - Z 105 mm lens used for imaging the particles

C

Particle density estimation

Once the average particle size was determined, the density of of these particles needed to be estimated. A simple experiment was conducted for this purpose. Two identical glass jars were filled with different ratios of glycerine and water. The ratios were pre-determined and thus the effective density could be calculated based on equation C.1.

$$\rho_{mix} = \frac{m_w \rho_w + m_g \rho_g}{m_g + m_w} \tag{C.1}$$

Particles were then added to the jars and mixed using a magnetic mixer. In order to reduce the surface tension *1 g* of Twene was also added to the suspension. The particles were left overnight in the sealed jars to allow them to absorb water. This step was crucial to mimic the experimental conditions as the particles that were added while performing experiments remain in the system for the entire experimental campaign and thus would absorb water and thereby changing the density. Once the suspension was kept undisturbed for a day, the solution was agitated using the magnetic mixer until particles were homogeneously mixed with the suspension. The heights of the particles floating and sinking were measured after few hours. The ratio of height was used to calculate the mean and standard deviation in the particle density. This was made possible by assuming a Gaussian distribution for particle density.

The figure C.1 shows the containers with which the ratio of heights was calculated. Since the assumed distribution was Gaussian and that the density of the fluid was known, the mean and standard deviation of the particle density could be calculated. The expression describing a Gaussian function is given by the equation C.2.

$$h_r = \frac{0.5\left(1 + erf\left(\frac{\rho_{mix} - \rho_{p,m}}{\sqrt{2}\rho_{p,\sigma}}\right)\right)}{1 - 0.5\left(1 + erf\left(\frac{\rho_{mix} - \rho_{p,m}}{\sqrt{2}\rho_{p,\sigma}}\right)\right)} \tag{C.2}$$

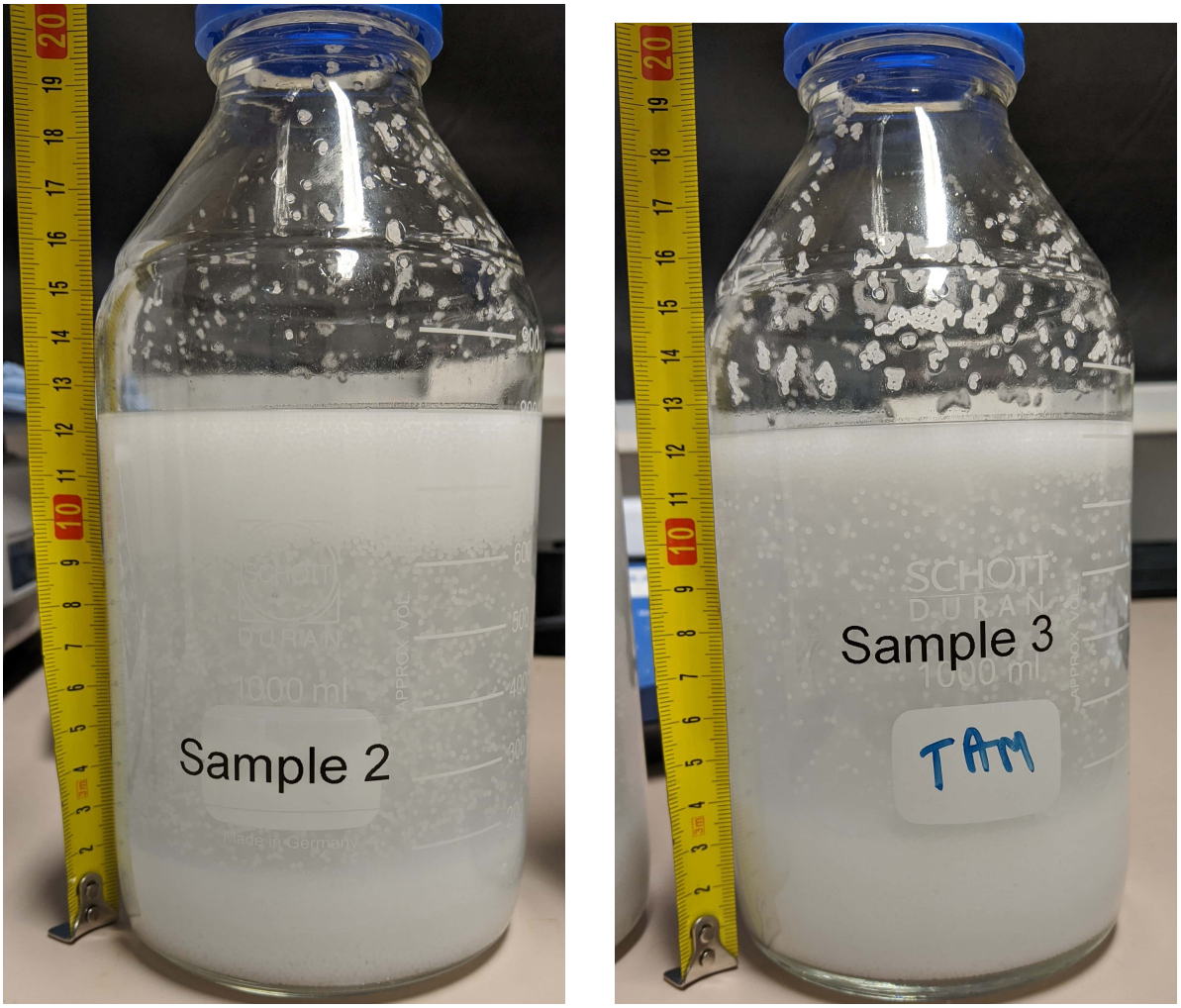

Figure C.1: The height ratio was calculated based on the heights measured using a measurement tape as shown in the figure

Since h_r can be determined for the 2 cases as shown in figure C.1, the mean and standard deviation in density of the particles can be estimated by solving the system of linear equations. The mean and standard deviation of the particles were estimated as $1033.4 kg/m^3$ and $1.4 kg/m^3$ respectively.

D

Experimental procedure

In order to perform the experiments in an efficient way and minimise errors, a strict protocol was followed when conducting experiments. The section lists the measures taken while setting up the experiment and procedure followed while performing them.

1. Before starting the pump, the pressure ports and the injection ports were inspected to check presence of air bubbles and/or particles. The tubes connecting the pressure sensor to the pipes were also inspected for presence of air bubbles. If found, the bubbles were made to reach the tip of the pressure ports.

2. The pump was turned ON and the head was raised to provide mass flux of *5 L/min* approximately. The return tank was well mixed if experiments are conducted with particles. The pump was run for 10 - 15 minutes to ensure the system was well mixed. While performing this step, any air bubbles/particles trapped at the pressure ports were removed.

3. The air bubbles were removed by flushing through the pipe to the return tank. The flow meter was placed in the return section on the ground while the return tank was placed at a higher level. The flow meter was lifted in order to flush the bubbles and prevent them being stuck in the flow meter. This is very important as air bubbles in the flow meter results in erroneous reading for density and mass flow rate.

4. The flow was stopped by closing the valve and the pump was switched OFF. The head was then reduced to the required level and the zero reading of the pressure sensors was checked and set properly. When starting experiments for a new particle concentration, the system was ensured to be neutrally buoyant. The particles were monitored for 4 minutes and if their displacement in radial direction was negligible the system was considered neutrally buoyant. Otherwise, water or glycerol was added to adjust the density and this step was repeated.

5. The pump was then switched ON and the valve opened to take measurements. Once the valve was opened, measurements were taken after a duration of 2 minutes in order to achieve a stable reading for pressure drop and flow rate.

6. The measurements were taken using a Labview interface where the pressure drop, temperature and mass flow rate was recorded. The duration of measurement was dependent on the flow regime as transition regime required a longer measurement time (5 minutes) in comparison to laminar and turbulent regime (2 minutes).

7. The perturbation mechanism was switched ON and the program was run for 30 s approximately to account for the advection of the first puffs to the pressure sensors. Failing to do so will give an not provide the correct value of pressure drop for the given Reynolds number and particle concentration.

8. As the perturbation mechanism had a small residual voltage after every injection/extraction stroke, the DC motor continues to rotate at a very small speed. Therefore, after taking 5 measurement points with the perturbation mechanism the linear guide was ensured to be within its range.

9. The head was raised for increasing the flow rate and consequently the Reynolds number of the flow. After increasing the head, the measurements are taken after a time gap of 2 minutes to allow the flow to stabilize and the measurements to be constant.

10. Once the measurements were complete, the head was reduced slowly without closing the valve. This was done to ensure the sudden closure of the valve did not damage the membrane in the pressure sensor.

11. The valve was closed and the pump was stopped. The frequency controller was switched OFF along with the perturbation mechanism.

E

Uncertainty analysis

The uncertainty analysis was performed for parameters like pressure drop and Reynolds number. The uncertainty in individual parameters are listed below.

- Uncertainty in pressure:
  1. Accuracy of sensor ($u_{1,pr}$) = ± 2.05 Pa
  2. Average repeatability for measurement duration ($u_{2,pr}$) = ± 0.25 Pa
  3. Zero error ($u_{0,pr}$) = ± 0.15 Pa
- Uncertainty in measurement of ρ (u_ρ) = ± 2 kg/m^3
- Uncertainty in velocity measurement (u_u) = ± 1 % of measured value
- Uncertainty in calculating viscosity of water-glycerol mixture (u_μ) = 0.07 % of measured value

Error propagation analysis was performed to calculate the total error in pressure drop and Reynolds number.

The total uncertainty in estimation of pressure is given by:

$$u_{\Delta p} = \sqrt{((u_{1,pr})^2 + (u_{2,pr})^2 + (u_{0,pr})^2} \tag{E.1}$$

The friction factor is given by equation 1.4 while the Re using 1.3. The propagation of uncertainty from individual sources is shown below.

$$\frac{\partial f}{\partial \Delta p} = \frac{1}{0.5\rho u^2 (L/D)} u_{\Delta p} = \frac{f}{\Delta p} u_{\Delta p} \tag{E.2}$$

$$\frac{\partial f}{\partial \rho} = \left| - \frac{\frac{\Delta p}{2} u^2 (L/D)}{\left(0.5\rho u^2 (L/d)\right)^2} u_\rho \right| = \frac{f}{\rho} U_\rho \tag{E.3}$$

$$\frac{\partial f}{\partial u} = \left| - \frac{(\Delta p)\rho u (L/D)}{\left(0.5\rho u^2 (L/d)\right)^2} \right| u_u = \frac{2f}{u} u_u \tag{E.4}$$

The total error in estimation of f is :

$$u_f = f \left[\left(\frac{u_{\Delta p}}{\Delta p} \right)^2 + \left(\frac{u_\rho}{\rho} \right)^2 + \left(\frac{u_u}{u} \right)^2 \right]^{\frac{1}{2}} \tag{E.5}$$

Similarly the error propagation analysis was performed for parameters to estimate the overall uncertainty in determining *Re*.

$$\frac{\partial Re}{\partial \rho} = \left(\frac{uD}{\mu}\right) u_\rho = \frac{Re}{\rho} u_\rho \tag{E.6}$$

$$\frac{\partial Re}{\partial u} = \left(\frac{\rho D}{\mu}\right) u_u = \frac{Re}{u} u_u \tag{E.7}$$

$$\frac{\partial Re}{\partial \mu} = \left| -\frac{\rho u D}{\mu^2} \right| u_\mu = \frac{Re}{\mu} u_\mu \tag{E.8}$$

The total error in estimating *Re* is:

$$u_{Re} = Re\left[\left(\frac{u_\mu}{\mu}\right)^2 + \left(\frac{u_\rho}{\rho}\right)^2 + \left(\frac{u_u}{u}\right)^2\right]^{\frac{1}{2}} \tag{E.9}$$

F

Adjusted viscosity and density

The code used to calculate the density of water-glycerol mixtures for different concentrations of glycerol and temperatures is given below [36].

Listing F.1: Error computation in dgcl_BE.m and dgcl_BDF2.m

```
function [rho_s, mu_s] = densityViscosityWaterGlycerolSolution(w_g, T)
% Calculation of density of aqueous glycerol solutions.
%
%rho_s = rho_GlySol(T,w_g)
%
%rho_GlySol calculates the density of aqueous glycerol solutions based on
%measured data of [1] and [2]. As [1] only covers temperatures in the range
%15-30 C , the accuracy of <0.07% can only be proven for these temperatures.
%However, it is assumed that the calculation also gives a good approximation
%of the densitiy for temperatures in the range 0-100 C .
%
%     [1] L. Bosart and A. Snoddy, Industrial & Engineering Chemistry 20,
%         1377 (1928).
%     [2] P. Linstrom and W. Mallard, NIST standard reference
%         database (2005).
%     [3] N.S. Cheng, Industrial & engineering chemistry research 47(9),
%         3285  3288   (2008)
%
%Input arguments
%
%     w_g     weight fraction of glycerol in solution
%             [0.00-1.00]
%     T       Temperature in   C
%             [0-100] (<0.07% accuracy for 15-30)
%
%Output arguments
%
%     rho_s  density of aqueous glycerol solution in kg/m^3
%     mu_s   dynamic viscosity of aqueous glycerol solution in Ns/m^2
%
```

```
%Other used variables
%
%     a,b,c,A,alpha    coefficients for calculations
%     rho_w            density of water in kg/m^3
%     rho_g            density of glycerol in kg/m^3
%     contraction      volume contraction of solution
%     mu_w             dynamic viscosity of water in Ns/m^2
%     mu_g             dynamic viscosity of glycerol in Ns/m^2
%
% Authors: Andreas Volk, Chris Westbrook 21. November 2017
% andreas.volk[at]unibw.de, c.d.westbrook[at]reading.ac.uk

% error checking
if ~isnumeric(T) || max(T<0) || max(T>100)
    error('T must be in the range 0-100')
end

if ~isnumeric(w_g) || max(w_g<0) || max(w_g>1)
    error('w_g must be in the range 0-1')
end

%contraction (distorted sine approximation fitted to data of [1])
c=1.78E-6*T.^2-1.82E-4*T+1.41E-2;
contraction=1+(c.*sin((w_g).^1.31.*pi).^0.81);

%density of pure water (fitted to data of [2])
rho_w=1000.*(1-abs((T-3.98)./615).^1.71);

%density of pure glycerol (fitted to data of [1])
rho_g=1273-T*0.612;

%density of specific ww solution glycerol
rho_s=contraction.*(rho_w+(rho_g-rho_w)./(1+rho_g./rho_w.*(1./w_g-1)));

%empirical formulas for dynamic viscosities of water and glycerol [3]
mu_w=0.001*1.790*exp((-1230-T)*T/(36100+360*T));  %Ns/m^2, [3] equation
    (21)
mu_g=0.001*12100*exp((-1233+T)*T/(9900+70*T));    %Ns/m^2, [3] equation
    (22)

%empirical formulas for dynamic viscosities of water-glycerol mixtures
   [3]
a=0.705-0.0017*T;                                 %[3] equation (12)
b=(4.9+0.036*T)*a^2.5;                            %[3] equation (13)
alpha=1-w_g+(a*b*w_g*(1-w_g))/(a*w_g+b*(1-w_g));  %[3] equation (11)
A=log(mu_w/mu_g);                                 %Note this is NATURAL
    LOG (ln), not base 10.
mu_s=mu_g*exp(A*alpha);                           %Ns/m^2, [3] equation
    (6)

end
```

G

Moody chart - Multiphase flows

The Moody plots for multiphase flows for perturbed and unperturbed condition are shown below. The plots in figure G.1 show the results for all particle concentrations.

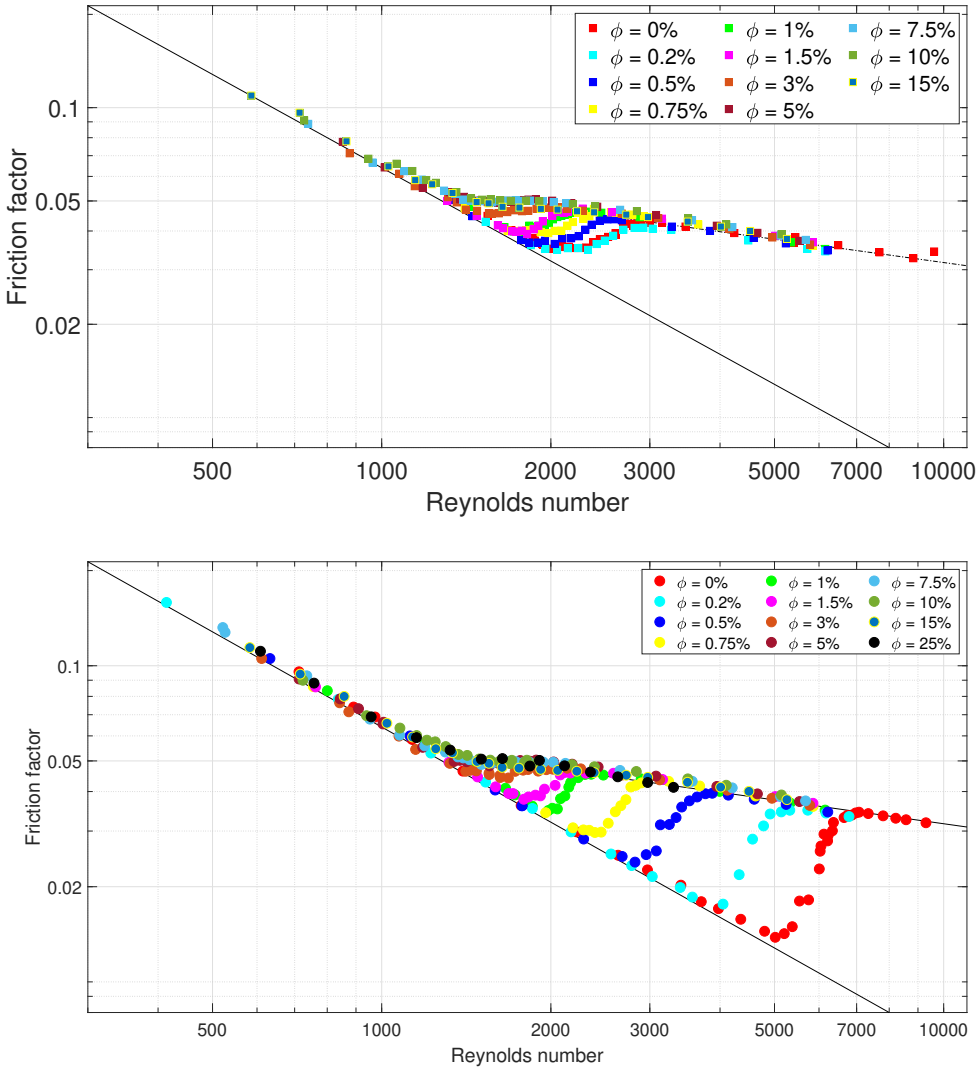

Figure G.1: Moody plots shown for all particle concentrations for perturbed and unperturbed flow

H

Puff splitting

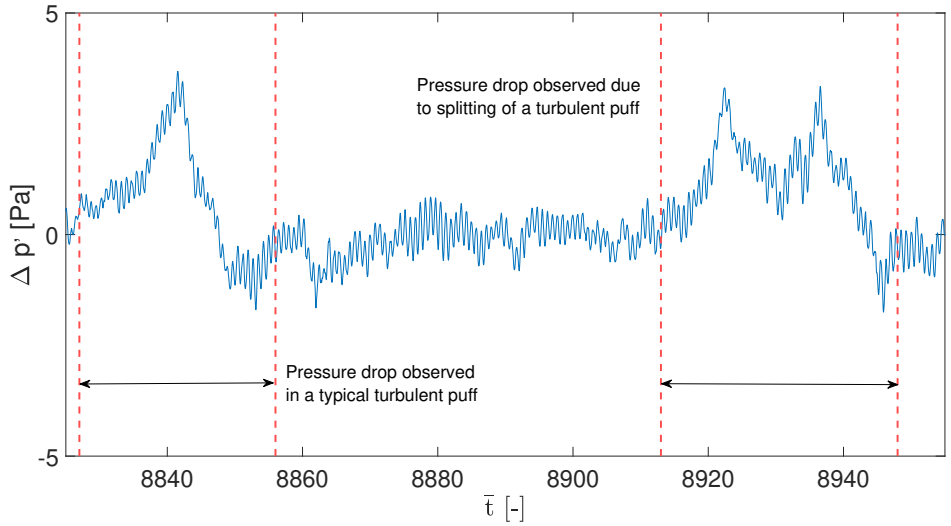

Figure H.1: Pressure drop observed for a turbulent puff alongside a puff splitting as it advects pass the pressure sensors. This splitting process is represented as $L_{puff} \geq$ 40D in puff statistics

Bibliography

[1] Baofang Song, Dwight Barkley, Björn Hof, and Marc Avila. Speed and structure of turbulent fronts in pipe flow. *Journal of Fluid Mechanics*, 813:1045–1059, Jan 2017.

[2] T. Mullin. Transition to turbulence in pipe flow. *Fluid Mechanics and its Applications*, 77(1995):221–231, 2005.

[3] Mina Nishi, Bülent Ünsal, Franz Durst, and Gautam Biswas. Laminar-to-turbulent transition of pipe flows through puffs and slugs. *Journal of Fluid Mechanics*, 614:425–446, 2008.

[4] Vasudevan Mukund and Björn Hof. The critical point of the transition to turbulence in pipe flow. *Journal of Fluid Mechanics*, 839(2018):76–94, 2018.

[5] D. J. Kuik, C. Poelma, and J. Westerweel. Quantitative measurement of the lifetime of localized turbulence in pipe flow. *Journal of Fluid Mechanics*, 645:529–539, 2010.

[6] Rory T. Cerbus, Chien Chia Liu, Gustavo Gioia, and Pinaki Chakraborty. Laws of Resistance in Transitional Pipe Flows. *Physical Review Letters*, 120(5):54502, 2018.

[7] Avila Kerstin, Moxey David, Lozar Alberto, De, Avila Marc, Barkley Dwinght, and Hof Bjorn. The Onset of Turbulence in Pipe Flow. *Science*, 333(July):192–197, 2011.

[8] T. Mullin and J. Peixinho. Finite-amplitude thresholds for transition in pipe flow. *Journal of Fluid Mechanics*, 582:169–178, 2007.

[9] Alberto De Lozar and Björn Hof. An experimental study of the decay of turbulent puffs in pipe flow. *Philosophical Transactions of the Royal Society A: Mathematical, Physical and Engineering Sciences*, 367(1888):589–599, 2009.

[10] J. P. Matas, J. F. Morris, and Guazzelli. Transition to Turbulence in Particulate Pipe Flow. *Physical Review Letters*, 90(1):4, 2003.

[11] François Boyer, Élisabeth Guazzelli, and Olivier Pouliquen. Unifying suspension and granular rheology. *Physical Review Letters*, 107(18):1–5, 2011.

[12] Iman Lashgari, Francesco Picano, Wim Paul Breugem, and Luca Brandt. Laminar, turbulent, and inertial shear-thickening regimes in channel flow of neutrally buoyant particle suspensions. *Physical Review Letters*, 113(25):1–5, 2014.

[13] Zhaosheng Yu, Tenghu Wu, Xueming Shao, and Jianzhong Lin. Numerical studies of the effects of large neutrally buoyant particles on the flow instability and transition to turbulence in pipe flow. *Physics of Fluids*, 25(4), 2013.

[14] Nishchal Agrawal, George H. Choueiri, and Björn Hof. Transition to Turbulence in Particle Laden Flows. *Physical Review Letters*, 122(11):114502, 2019.

[15] Willian Hogendoorn and Christian Poelma. Particle-Laden Pipe Flows at High Volume Fractions Show Transition Without Puffs. *Physical Review Letters*, 121(19):194501, 2018.

[16] R N Hof. Experimental investigation of laminar turbulent intermittency in pipe flow. 681:193–204, 2011.

[17] L. F. MOODY. Friction factors for pipe flow. *Trans. ASME*, 66:671–684, 1944.

[18] Stephen B. Pope. *Turbulent Flows*. Cambridge University Press, 2000.

[19] H Blasius. The similarity law in friction processes. *Physikalische Zeitschrift*, 12:1175–1177, 1911.

[20] J. NIKURADSE. Stromungsgesetze in rauhen rohren. *VDI-Forschungsheft*, 361:1, 1933.

[21] G I Taylor. Experiments with fluid friction in roughened pipes. *Proceedings of the Royal Society of London. Series A - Mathematical and Physical Sciences*, 161(906):367–381, 1937.

[22] Frans TM Nieuwstadt, Jerry Westerweel, and Bendiks J Boersma. *Turbulence: introduction to theory and applications of turbulent flows*. Springer, 2016.

[23] I. J. Wygnanski and F. H. Champagne. *On transition in a pipe. Part 1. The origin of puffs and slugs and the flow in a turbulent slug*, volume 59. Technische Universiteit Delft, 1973.

[24] Osborn Reynolds. An experimental investigation of the circumstances which determine whether the motion of water shall be direct or sinuous and the law of resistance. *Philosophical Transactions of the Royal Society*, 174(1883):935–982, 1887.

[25] Björn Hof, Casimir W.H. Van Doorne, Jerry Westerweel, and Frans T.M. Nieuwstadt. Turbulence regeneration in pipe flow at moderate reynolds numbers. *Physical Review Letters*, 95(21):1–4, 2005.

[26] Franz Durst and Bülent Ünsal. Forced laminar-to-turbulent transition of pipe flows. *Journal of Fluid Mechanics*, 560:449–464, 2006.

[27] B Hof, A Juel, and T Mullin. Scaling of the Turbulence Transition Threshold in a Pipe. (December):1–4, 2003.

[28] Tom Mullin and J. Peixinho. Transition to turbulence in pipe flow. *Journal of Low Temperature Physics*, 145(1-4):75–88, 2006.

[29] A. P. Willis, J. Peixinho, R. R. Kerswell, and T. Mullin. Experimental and theoretical progress in pipe flow transition. *Philosophical Transactions of the Royal Society A: Mathematical, Physical and Engineering Sciences*, 366(1876):2671–2684, 2008.

[30] R. K. McGEARY. Mechanical packing of spherical particles. *Journal of the American Ceramic Society*, 44(10):513–522, 1961.

[31] A. A. Draad, G. D.C. Kuiken, and F. T.M. Nieuwstadt. *Laminar-turbulent transition in pipe flow for Newtonian and non-Newtonian fluids*, volume 377. Technische Universiteit Delft, 1998.

[32] R. R. Kerswell. Recent progress in understanding the transition to turbulence in a pipe. *Nonlinearity*, 18(6), 2005.

[33] Nian-Sheng Cheng. Formula for the viscosity of a glycerolwater mixture. *Industrial & Engineering Chemistry Research*, 47(9):3285–3288, 2008.

[34] F Durst, Subhashis Ray, Bülent Ünsal, and OA Bayoumi. The development lengths of laminar pipe and channel flows. 2005.

[35] Jonathan J. Stickel and Robert L. Powell. Fluid mechanics and rheology of dense suspensions. *Annual Review of Fluid Mechanics*, 37:129–149, 2005.

[36] Andreas Volk and Christian J Kähler. Density model for aqueous glycerol solutions. *Experiments in Fluids*, 59(5):1–4, 2018.